INFORMATION TO USERS

This manuscript has been reproduced from the microfilm master. UMI films the text directly from the original or copy submitted. Thus, some thesis and dissertation copies are in typewriter face, while others may be from any type of computer printer.

The quality of this reproduction is dependent upon the quality of the copy submitted. Broken or indistinct print, colored or poor quality illustrations and photographs, print bleedthrough, substandard margins, and improper alignment can adversely affect reproduction.

In the unlikely event that the author did not send UMI a complete manuscript and there are missing pages, these will be noted. Also, if unauthorized copyright material had to be removed, a note will indicate the deletion.

Oversize materials (e.g., maps, drawings, charts) are reproduced by sectioning the original, beginning at the upper left-hand corner and continuing from left to right in equal sections with small overlaps.

Photographs included in the original manuscript have been reproduced xerographically in this copy. Higher quality 6" x 9" black and white photographic prints are available for any photographs or illustrations appearing in this copy for an additional charge. Contact UMI directly to order.

Bell & Howell Information and Learning
300 North Zeeb Road, Ann Arbor, MI 48106-1346 USA
800-521-0600

UMI®

INFRARED PROPERTIES OF HIGH-TEMPERATURE SUPERCONDUCTORS WITH SINGLE AND TRIPLE COPPER OXYGEN PLANES

By

Tatiana Startseva

M. Sc. (Physics) Brock University

A THESIS SUBMITTED TO

THE FACULTY OF GRADUATE STUDIES

IN PARTIAL FULFILLMENT OF

THE REQUIREMENTS FOR THE DEGREE OF

DOCTOR OF PHILOSOPHY

MCMASTER UNIVERSITY

July 1998

IR PROPERTIES OF HTSC WITH SINGLE AND TRIPLE CuO_2 PLANES

DOCTOR OF PHILOSOPHY (1998) McMaster University

(Physics) Hamilton, Ontario

TITLE: Infrared Properties of High-Temperature Superconductors with Single and Triple CuO_2 Layers

AUTHOR: Tatiana Startseva, M.Sc. (Brock University)

SUPERVISOR: Professor T. Timusk

NUMBER OF PAGES: xiii, 109

Abstract

This thesis includes work on two high temperature superconducting systems (HTSC), namely, $La_{2-x}Sr_xCuO_4$ and $HgBa_2Ca_2Cu_3O_{8+\delta}$. The CuO_2 planes contained within the crystal structure of these materials, as well as in all the other HTSC, hold the key to superconductivity. From one point of view the two systems described in this thesis represent two extremes within a wide variety of HTSC. $La_{2-x}Sr_xCuO_4$ is the classic representative of a material with a single CuO_2 plane per unit cell and has one of the lowest critical temperatures. On the other hand, the crystallographic structure of $HgBa_2Ca_2Cu_3O_{8-\delta}$ is based on three CuO_2 planes. Despite the fact that both of these systems were discovered quite some time ago relatively little work has been done on them.

Infrared spectroscopy has established itself as a very powerful technique for studying the properties of superconductors. One out of the vast majority of excitations that infrared spectroscopy can probe is the excitation responsible for the pairing mechanism in superconductivity. Furthermore, the energy range covered is compatible with the predicted value of the superconducting energy gap.

This work is focused on, but not confined to, the infrared study of the normal properties of both $La_{2-x}Sr_xCuO_4$ and $HgBa_2Ca_2Cu_3O_{8+\delta}$. The reflectivity of $La_{2-x}Sr_xCuO_4$ single crystals has been measured in the frequency range 30 - 9,000 cm^{-1} (0.004 - 1 eV) in directions parallel and perpendicular to the CuO_2 planes (*ab*-plane), whereas $HgBa_2Ca_2Cu_3O_{8+\delta}$ single crystals were studied only in the direction of the *ab*-plane. Both the doping and the temperature dependence were studied. For the first time, the high-temperature optical spectra were obtained. This allowed us to investigate the charge dynamics of the anomalous normal state up to 400 K.

We observe a gap-like depression in the effective scattering rate $1/\tau(\omega, T)$ below a temperature T^* in both systems. This characteristic behavior of the frequency and temperature dependent scattering rates suggests the existence of a pseudogap state in both the under- and overdoped regimes of the single-layer HTSC system $La_{2-x}Sr_xCuO_4$ for temperatures exceeding 300 K as well as in the underdoped regime of $HgBa_2Ca_2Cu_3O_{8-\delta}$. The signature of the pseudogap state in the direction perpendicular to the CuO_2 planes is also discussed.

Acknowledgment

I would like to take this opportunity to thank my supervisor, Tom Timusk, with whom I have had the pleasure to work for the past four years, for his invaluable insights, guidance, enthusiasm and patience. He spent a tremendous amount of time advising, reassuring and supporting me.

I wish to thank Prof. Jules Carbotte who encouraged my interest and spent his time in discussions as well as for providing the opportunity to meet and collaborate with the other physicists in Canada through series of CIAR meetings. I offer sincere thanks to Profs. Bruce Gaulin, John Preston and Carl Stager for their useful advises and for providing me with many unique opportunities throughout my graduate studies.

A warm "thank you" goes out to all the members of the Department of Physics and Astronomy, in particular, Cheryl, Jackie, Marg, Rose and Wendy, for their support and help. As well, thanks to Gord Hewitson, Venice Perno and the guys from the machine and electronic shops for their excellent, speedy work which kept the lab running smoothly. Gord, your tastefully arranged fruit baskets and exquisite flower bouquets will never be forgotten. Thanks should also be given to " the basement community": Dimitri Basov, Andy Duft, Andy Duncan, Ron Francis, Jim Garrett, Jeff McGuire, Steve Moffat, Tadek Olech, Jason Palidwar, Anton Puchkov, Toomas Rõõm, and, last but not least, Rob Hughes for their huge contribution to this thesis and for providing such a delightful work atmosphere. It is without a sarcasm (for once) that I say, it's been great having you around. My dear friends, Andy "the pie man" Düft and " short & snappy" Susie, deserve extra thanks. Discussions with them (mostly starting before 8:00 AM) were always enlightening and often led to a new avenues of thoughts.

My genuine thanks and appreciation are extended to my friends: Peter and Anita Mason, Jason and Melonie Palidwar, Ron and Sonia Francis, Frank Hayes and Carol Rogerson. The last four years were both pleasant and memorable.

I am fortunate to feel the love, support and encouragement of my mother and my grandparents. Thank you for trying to understand what it is that I do and making me believe that I could succeed in whatever I chose. You have been a wonderfully positive influence.

Finally, to my perfect companion, Jim, who convinced me to undertake the study at McMaster and filled all these years with the encouragement, love, faith and constant support, I express my deepest admiration and appreciation.

Table of Contents

List of Tables

List of Figures

In nature's infinite book of secrecy

A little can I read.

- William Shakespeare

Chapter 1

INTRODUCTION

1.1 On a historical note

In many conductors the electrons responsible for the current undergo a transition into an ordered state, i.e., a superconducting state, with many unique properties. The difference between the superconducting and normal states is very small in energy, but it is tremendous as far as the resistivity and magnetism are concerned. Both zero resistance and perfect diamagnetism are the hallmarks of superconductivity. The vanishing of resistance to the flow of electric current below a critical temperature, T_c, was discovered by H. Kamerlingh Onnes in 1911 while studying the temperature dependence of the electrical resistance of mercury. The critical temperature of the first superconductor was 4.2 K. The immeasurable resistance at temperatures below T_c suggested the name for the phenomenon. The other key property of a superconductor is the appearance of a large diamagnetism in the superconducting state. This was discovered by W. Meissner and R. Ochsenfeld in 1933. A bulk superconductor at temperatures below T_c behaves as if the magnetic induction B is equal to zero inside the sample.

An explanation for this challenging problem was not found for decades. This was partially due to the fact that it required a lot of imagination to deal with such dramatic changes on a very small energy scale. For example, in the case of aluminum the energy difference between an electron in the normal and superconducting state is 0.14×10^{-8} eV per electron. This is an insignificant change compared to the electron's kinetic energy of

1-10 eV. Only in 1957 did J. Bardeen, L.N. Cooper, and J.R. Schrieffer establish the first successful macroscopic theory for superconductivity called the BCS theory. This theory proves that it is energetically favorable for electrons to form pairs of carriers with opposite spin and momentum, via phonon mediated processes, called Cooper pairs.[Bardeen57] In order to break the pair an energy of magnitude 2Δ is needed. The energy gap, Δ, a fundamental property of superconductors, is related to the critical temperature by the fundamental BCS relation,

$$2\Delta = 3.54 k_b T_c, \tag{1.1}$$

where k_b is a Boltzman constant.

Table 1.1: Measured values of Δ.

The value of the gap taken from tunneling experiments.[Ashcroft76]

element	$2\Delta(0)/k_bT_c$
Al	3.4
Hg	4.6
Nb	3.8
Zn	3.2
In	3.6

The experimental gaps follow this equation very closely with an accuracy of 10%. Table 2.1 shows the results of $2\Delta/k_bT_c$ based on tunneling data.[Ashcroft76] One of the first experiments, however, where the energy gap was directly observed was an infrared absorption experiment.[Richards60]

Between 1911 and 1986 hundreds of superconducting compounds were found, but the highest critical temperature, T_c, was only 23 K. The discovery of $La_{2-x}Ba_xCuO_4$ by J.G. Bednorz and K.A. Müller in 1986 started a new era in history of superconductivity:

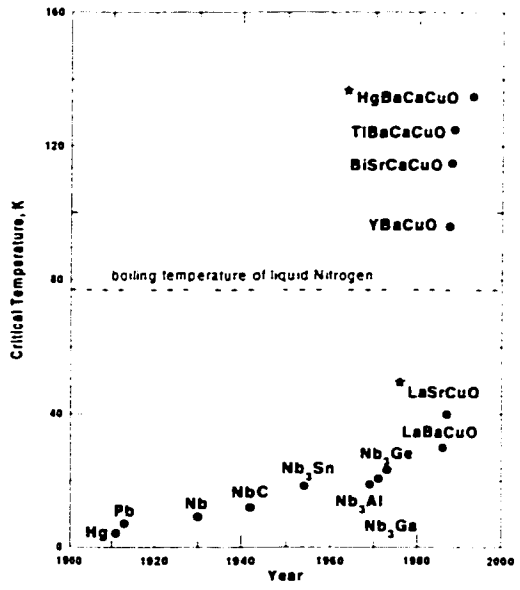

Figure 1.1: Evolution of the critical temperature since the discovery of superconductivity by K. Onnes in 1911.
The discovery of the cuprates started a new exciting era in the history of superconductivity. (La,Sr)CuO and HgBaCaCuO, cuprate superconductors with one of the lowest and highest critical temperatures are discussed in this thesis.

the era of high temperature superconductors (HTSC). $La_{2-x}Ba_xCuO_4$ has a T_c equal to 30 K.[Bednorz86] In itself a jump in T_c of 7 K was not a revolutionary discovery at the time. However, Cu oxides (cuprates) opened up a whole new family of superconducting materials with higher transition temperatures. Since 1986 other copper-oxide superconductors with critical temperatures above liquid nitrogen's boiling point were discovered. The HTSC material with the highest T_c is $HgBa_2Ca_2Cu_3O_{8+\delta}$(Hg1223) which was discovered by Schilling *et al.*[Schilling93] in April 1993(Fig 1.1). At the optimal oxygen concentration, T_c is equal to 135 K, a record at ambient pressure that remains valid to this day. Superconductivity at such high temperatures generated enthusiasm in the technological world and attracted the attention of the public. Visions of many practical applications were proposed. Powerful superconducting magnets, magnetic resonance

imaging, brain and heart measurements with superconducting SQUIDs, long distance lossless transmission lines, levitated trains, lossless computer elements are just some of them. The most promising application of the HTSC materials are passive microwave devices for use in satellite communications.

1.2 HTSC and conventional superconductors

1.2.1 Coupling mechanism

There are many differences between high-temperature and conventional superconductors. The major difference is the magnitude of the critical temperature. Often, the T_c of the cuprates is almost an order of magnitude larger than the T_c of conventional superconductors.

The strongly-coupled BCS theory describes conventional superconductors very well. Phonon-mediated pairing is responsible for the superconductivity in these materials. This was proven by the isotope effect. In conventional superconductors T_c is proportional to the frequency of phonons which is in turn inversely proportional to the mass.

$$T_c \sim \Theta_D \sim M^{-\alpha} \tag{1.2}$$

For superconductors such as Hg, Tl and Pb $\alpha = 0.5$.[Kittel86] However, in case of optimally doped HTSC α is between 0 and 0.1. A very small α and an extremely high T_c suggest that phonons are not the major contributor to the pairing mechanism. Nevertheless, the origin of the isotope effect in HTSC is still under dispute.

Difficulties in explaining the isotope effect in HTSC could be related to a very complicated crystallographic structure. Most conventional superconductors have the simplest crystal structures, such as body-centered cubic or face-centered cubic with only several atoms per unit cell. The HTSC's crystallographic structure is perovskite-like with two

types of copper-oxide layers commonly referred to as layers and chains, and up to a dozen other atoms in a chemical unit cell. The other layers in the cuprates are often called the charge reservoir layers or the doping block. Figure 1.2 reflects these general features of the HTSC's crystal structure. The "openness" of the crystal structure allows one to introduce dopants by adding oxygen or by chemical substitution. For example, La_2CuO_4 is the parent compound for $La_{2-x}Sr_xCuO_4$. The replacement of some of the trivalent La by divalent Sr varies the critical temperature from 0 K up to 40 K (see Fig 1.3). The undoped phase of the HTSC material is an antiferromagnetic insulator with a gap of 1.5-2 eV. However, considering that the valency of La is +3 and the valency of oxygen is −2, then the valency of Cu should be +2. This leads to one hole per formula unit and suggests that La_2CuO_4 is metallic with a half-filled band. In reality strong electron correlations can split the half-filled conduction band into two bands. One of them is filled and the other is empty. A charge transfer gap between the bands results in semiconducting properties.

1.2.2 Gap symmetry

Perhaps one of the hottest issues in the history of HTSC was the symmetry of the Cooper pairs. For conventional superconductors the wavefunction of the Cooper pair is isotropic with an angular momentum equal to zero. It is widely known as an s-wave superconducting order parameter. The HTSC's are highly anisotropic materials. An important experimental manifestation of the type of mechanism for HTSC is the degree of gap anisotropy. For s-wave pairing the gap parameter $\Delta(\vec{k})$ remains nonzero, but may vary somewhat as the wavevector $\vec{k}$ moves around the Fermi surface, while for p- and d-wave pairing $\Delta(\vec{k})$ goes to zero at points or along lines on the Fermi surface. The wealth of experimental data has narrowed the question about the symmetry of the order parameter generally to two scenarios: pure d-wave or a mixture of d and s wave. The difference

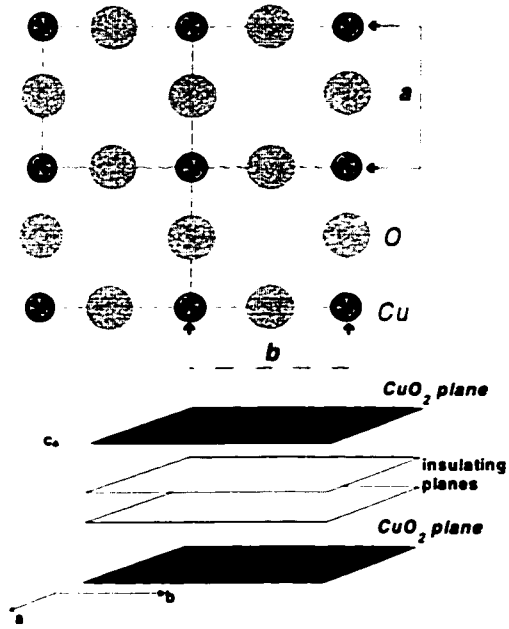

Figure 1.2: A schematic diagram of the CuO_2 plane and HTSC's crystal structure. The upper figure shows the planar arrangement of Cu and O atoms. Cu atoms have magnetic moments which form an antiferromagnetic sublattice. The lower figure is mostly based on (La,Sr)CuO's crystal structure. It emphasizes the conducting CuO_2 layers separated by a couple of insulating planes. The direction of CuO_2 structure is called the ab-plane. The perpendicular direction is called the c-axis.

between d and s wave symmetry is not just in the shapeof the order parameter, but also in the fact that d-wave has a sign change associated with it. In k-space the order parameter is related to the energy gap, Δ. The particular direction in k-space where the gap vanishes would ultimately be reflected in the experimental data as the presence of excitations starting at zero energy for the experimental techniques that represent an averaged over all (or the majority) k space. Such experiments include infrared (IR) spectroscopy, microwave conductivity, NMR and specific heat measurements. For example, one of the first experiments to suggest d-wave symmetry in the order parameter was

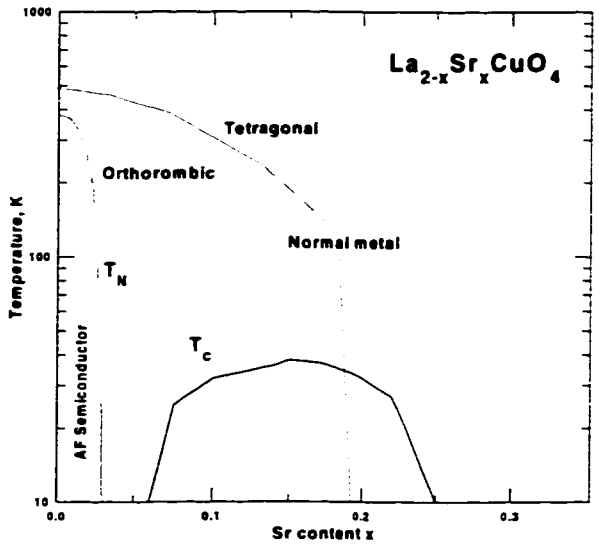

Figure 1.3: Phase diagram of $La_{2-x}Sr_xCuO_4$.
The general features, such as the presence of the antiferromagnetic phase and the superconducting state, are present in all HTSC.(from Ref. [Schilling93])

the measurements of the linear-in-temperature(as opposed to T^2) penetration depth in $YBa_2Cu_3O_{6.95}$(Y123) by Hardy *et al.*[Hardy93] This shows that the density of excitations drops more slowly with temperature than it would for a constant gap.

There are several experiments that can actually resolve the k dependence of the gap symmetry. Polarization-dependent angle-resolved photoemission studies by Z.-X. Shen and Campuzano's groups on high-quality untwinned single crystals of Y123 and $Bi_2CaCu_2O_{8+\delta}$ (Bi2212) reveal modifications to the near-Fermi-edge spectral weight that are indicative of an anisotropic superconducting energy gap.[Shen93, Harris96, Ding96, Ding97] The measured magnitude of the shift of the leading edge increases monotonically, reaching a maximum value of approximately 25 meV. The authors note that within experimental

error their results are consistent with a $d_{x^2-y^2}$ order parameter, where $\Delta(\vec{k})$ is proportional to $\cos(\vec{k}_{xa}) - \cos(\vec{k}_{ya})$, but qualitatively incompatible with an extended s-wave gap proportional to $\cos(\vec{k}_{xa}) + \cos(\vec{k}_{ya})$. However, they point out that they cannot distinguish between pure $d_{x^2-y^2}$ symmetry and mixed $s + id$ symmetry because they are unable to prove that the gap really is zero.

Several phase-sensitive experiments using DC-SQUIDs, tricrystal substrates, and thin-film superconducting rings containing three grain-boundary junctions have provided the strongest evidence for d-wave symmetry of the order parameter in Y123 and $Tl_2Ba_2CuO_{6+\delta}$ (Tl2201) samples.[Tsuei94, Kirtley95, Tsuei96] The authors of the first experiment on Y123 had difficulties interpreting their results based on the effects of the CuO_2 bilayers in the unit cell, the orthorhombic crystal structure, and the CuO chains. These objections were overcome in experiments involving cuprates such as Tl2201 with a single CuO_2 layer in the unit cell, a tetragonal crystal structure, and no CuO chains. A high-resolution scanning-SQUID-microscopy study demonstrates the effect of spontaneously generated half flux quanta (π phase shifts) in superconducting rings containing three grain-boundary junctions. Half-integer Josephson vortices (containing flux $h/4e$) were also observed in a Tl2201 film, but only at the tricrystal point (the point where the three grain boundaries of the tricrystal substrate come together), whereas only ordinary Josephson vortices (flux $h/2e$) were trapped at the bicrystal grain boundaries. These observations show that the order-parameter symmetry in Tl2201 is consistent with a pairing state with $d_{x^2-y^2}$ symmetry as observed in Y123.

1.2.3 Anomalous normal state properties

The extensive search for the superconducting gap and its symmetry directed attention towards a different problem: the anomalous normal state properties of the cuprates.

Since the discovery of HTSC, it has been noted[Gurvitch87] that normal state resistivity is linear up to extremely high temperatures. A tremendous amount of experimental work concentrating on the normal properties of HTSC has been collected over the last three years. However, there is still no consensus about the mechanism behind these unusual phenomenon.

An NMR study of Y123 was the first experiment showing the so-called "spin gap" or "pseudogap". [Warren89] As a function of temperature, both the spin susceptibility and the nuclear spin-lattice relaxation rate was suppressed below a characteristic temperature T^*, a temperature that can significantly exceed the superconducting transition temperature T_c. The spin susceptibility is proportional to the number of electrons with spins aligned along the applied field. It takes more energy to flip the paired spin rather than a single spin. Thus, the spin susceptibility is suppressed. This argument produced the idea that the preformed pairs already exist in the normal state. The name 'pseudogap' developed because, first of all, it was observed above T_c and, secondly, an actual zero value in the gap was never observed.

The normal state transport properties of HTSC are strongly affected by the presence of the pseudogap.[Batlogg94, Bucher93, Ito93, Walkes93] The resistivity of $YBa_2Cu_3O_7$ is a linear function in temperature well above 300 K. However, if the oxygen concentration is reduced, the slope of the resistivity becomes steeper developing almost a T^2-behavior. The temperature at which the slope of the resistivity changes is called T^*. The value of T^* as well as its doping dependence suggests a common origin between the transport phenomenon and the NMR data. The spin fluctuations responsible for a suppression of the Knight shift could be the source of the reduction in the scattering seen in the resistivity data. On the other hand, the specific heat measurements[Loram93, Loram94] show that the mechanism behind the anomalous normal properties of HTSC is not limited to a magnetic origin but also has a charge origin.

Several groups have studied the k-space dependence of the pseudogap using angle-resolved photoemission spectroscopy (ARPES).[Marshall96a, Loeser96, Ding96, Ding97] The photoemission spectrum gives information about the electronic energy as a function of k. For a normal metal at zero temperature the spectrum is constant down to the Fermi energy, ϵ_F. Below this energy a sharp drop develops. If there were a gap at the Fermi surface then the density of states would descend for energies less than ϵ_F. In underdoped Bi2212 it was found that the drop below the Fermi energy occurs above T_c. The size of the pseudogap was independent on the doping level. It also seems to dissappear above optimal doping.

Several other techniques were used to study the pseudogap. Vacuum tunneling spectroscopy[Renner98], Raman spectroscopy,[Blumberg97, Nemetschek97] and neutron scattering experiments[Rossat-Mignod91, Tranquada92] have all shown evidence of a gap-like feature in the normal state of various materials.

The infrared reflectance technique is also suitable for investigating both the normal and superconducting properties. The term "pseudogap" was first introduced by C.C. Homes while studying the c-axis conductivity of Y123.[Homes93b] A. V. Puchkov et al.[Puchkov96d] reported studies on the electromagnetic response of three different families of HTSC (Y123 and Y124, Bi2212, and Tl2201) which together allowed the authors to cover the entire doping range from under- to overdoped. The evolution of the pseudogap response by changing the doping level, by varying the temperature from above to below T^*, or by introducing impurities in the underdoped compound was explored. A memory-function analysis of the ab-plane optical data most clearly revealed the effect of the pseudogap. It was found that it occurs in underdoped samples. One exception to this rule was the compound Bi2212 where T^* was higher than T_c in the optimally doped regime. The main conclusion was that the scattering rate of underdoped HTSC is linear and temperature independent over a significant frequency range (750 cm^{-1} up to

3000 cm^{-1}). Below 750 cm^{-1} the scattering rate drops off faster, almost as ω^2. The region where strong suppression of the effective scattering rate occurs is called the "pseudogap".

The vast majority of the experiments described above were done mostly on two materials: Bi2212 and Y123. The technical aspects of working with Y123 are better developed. The latter's critical temperature of 93 K allows an experimentalist to perform the study using relatively inexpensive refrigeration equipment. In addition, the methods of growing and working with Y123 are well advanced. Nevertheless, the easily cleaved surface having atomic smoothness made Bi2212 the material of the choice for the tunneling and ARPES spectroscopies. However, there are some drawbacks to the measurements done on Bi2212 and Y123. Both systems possess two CuO_2 planes per unit cell. This makes an explanation of the role of the CuO_2 plane in HTSC extremely difficult. In addition Y123 has a more complicated structure because of its CuO chains. It has been determine from DC resistivity,[Gagnon94] penetration depth measurements,[ZhangK94] and the IR data [Basov95a] that both the CuO chains and the CuO_2 planes bring an equal contribution to the conductivity. This makes the study of the role that the CuO_2 planes play in superconductivity more complicated. Furthermore, Y123 and Bi2212 are limited as far as doping possibilities are concerned. In order to obtain a general picture about the doping dependence of the pseudogap it is necessary to include different families of HTSC.

LSCO is an excellent prototype system for studying the doping dependence. With Sr substituted for La, it is possible to go through a complete doping range from under- to overdoped. In contrast, Y124 is invariably underdoped, Y123 and Bi2212 can be underdoped and slightly overdoped, and Tl2201 is always overdoped. Moreover, the fact that LSCO consists of only one CuO_2 plane per unit cell helps to pinpoint the role of the planes without complications due to chain-plane interactions and the presence of closely coupled CuO_2 planes.

Another aspect of LSCO should be mentioned. Based on NMR results the pseudogap has been attributed only to cuprates with more than one CuO_2 layer per unit cell.[Millis93] According to the authors, the weakly coupled CuO_2 planes in LSCO would prevent long-range spin density wave ordering because of the low dimensionality. This implies that a spin-gap or a pseudogap cannot be observed in LSCO. However, the transport measurements on LSCO indicate anomalous normal properties similar to those found in Y123. Additionally, the IR optical measurements by Uchida *et al.*[Uchida96] confirmed that a suppression of c-axis conductivity similar to Y123 was present in underdoped LSCO with $x = 0.12$. This, along with the several reasons mentioned above, stimulated our study of IR optical properties of LSCO.

Apart from the fact that the data presented in this thesis for the Hg1223 compound are the first optical spectra for this material, the behavior of the pseudogap is extremely intriguing because it has a triple CuO_2 layer structure. In all other measurements the size of the pseudogap in the direction of ab-plane was both material and doping independent. Would it hold for the highest-yet-found HTSC described in this work?

1.2.4 Thesis overview

The main focus of this research is the study of pseudogap as a function of doping, temperature and the number of CuO_2 planes by means of infrared optical spectroscopy. The choice of infrared spectroscopy as a primary tool for this study is a result of a compromise between a desire to investigate the broadest range of properties and using a single experimental technique. It permits one to study such phenomena as electronic transitions, phonons, pseudogaps, superconducting gap, and the scattering rates of conducting carriers in the energy range from 10 cm^{-1} up to 10000 cm^{-1}. This frequency range allows one to establish a connection between low-frequency experiments, for example DC transport, microwave, tunneling, Raman, to the high-energy measurements, such as ARPES and

X-ray spectroscopy.

Chapter 2 will provide the necessary background for the analysis of the optical data as well as some details of the experimental apparatus.

Chapter 3 will discuss the optical properties of the underdoped LSCO. A comparison with the double layer cuprates is made. Pseudogap features along both the ab-plane and c-axis directions are presented.

Chapter 4 deals with the widely believed statement that the pseudogap is a signature of only the underdoped families of HTSC. The manifestation of the pseudogap in overdoped LSCO is described and compared to the recent data obtained from an identical sample using Raman spectroscopy.

Chapter 5 provides new insights into the charge dynamics of the triple layer HTSC Hg1223.

Chapter 2

THEORY AND METHODS: IR Optical Properties of Solids

2.1 Reflectance measurements

Infrared spectroscopy has established itself as a very powerful technique for studying the properties of superconductors. One out of the vast majority of excitations that can be probed by infrared spectroscopy is the excitation responsible for the pairing mechanism in superconductivity. Furthermore, the energy range covered is compatible with the predicted value of the superconducting energy gap as well as many other interactions in the HTSC systems. Figure 2.1 exhibits some of the important energy scales in metals and superconductors.

The instrument used in the study is a Fourier transform Michelson interferometer. The reflectance obtained in these experiments usually covers the range from 20 cm^{-1} up to 9,000 cm^{-1}.

Since the information obtained is only the real part of the complex reflectance then Kramers-Kronig analysis must be used to extract both parts of the complex optical

Table 2.1: Combination of the lamps, beam splitters and detectors used in the Michelson interferometer.

Range, cm^{-1}	Lamp	Beam splitter	Detector
20 - 250	Hg arc	12.5μ(50G)Mylar	1.2 K Si bolometer
100 - 800	Hg arc	3μ(12G)Mylar	4.2 K Si bolometer
450 - 9,000	Tungsten	KBr	77 K HgCdTe(MCT)
600 - 8,000	Tungsten	KBr	77 K HgCdTe(MCT)(JD16 EG&G)

constant. The mathematical aspects of the analysis are discussed below. However, it is important to mention here the necessity of the high-frequency data in the Kramers-Kronig calculations. Obtaining this data requires the use of a grating spectrometer and an ellipsometer (Fig. 2.1). Besides supplying the information for the high-frequency extrapolation, ellipsometry allows one to obtain both the real and imaginary parts of the optical constants in the near IR, visible and near ultraviolet regimes directly from the experiment. It is useful to check the accuracy of a Kramers-Kronig calculation by comparing it to the ellipsometric data. The avaliable ellipsometric apparatus, however, is limited to room temperature measurements and the programs are for isotropic samples.

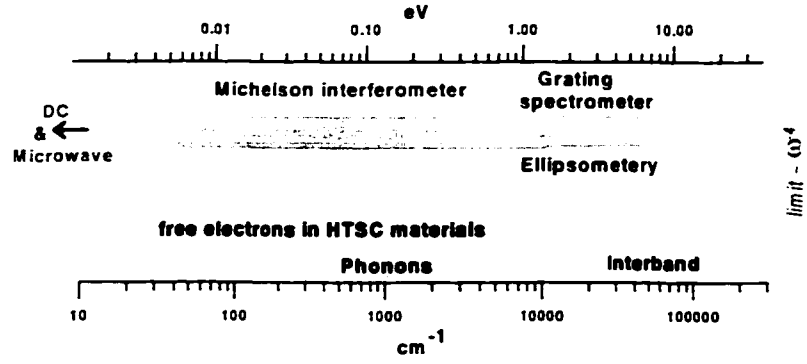

Figure 2.1: The energy scales involved in superconductivity.

A prototype of the interferometer was developed by Michelson in 1880. Despite its age it has still been used as the primary device in infrared spectrometry. A sketch of the experimental setup is shown in Figure 2.2. Such instruments allow one to measure the

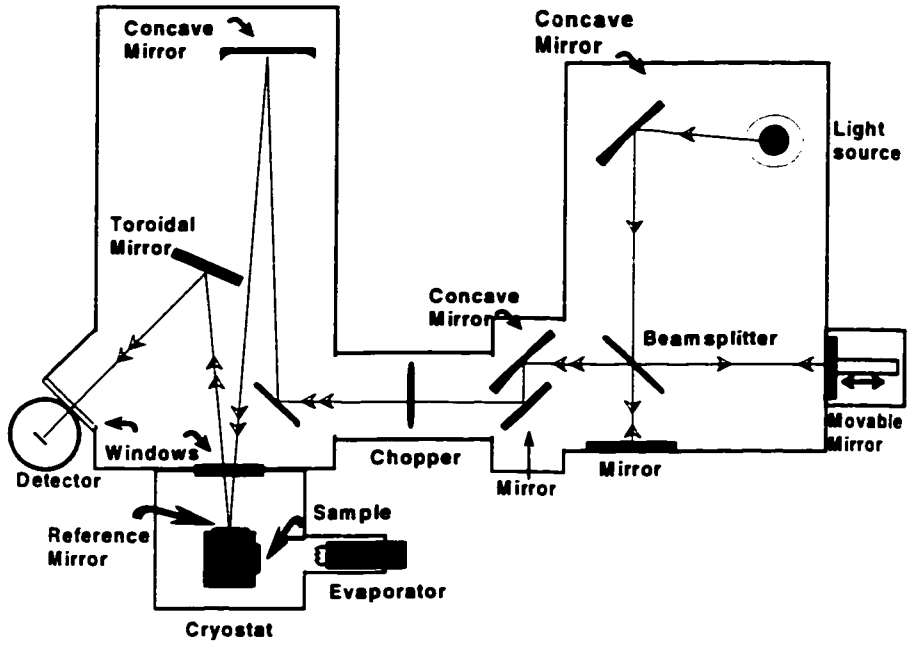

Figure 2.2: Schematic diagram of the apparatus used to measure IR reflectance. Usually three different detectors are used.

infrared reflectance as a function of both frequency and temperature. The broad band light source used was either a mercury arc lamp or a tungsten lamp. The light from the source is directed by a mirror onto a mylar beam splitter which has the property of being able to reflect and transmit equal amounts of light. The two beams divided by the beam splitter are reflected back by one stationary and one movable mirror. The recombined beams will then interfere with each other. Whether the interference is constructive or destructive depends on the path difference and the frequency of the light. After passing a set of mirrors the beams travel through a chopper that is only used in the alignment procedure. Finally, the light hits the sample positioned inside of the cryostat.

The sample is glued to the apex of a cone (see Figure 2.3). To utilize the whole sample, an overfilling technique is used so that light that misses the sample is scattered out of the optical path.[Homes93a] The reflectance of the sample (R_s) is compared to the reflectance of a stainless-steel reference mirror (R_m). By alternating between the sample and reference mirror every few minutes one can eliminate the effects of long term drifts in both the detector response and in the light source. The rotation also allows one to place the sample in front of an evaporator. To correct for the sample size and any irregularities in the surface, and to eliminate the effects of the reference mirror, an *in situ* evaporation of a metallic film (Au or Al) onto the surface of the sample was used. The coated sample was then remeasured (R_{gs}) and the absolute value of R was given by the ratio of spectra before and after plating, corrected for the absolute reflectance of the metallic film. [Palik85]

$$\left(\frac{R_s}{R_m}\right)\left(\frac{R_{gs}}{R_m}\right)^{-1} = \frac{R_s}{R_{gs}}. \tag{2.1}$$

The accuracy of the absolute reflectance is estimated to be $\leq \pm 1\%$.

The brass cone holding the sample was anchored with a copper braid to the cold finger of a continuous flow cryostat to insure proper thermal contact. The available temperature

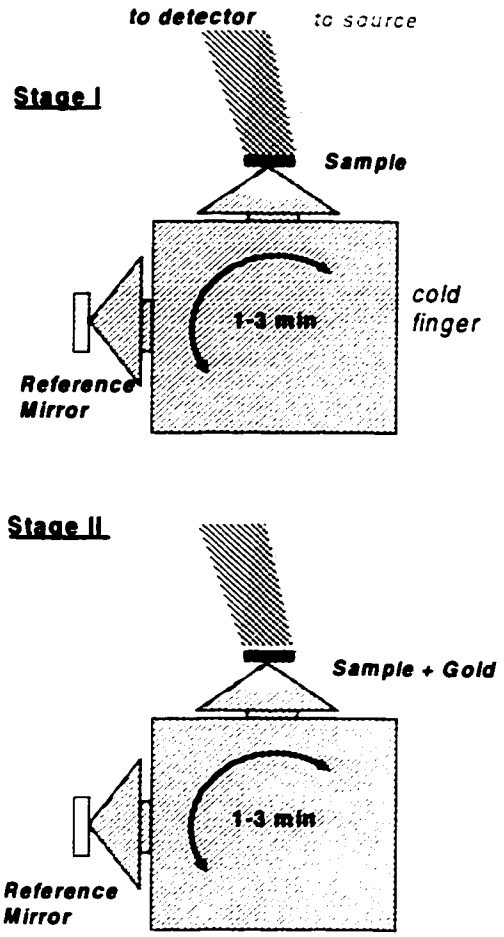

Figure 2.3: Diagram of the sample holder and the cold finger.
Stage I: The light from the source hits the sample and the reflected light is detected. The rotation of the cryostat allows one to compare the reflectance of a sample to that of a reference mirror. Stage II: Similar measurements are repeated with the thin layer of gold evaporated on the surface of a sample. The ratio between the data obtained from Stage I and the data from Stage II gives an absolute value of the sample's reflectance.

range varies from 10 K up to 850 K. However, in the present study the highest measured temperature was 400 K.

It is also possible to measure the reflectance along different crystallographic directions. This can be accomplished by introducing a polarizer at the chopper position. The orientation of the chosen axis can be calibrated by plotting the reflectance ratio as a function of the polarizer angle, and then least-squares fitting it to a $\sin^2\theta$ function. The estimated error in the angle between the chosen axis of the crystal and the polarizer axis is less than 1°. The polarizer leakage of other polarizations is less than 0.4% of the signal.

After passing the cryostat the light is collected by a toroidal mirror and is focused onto a detector. The plot of the detector signal as a function of mirror position, which is referred to as the interferogram, can be Fourier-transformed into the light signal as a function of frequency.

2.2 Theory

In order to interpret the reflectance data, the electromagnetic theory of light should be used to derive the complex reflection coefficients in terms of the macroscopic optical properties that characterize the specific sample under study. A considerable amount of work has been done on this topic. A detailed discussion can be found in a number of books and articles.[Ashcroft76, Kittel86, Timusk89, Wooten72, Landau84] The purpose of this chapter is to provide the background information that is essential for the analysis of the reflectance data where the angle of incidence is close to normal.

2.2.1 Dielectric response function

Consider a medium which is isotropic, linear in response, and homogeneous.[1] If the magnetic field does not vary with frequency (static case) then the definition of the dielectric constant ϵ is described by the following expression:

$$\vec{D} = \vec{E} + 4\pi\vec{P} = \epsilon\vec{E}, \tag{2.2}$$

where ϵ is the static dielectric constant, $\vec{D}$ is the displacement and $\vec{E}$ is the electric field.

In the dynamic case, i.e. when $\epsilon = \epsilon(\omega)$ Eq. 2.2 would transform into.

$$D(\vec{\omega}) = E(\vec{\omega}) + 4\pi P(\vec{\omega}) = \epsilon(\omega)E(\vec{\omega}). \tag{2.3}$$

The reflectivity defined in terms of the dielectric function is:

$$r = \left|\frac{\sqrt{\epsilon}-1}{\sqrt{\epsilon}+1}\right|^2. \tag{2.4}$$

The complex index of refraction, $N(\omega)$, is given by:

$$N(\omega) = n(\omega) + ik(\omega) = (\epsilon_1(\omega) + i\epsilon_2(\omega))^{1/2}, \tag{2.5}$$

so that,

$$\epsilon_1(\omega) = n^2(\omega) - k^2(\omega) \tag{2.6}$$

$$\epsilon_2(\omega) = 2n(\omega)k(\omega). \tag{2.7}$$

Finally, the power absorption coefficient is:

$$\alpha(\omega) = \frac{2\omega}{c}k(\omega) = \frac{\omega\epsilon_2(\omega)}{cn}. \tag{2.8}$$

[1] The units used in this thesis are CGS

The physical meaning of the imaginary part of the dielectric function is it describes how much energy is dissipated.

2.2.2 Kramers-Kronig transformations

The Kramers-Kronig transformations relate the real and imaginary part of the complex response at all frequencies. However, certain conditions have to be satisfied. Consider the response function $f(\omega) = Ref(\omega) + iImf(\omega)$.[Kittel86] First of all, the poles of $f(\omega)$ must be below the real axis. Secondly, the integral should vanish around an infinite semicircle in the upper half of the complex ω-plane and $f(\omega)\to 0$ uniformly as $|\omega|\to\infty$. Finally, and most importantly the response must be linear.

The Kramers-Kronig relations for f are:

$$Ref(\omega) = \frac{1}{\pi}\mathcal{P}\int_{-\infty}^{\infty}\frac{\Omega Imf(\Omega)}{\Omega-\omega}d\Omega \tag{2.9}$$

$$Imf(\omega) = -\frac{\omega}{\pi}\mathcal{P}\int_{-\infty}^{\infty}\frac{Ref(\Omega)}{\Omega-\omega}d\Omega \tag{2.10}$$

Here, $\mathcal{P}$ means "principal part".

The Kramers-Kronig transformations are a direct consequence of the causality principle. Ref and Imf must be related to each other to satisfy causality.

Applying Eq 2.10 to the dielectric function one gets the following:

$$\epsilon_1(\omega) - 1 = \frac{2}{\pi}\mathcal{P}\int_0^{\infty}\frac{\Omega\epsilon_2(\Omega)}{\Omega^2-\omega^2}d\Omega \tag{2.11}$$

$$\epsilon_2(\omega) = -\frac{2\omega}{\pi}\mathcal{P}\int_0^{\infty}\frac{\epsilon_1(\Omega)-1}{\Omega^2-\omega^2}d\Omega + \frac{4\pi\sigma_{dc}}{\omega}, \tag{2.12}$$

where σ_{dc} is the DC conductivity.

Finally, the complex reflectance is defined as,

$$r(\omega) = |R(\omega)|^{1/2}\exp(i\theta(\omega)). \tag{2.13}$$

In an experiment only reflectance, R, is obtained. The Kramers-Kronig relations are used to extract the phase shift. Therefore, it is important to gain experimental information about R over as wide a frequency range as possible. Typically, the extrapolation is used to extend the data beyond the measured frequency interval. At high frequencies a $R \sim \omega^{-p}$ relationship with $0 \leq p \leq 4$ is used. For an insulator the reflectance is considered to be constant at low frequency. For a metal the reflectance follows the Hagen-Rubens relation, $R = 1 - (2\omega\rho_{dc}/\pi)^{1/2}$, where ρ_{dc} is the dc resistivity.[Timusk89]

After putting together the data and the extrapolation the Kramers-Kronig relations can be applied:

$$\theta(\omega) = \frac{\omega}{\pi} \int_0^\infty \frac{\ln R(\Omega)}{\omega^2 - \Omega^2} d\Omega. \tag{2.14}$$

By knowing both $r(\omega)$ and $\theta(\omega)$ the rest of the optical constants can be determined from the Fresnel equations.

2.2.3 The free electron's dielectric function

Using the equation of motion of a free electron in an electric field one can get an expression:

$$m\frac{d^2\vec{x}}{dt^2} = -e\vec{E}. \tag{2.15}$$

By substituting the following equations,

$$\vec{E} = \vec{E}_0 \exp(-i\omega t), \tag{2.16}$$

$$\vec{x} = \vec{x}_0 \exp(-i\omega t), \tag{2.17}$$

into Eq 2.15 one can obtain the expression for the dipole moment of the electron:

$$-ex = -\frac{e^2\vec{E}}{m\omega^2}. \tag{2.18}$$

Then the polarization which is the dipole moment per unit volume is equal to:

$$P = -nex = -\frac{ne^2\vec{E}}{m\omega^2}. \tag{2.19}$$

The dielectric function in this case is given by,

$$\epsilon(\omega) = \frac{\vec{D}(\omega)}{\vec{E}(\omega)} \tag{2.20}$$

$$= 1 + \frac{4\pi\vec{P}(\omega)}{\vec{E}(\omega)} \tag{2.21}$$

or by substituting Eq. 2.19 it will take the form of

$$\epsilon(\omega) = 1 - \frac{4\pi ne^2}{m\omega^2}. \tag{2.22}$$

The plasma frequency ω_p is defined by the relation:

$$\omega_p^2 = \frac{4\pi ne^2}{m}. \tag{2.23}$$

Usually, the contributions from high-energy interband processes and atomic cores give rise to a background which can be included as $\epsilon(\infty)$. Eq 2.22 would now look like:

$$\epsilon(\omega) = \epsilon(\infty) - \frac{4\pi ne^2}{m\omega^2}. \tag{2.24}$$

Note that one of the ways to determine a plasma frequency is to find the conditions where the dielectric function is zero.

2.2.4 Drude theory

Frequently, particularly in the case of metals, the complex optical conductivity $\sigma(\omega) = \sigma_1(\omega) + i\sigma_2(\omega)$ is considered. The dielectric function and the optical conductivity are related by the equation:

$$\sigma(\omega) \equiv i\frac{\omega}{4\pi}(1 - \epsilon(\omega)). \tag{2.25}$$

P. Drude established a simple model of metallic conduction in 1890.[Ashcroft76] The theory is still used as a starting approximation in complicated situations. There are several assumptions that have to be made when applying this model. The first is the free electron approximation. The second assumption is that the collisions occur between two or more electrons and static defects instead of between electrons or between electrons and other excitations such as phonons and magnons. The probability of a collision per unit time is given by $1/\tau$. The third assumption states that the average time between collisions is independent of position and velocity. Finally, it is assumed that electrons achieve thermal equilibrium only through collisions.

Consider that all the above assumptions are satisfied and under the influence of an external field the Fermi surface moves in the opposite direction to the field by an amount proportional to current density. The equation of motion of an electron with momentum $\vec{p}$ experiencing a periodic electric field is,

$$\frac{d\vec{p}}{dt} = -\frac{\vec{p}}{\tau} - e\vec{E}. \tag{2.26}$$

Substituting $\vec{E} = \vec{E}_0 \exp(-i\omega t)$ and $\vec{p} = \vec{p}_0 \exp(-i\omega t)$ one can obtain

$$-i\omega\vec{p}(\omega) = -\frac{\vec{p}(\omega)}{\tau} - e\vec{E}(\omega). \tag{2.27}$$

The current density is,

$$\vec{j}(\omega) = \frac{-ne\vec{p}(\omega)}{m} \tag{2.28}$$

$$= \frac{(ne^2/m)\vec{E}(\omega)}{1/\tau} - i\omega \tag{2.29}$$

$$= \sigma(\omega)\vec{E}(\omega). \tag{2.30}$$

Consequentially, the optical conductivity in the Drude model takes the form:

$$\sigma(\omega) = \frac{\sigma_{dc}}{1 - i\omega\tau}, \tag{2.31}$$

where $\sigma_{dc} = ne^2\tau/m$ is the dc conductivity.

The real and imaginary parts of the Drude conductivity can be presented as

$$\sigma_1(\omega) = \frac{\omega_p^2}{4\pi}\frac{\tau}{1+\omega^2\tau^2} \tag{2.32}$$

$$\sigma_2(\omega) = \frac{\omega_p^2}{4\pi}\frac{\omega\tau}{1+\omega^2\tau^2}. \tag{2.33}$$

Here, $\omega_p = 4\pi ne^2/m$ is the plasma frequency of the free carriers. A typical curve of the real conductivity given by Eq.s 2.32 and 2.33 is shown in Fig. 2.4.

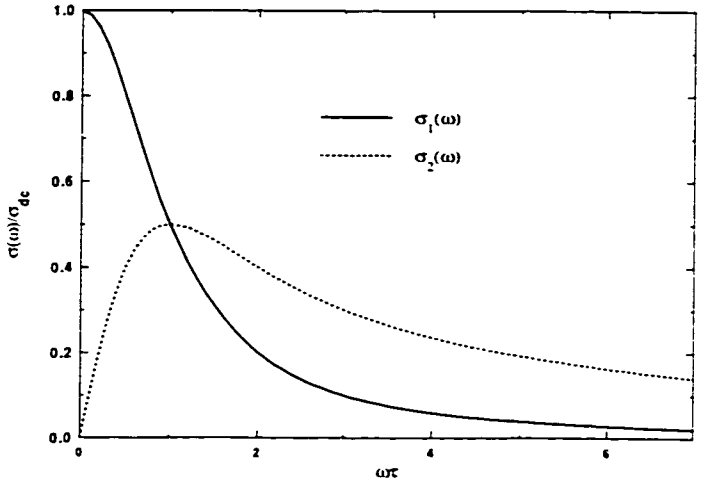

Figure 2.4: The frequency dependence of the real and imaginary parts of optical conductivity given by the Drude theory.

2.2.5 Extended Drude formalism

In real systems such as HTSC, the conductivity has a more elaborate form than that described by a simple Drude model. Two models have been used for HTSC: one and two component models. In the one component model, the optical response is due to absorption of energy by one source of carriers, the itinerant conduction electrons, with a

frequency dependent scattering rate $1/\tau(\omega)$ and a frequency dependent mass m^*. This is a result of the strong interactions with dynamic excitations arising from the strong electron-electron interactions. The single component formalism is commonly referred as the extended Drude model. For the two component model, one assumes that there are two contributions to the frequency spectrum: one comes from the conduction electrons and the other is related to the polarizable bound-state electron (mid infrared) carriers. The two component model can also be regarded as arising from a double relaxation process, two different scattering mechanisms, rather than two sets of carriers.[Allen76]

Both models have their advantages and drawbacks. For HTSC, the spectra obtained from lightly doped cuprates reveal distinct and well separated absorption features well separated from the Drude band.[Timusk89] Thus, a two component model seems appropriate. The low frequency Drude band dominates more as the doping increases and the single-component approach gives better treatment of the optical response at low frequencies below 1 eV. The effective mass loses its physical meaning and becomes negative above 7,000 cm^{-1}[Puchkov96c] suggesting the influence of additional excitations.

It has been suggested that it is safe to apply the single component model to analyze the data at energies below 4,000 cm^{-1}.[Basov98a] Thomas *et al.*[Thomas88] noted that the number of carriers estimated from the optical spectra corresponds to the value obtained from the chemical valence argument if a cut-off frequency of 8,000 cm^{-1} is used. Hence, the response of conducting carriers is dominant up to 4,000 cm^{-1}. Also, by examining the temperature dependence of the real part of the conductivity and considering that the temperature dependence is usually assigned to "free" carriers, one can conclude that the one component model can be used up to 3,000 or 4,000 cm^{-1}. Furthermore, theoretical calculations by Atkinson and Carbotte [Atkinson97] point out that in the case of Y123 the interband contribution from chain-plane transition introduces a minor factor for a *ab*-plane conductivity at frequencies below 2,000 cm^{-1}. This suggests that the main

response comes from intraband processes.

However, the main deficiency of the extended Drude model is the fact that it is based on an oversimplified version of Fermi liquid theory. This theory is highly questionable in HTSC. One way to avoid this shortcoming is to calculate the conductivity, first, by using a more complicated anisotropic theory with a k dependent Fermi velocity and then using the calculated conductivity to find the effective scattering rates and the effective masses. This approach was used by Branch *et al.*[Branch97] and Stojković *et al.*[Stojković96]

Despite the possible disadvantages of the extended Drude model it has been widely accepted in the infrared community as an extremely fruitful tool to analyze the charge dynamics in cuprates.[Thomas88, Collins90, Rieck95, Basov96, Puchkov96a] An overview of the model is offered below based on the work of several theoretical groups.[Allen71, Dolgov95, Shulga91, Götze72, Allen76, Webb86]

In the extended Drude model the optical conductivity can be described by making the damping term in the Drude formula complex and frequency-dependent: $M(\omega,T) = 1/\tau(\omega,T) - i\omega\lambda(\omega,T)$, where $M(\omega)$ is called a memory function.

$$\sigma(\omega,T) = \frac{1}{4\pi}\frac{\omega_p^2}{M(\omega,T) - i\omega} = \frac{1}{4\pi}\frac{\omega_p^2}{1/\tau(\omega,T) - i\omega[1+\lambda(\omega,T)]} \tag{2.34}$$

To recover the classical Drude result the memory function can be expanded for small frequencies into a Taylor series. The conductivity will then take the form:

$$\sigma(\omega,T) = \frac{1}{4\pi}\frac{\omega_p^2}{1/\tau(0) - i\omega(1+\lambda(0))}, \tag{2.35}$$

The alternative way to reduce Eq. 2.34 to the familiar Drude form is to introduce a renormalized scattering rate $1/\tau^*(\omega,T) = 1/[\tau(\omega,T)(1+\lambda(\omega,T))]$ and the effective plasma frequency $\omega_p^{*2}(\omega,T) = \omega_p^2/(1+\lambda(\omega,T))$:

$$\sigma(\omega,T) = \frac{1}{4\pi}\frac{\omega_p^{*2}(\omega,T)}{1/\tau^*(\omega,T) - i\omega} \tag{2.36}$$

$$1/\tau(\omega) = \frac{\omega_p^2}{4\pi} Re(\frac{1}{\sigma(\omega)}), \tag{2.37}$$

$1/\tau^*(\omega)$ is physically meaningless, at least when interpreted as a scattering rate. Equation 2.37 demonstrates that $1/\tau(\omega)$ and $1/\sigma(\omega)$ are identical except for a multiplication factor. Thus, it is the real part of a physical response function, $1/\sigma(\omega)$, and obeys a Kramers-Kronig relation. $1/\tau^*(\omega)$ does not obey a Kramers-Kronig relation and is not directly a physical quantity. If a theoretical calculation of electrons scattering off of some other boson-like excitation is made, then $1/\tau(\omega)$ is closely related to the imaginary part of the self-energy and the quantity conventionally written $i\omega m^*/m$ is the real part[Dolgov95]. Within such calculations, in the limit of zero frequency the normal-state optical conductivity is completely real and is equal to the dc conductivity. $1/\sigma_{dc}(T) = \rho_{dc}(T) = m_e/(\tau(T)ne^2)$, where $\rho_{dc}(T)$, is the dc resistivity. $1/\tau^*(\omega)$ does not enter at all. An alternative explanation is that the quantity with a clear physical meaning is the mean free path. When one tries to convert the latter into a lifetime, it is necessary to know the velocity and therefore the mass. The way to separate these two effects is to consider $1/\tau(\omega)$. $1/\tau^*(\omega)$ is the mean free path mixed up with the velocity renormalization, while $1/\tau(\omega)$ is the mean free path.

The mass enhancement factor $\lambda(\omega)$ is given as the imaginary part of $1/\sigma(\omega)$:

$$1 + \lambda(\omega) = -\frac{\omega_p^2}{4\pi}\frac{1}{\omega} Im(\frac{1}{\sigma(\omega)}). \tag{2.38}$$

The very narrow Drude peak is a consequence of the large mass, which makes it hard for carriers, even scattered ones, to stay in phase with the driving field. The total plasma frequency ω_p^2 in Eqs. 2.37 can be found from the sum rule $\int_0^\infty \sigma_1(\omega)d\omega = \omega_p^2/8$.

The detailed calculations in the frame of memory function analysis were developed for electron-phonon scattering.[Allen76, Allen71, Shulga91] In the case of finite temperatures Shulga et al. obtained an expression for the effective scattering rate:

$$\frac{1}{\tau}(\omega,T)=\frac{\pi}{\omega}\int_0^\infty d\Omega\alpha_{tr}^2(\Omega)F(\Omega)[2\omega\coth(\frac{\Omega}{2T})-(\omega+\Omega)\coth(\frac{\omega+\Omega}{2T})+$$
$$+(\omega-\Omega)\coth(\frac{\omega-\Omega}{2T})]+\frac{1}{\tau_{imp}}. \qquad (2.39)$$

where $\alpha_{tr}^2(\Omega)F(\Omega)$ is a phonon density of states weighted by the amplitude for large-angle scattering on the Fermi surface and T is measured in frequency units.

Eq. 2.39 gives an interpretation of the suppression of $1/\tau$. At low frequencies the number of energetically accessible states is small. As soon as the scattering channels become avaliable the scattering rate increases. Yet, one would expect the saturation of the scattering rate as soon as additional channels are no longer present. Farnworth and Timusk were among the pioneers in the inverting the spectra to obtain α^2F in BCS superconductors.[Farnworth74] In strong electron-phonon coupling, excited electrons emit phonons and produce a spectrum of conductivity related to $\alpha^2F(\omega)$. The features observed in the superconducting state are similar to that of the normal state except for a shift of twice the gap, i.e. $\omega_{ph}+2\Delta$. The results correlate well with the tunneling data. Moreover, the optical data carried more information. As seen from experiments the effective mass is strongly enhanced. This is a consequence of the enhanced scattering.

It should be clear from Eq. 2.39 that the extraction of $\alpha^2F(\omega)$ by optical measurements is a difficult task. The data must be free of noise as two derivatives are required. However, the analysis based on the optical data of K_3C_{60} has been successful.[Marsiglio98] The extracted $\alpha^2F(\omega)$ by inversion of reflectance data structure is proven to be in adequate agreement with similar data obtained from neutron scattering results.

A number of theoretical interpretation have been offered to explain the microscopic origin of the pseudogap. These include nearly antiferromagnetic spin fluctuations[Chubukov97], condensation of preformed pairs[Emery95b, Geshkenbein], SO(5) symmetry[Zhang97]

and spin-charge separation[Lee97].Several reviews exist[Randeria97, Timusk98]. [Emery95b]

2.3 Optical properties of superconductors

All of the HTCS's exhibit a dramatic departure from the Drude form of the reflectivity. Instead of being close to 100% for frequencies below the plasma edge as expected for a good metal, the reflectance of the cuprates drops gradually in a typical quasi-linear fashion until 1 eV. Departure from the optimally doped HTSC yields lower reflectance.

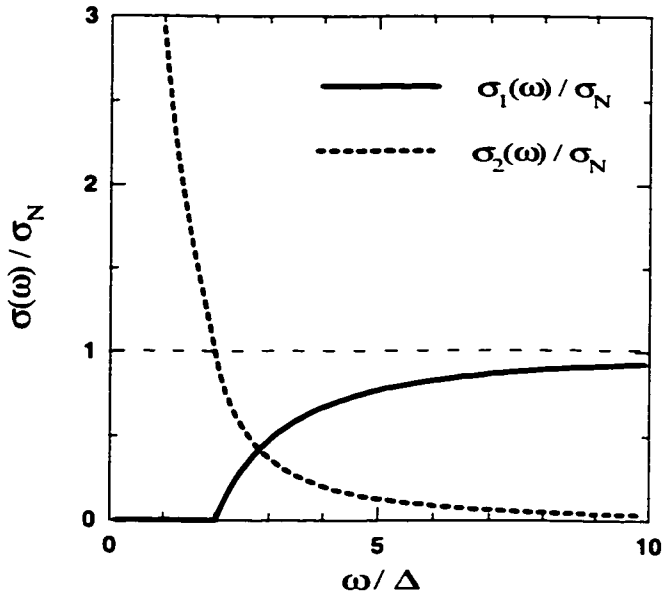

Figure 2.5: The real and imaginary parts of the optical conductivity of a superconductor. The calculation is based on an s-wave order parameter.

For a conventional superconductor, absorption cannot occur until enough energy is absorbed to break the Cooper pair. The threshold for absorption in an isotropic s-wave superconductor is at $\omega = 2\Delta$, rather than Δ; because it is necessary to excite both the particles forming the Cooper pair above the gap energy. In Figure 2.5 we plot σ_1 and σ_2 for the superconducting state of an isotropic s-wave superconductor. Since the physical

meaning of σ_1 is absorption then the real part of conductivity is identically zero below $\omega = 2\Delta$. Beyond this frequency the conductivity starts rising sharply until it reaches the value of normal state conductivity. Note that the difference in spectral weight between the normal (Fig. 2.4) and superconducting (Fig. 2.5) σ_1 is shifted to the delta function positioned at zero frequency.

It is generally believed that the superconducting state is rather conventional in the sense that most experiments can be explained within the framework of a BCS-type theory for a *d*-wave superconductor. The complete absence of absorption has never been detected in the conductivity spectra of cuprates. However, the suppression of conductivity, similar to a "gap-like" drop, has been seen in all HTSC. Most intriguing was the fact that this analogous superconducting behavior extends above the transition temperature. Consequentially, in the recent years the majority of studies on cuprate superconductors were focused on their unusual normal state properties.

In order to understand the electromagnetic response of HTSC in the normal state it is useful to discuss the results of other studies. The first insights into this problem were gained from quantitative charge and spin dynamics studies (resistivity, Hall effect and magnetic susceptibility) over wide range of temperatures and hole concentrations.[Batlogg94] The best example to discuss both the temperature and doping dependence is LSCO since the addition of Sr to La_2CuO_4 can vary the hole concentration from an underdoped to an overdoped regime.

Schematically, the general feature of the resistivity, susceptibility and Hall effect coefficient and the accepted way of determining T^* are summarized in Figure 2.6.

Near optimal doping, $0.15 < x < 0.20$ for LSCO, the in-plane resistivity exhibits a T-linear dependence stretched over a wide temperature range. In the underdoped regime, $0.05 < x < 0.15$, ρ_{ab} increases superlinearly below T^* and grows less rapidly with a near-linear T-dependence at the highest temperatures. In the metallic overdoped region, 0.2

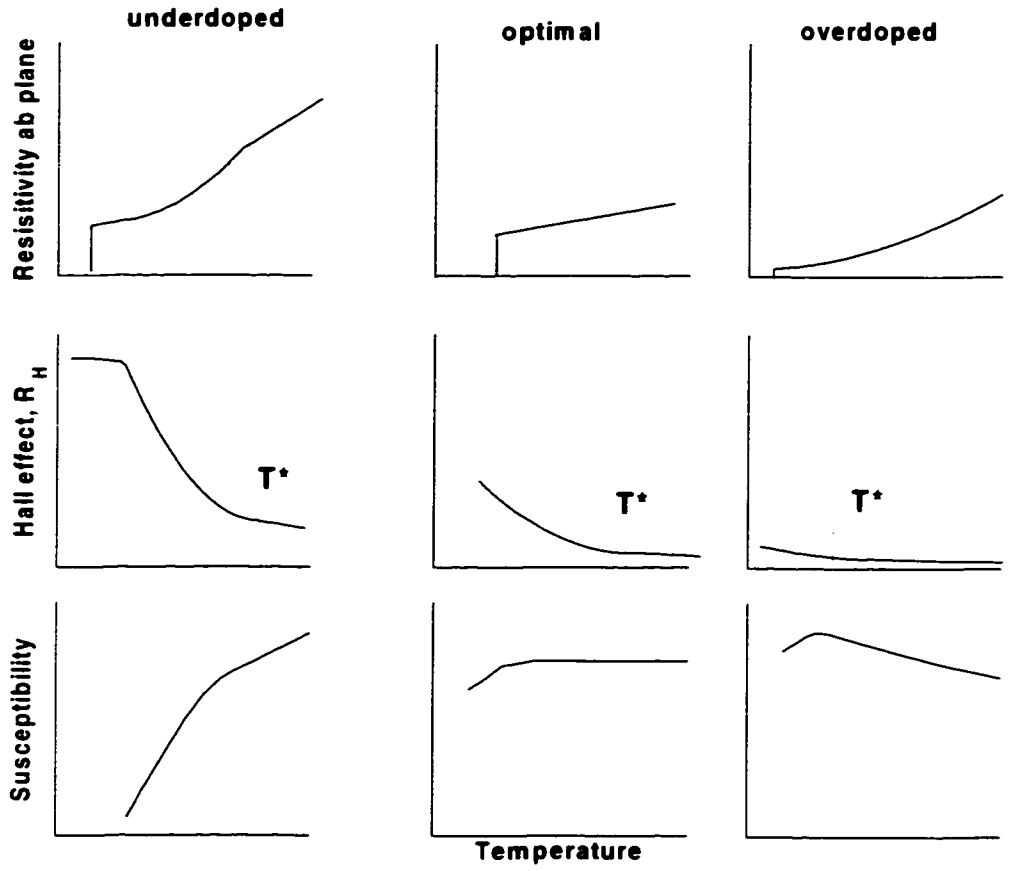

Figure 2.6: Signature of the pseudogap in the temperature dependence of the in-plane resistivity, the Hall effect coefficient and the susceptibility for the three regions of hole concentration.
(After Batlogg *et al.*[Batlogg94])

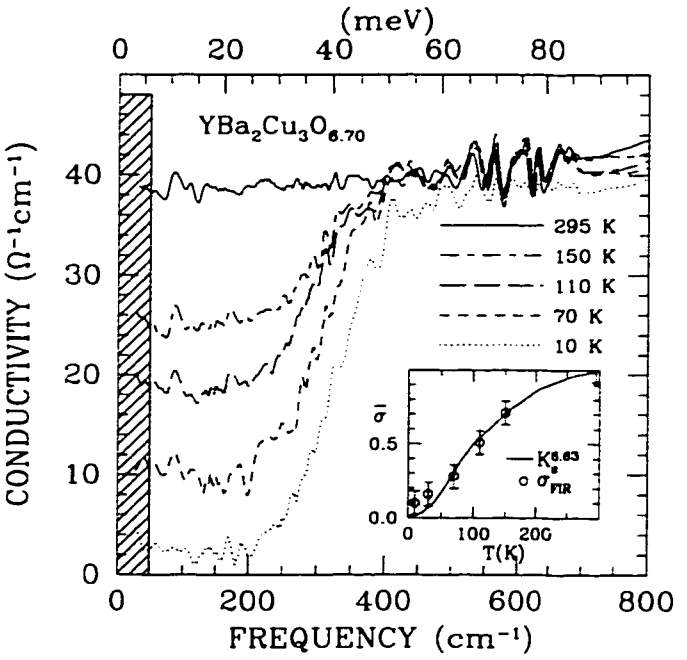

Figure 2.7: The c-axis conductivity of an underdoped Y123 crystal. (After Homes *et al.* [Homes95]) As the temperature is lowered the pseudogap develops. The inset: The NMR Knight shift (normalized at 300 K) is plotted as a function of temperature for an underdoped Y123 crystal. The circles show the low frequency c-axis conductivity for samples with the same doping level.

$< x <$0.4, the resistivity varies as T^n, where n increases from 1 towards 2 as the doping is increased. T* is determined by the increase of $d\rho/dT$ upon cooling.

A similar approach to parameterize the normal state properties in terms of the pseudogap temperature, T*, has been derived from Hall effect measurements. Well above T*, the Hall effect coefficient is constant, while below T* it has T-linear dependence.

In magnetic response measurements, T* is assigned to sharp decrease in $\chi(T)$. The signature of the normal-state gap-like features were observed in the infrared optical measurements as well. Several families of HTSC, Y123, Y124, LSCO and PSYCCO ($Pb_2Sr_2(Y/Ca)Cu_3O_8$),[Homes93b, Basov94, Tajima95, Basov95a, Uchida96, Startseva98a, Reedyk97] exhibit a gap-like suppression in the c-axis conductivity. Figure 2.7 shows that

the characteristic temperature scale where the suppression occurs matches T^* from spin susceptibility measurements. The size of the gap along the c-axis could be estimated either from the energy position where the full suppression takes place or from the starting point of the suppression. As a result, two values were obtained for Y123: 200 cm^{-1} and 400 cm^{-1}.

The extended Drude model has been widely used to describe the coherent response along the ab-plane direction. There is clearly a correlation between the suppression in the in-plane scattering rate and the pseudogap in the c-axis conductivity. This suggests a similar mechanism. However, the energy scale of the pseudogap along the ab-plane is twice as large as that along c-axis.

In the ab-plane the most dramatic manifestation of the pseudogap is observed in the scattering rate for $\omega < 700$ cm^{-1}.[Puchkov96d] By examining the optical results obtained from the underdoped cuprates the following features are noted(see Figure 2.8): (i) above the pseudogap temperature (above the T^*) the scattering rate is nearly ω-linear up to at least 3,000 cm^{-1}; (ii) for $T<T^*$ the scattering rate is suppressed below 700 cm^{-1}, (iii) the energy scale of the pseudogap (700 cm^{-1}) barely depends on the material, doping level and temperature; (iv) $1/\tau(\omega)$ is temperature independent above 700 cm^{-1} and (v) $1/\tau(\omega)$ in the superconducting state is almost indistinguishable from that of the pseudogap state.

A similar threshold structure of the scattering rate is observed in the optimally doped cuprates (see Figure 2.9). However, T^* is less than T_c in this case with the exception of Bi2212.[Puchkov96d] In contrast with the underdoped materials, the temperature dependence of the scattering rate seems to extend over a broader frequency range. Attention should also be drawn to the common feature for optimally doped cuprates, namely, an "overshoot" of the superconducting-state's scattering rate to values above those in the normal state.

Figure 2.10 illustrates the general features of the scattering rate curves for overdoped

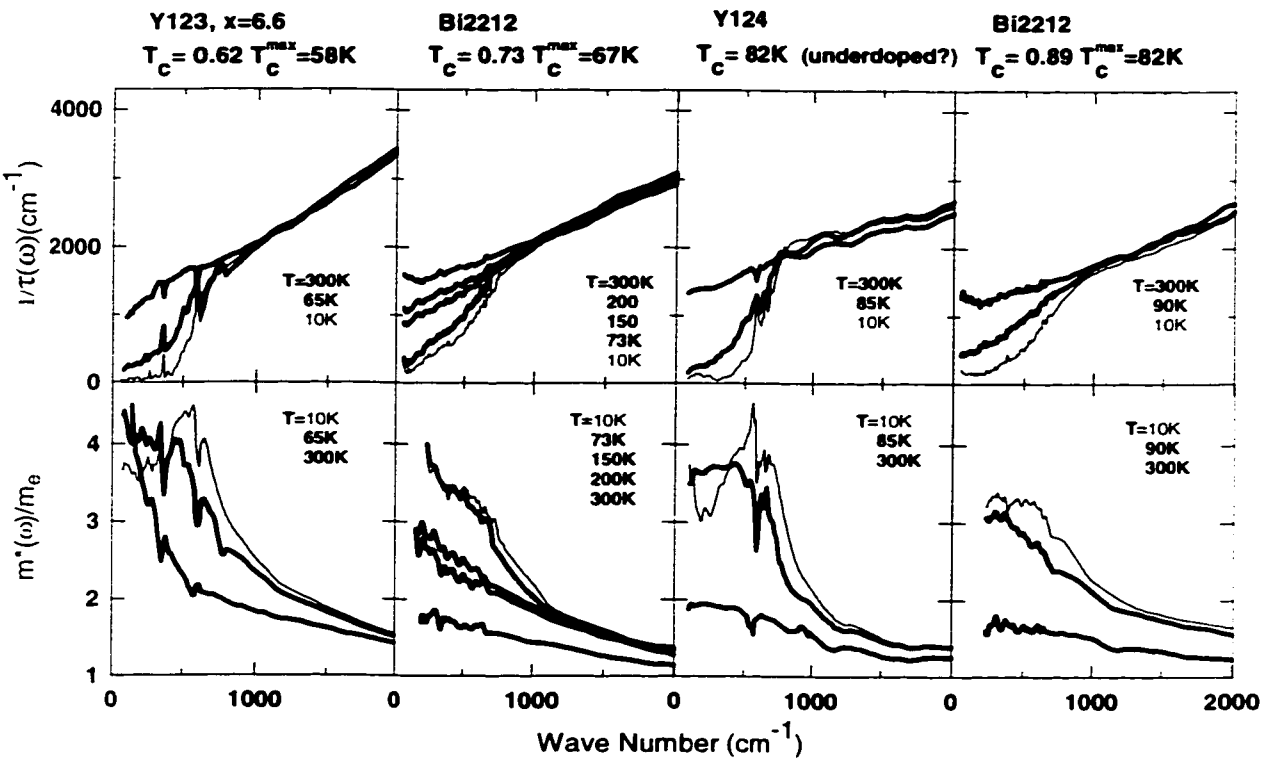

Figure 2.8: Scattering rate and effective mass for underdoped cuprates. (After Puchkov *et al.*[Puchkov96d]) The frequency dependent scattering rate, top row, and the mass renormalization, bottom row, for a series of underdoped cuprate superconductors. The scattering rate curves are essentially temperature independent above 700 cm^{-1}, but develop a depression at low temperatures and low frequencies. The effective mass is enhanced at low temperatures and low frequencies.

samples. The trends are (i) no suppression in the scattering rate is observed at $T>T_c$ with the exception of the slightly overdoped Bi2212 compound; and (ii) the T-dependence becomes more pronounced at high frequencies. It should be noted that for the strongly overdoped Tl2201 sample the frequency dependence of $1/\tau(\omega)$ is reminiscent of Fermi liquid behavior, but the temperature dependence is still linear whereas a quadratic dependence is expected for a pure Fermi liquid.

For completeness the effective masses are shown below the scattering rates. m/m^* peaks at the frequencies where scattering rate is suppressed. The maximum value of m/m^* varies between 1 and 4.

All of the previously measured materials represent a bilayer family of HTSC. The only single layer cuprate from the above study was Tl2201 which was avaliable as a strongly overdoped sample.

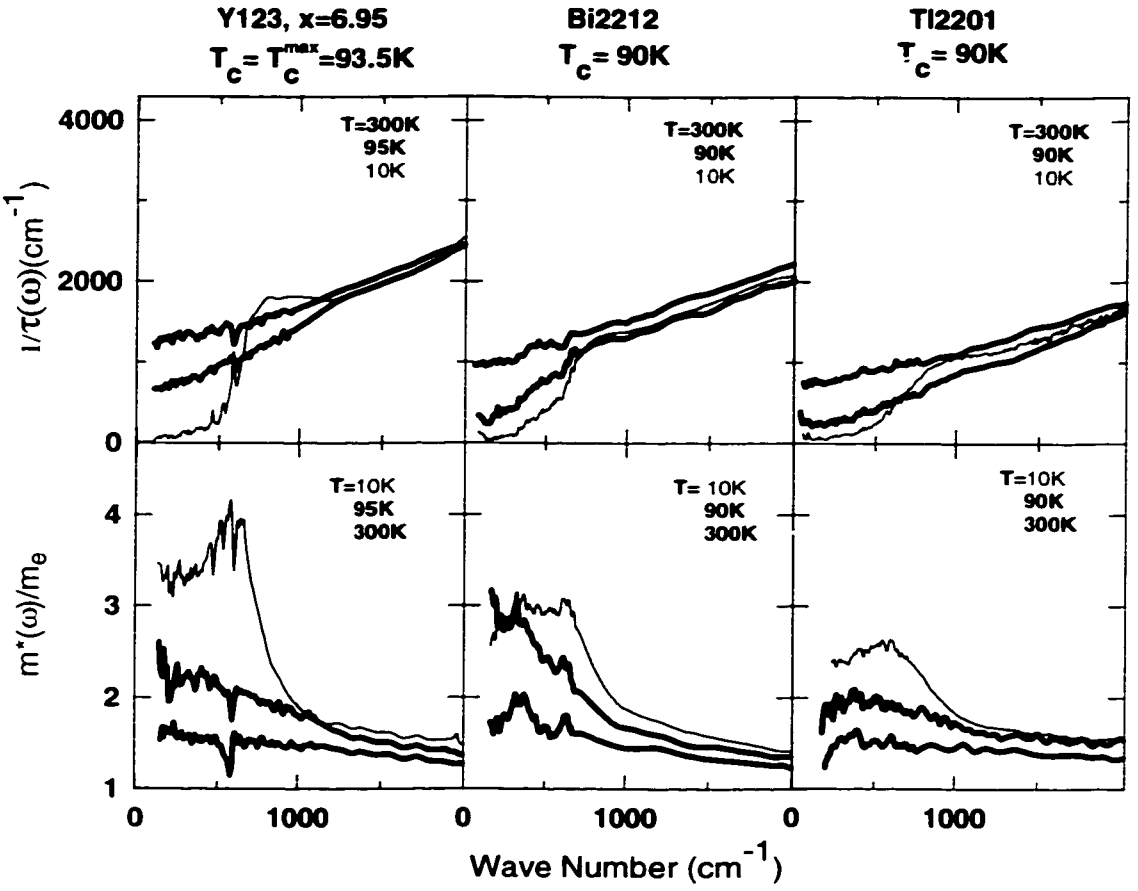

Figure 2.9: Scattering rate and effective mass for optimally doped cuprates. (After Puchkov *et al.*[Puchkov96d]) The scattering rate has a degree of temperature dependence at low frequencies. In the superconducting state the scattering rate is depressed at low frequencies.

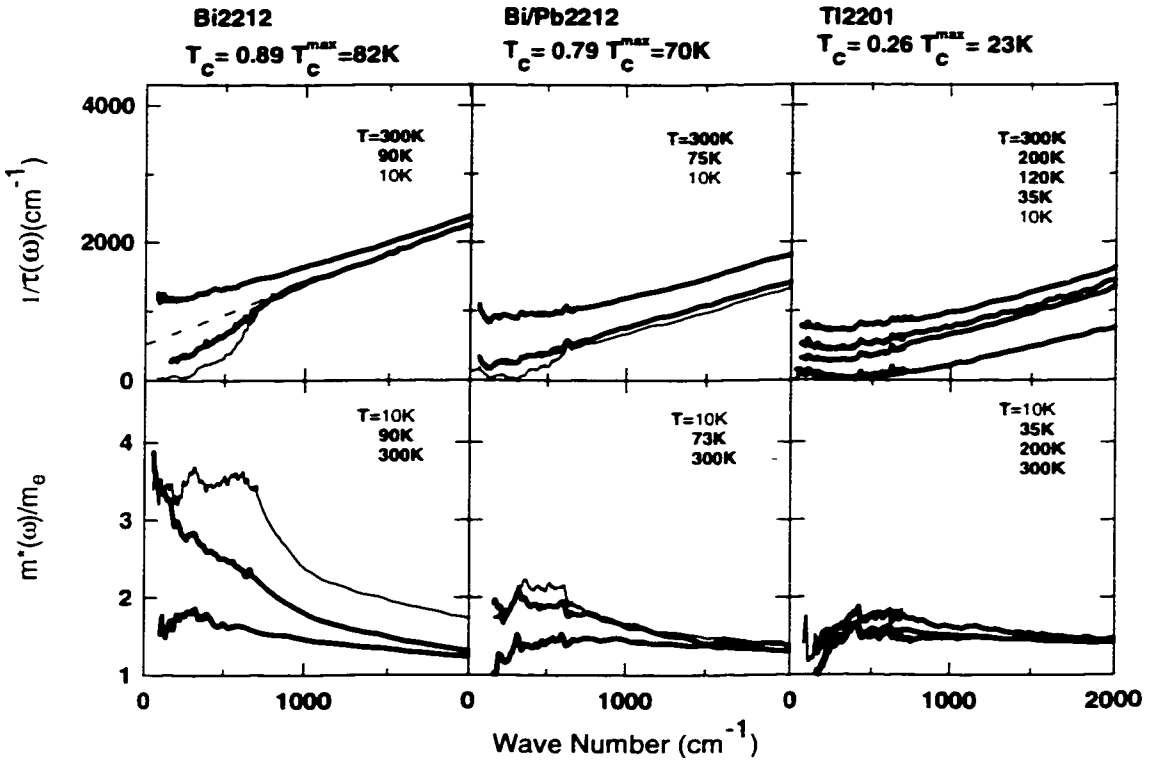

Figure 2.10: Scattering rate and effective mass for overdoped cuprates. (After Puchkov *et al.*[Puchkov96d]) In the overdoped samples the high-frequency scattering rate shows an increasingly strong temperature dependence. As part of the high-frequency scattering disappears at low temperatures, the low-frequency depression of $1/\tau(\omega)$ and the effective mass enhancement decrease in magnitude. This occurs even in the superconducting state.

Chapter 3

THE PSEUDOGAP STATE OF UNDERDOPED $La_{2-x}Sr_xCuO_4$

The presence of a pseudogap in the normal state of the underdoped high temperature superconductors is by now widely accepted.[Timusk98] The strongest evidence for the pseudogap state comes from recent measurements of angle resolved photoemission spectra [Marshall96a] as well as vacuum tunneling[Tao87, Renner98]. However, these techniques both demand extremely high surface quality and have therefore mainly been restricted to $Bi_2Sr_2CaCu_2O_{8+\delta}$ (Bi2212) and $YBa_2Cu_3O_{7-\delta}$ (Y123) materials, both with two CuO_2 layers per unit cell. Techniques that probe deeper into the sample such as dc transport[Bucher93, Ito93, Batlogg94], optical conductivity [Basov96, Puchkov96c, Puchkov96a] and NMR[Millis93] were not only the earliest to show evidence of the pseudogap, but have been extended to a much larger variety of materials, including several materials with one CuO_2 layer.[Batlogg94] In all cases evidence for a pseudogap has been reported.

The pseudogap in LSCO as seen by NMR and neutron scattering[Mason92] is rather weak and has led to the suggestion that the existence of the pseudogap in the spin excitation spectrum is only possible in bilayer compounds such as Y123 and $YBa_2Cu_4O_4$(Y124). In particular, Millis and Monien attribute the pseudogap (or the spin gap) to the strong antiferromagnetic correlations between the planes in the bilayer, which are responsible for a quantum order-disorder transition.[Millis93]

Apart from having only one CuO_2 layer, $La_{2-x}Sr_xCuO_4$ (LSCO) is also a good model system for the study of doping dependences since it can be doped by the addition of

strontium over a wide range: from the underdoped, where T_c increases with Sr content, to the optimally doped where T_c reaches its maximum value of ≈ 40 K at $x = 0.17$, and to the overdoped region where $T_c \rightarrow 0$ at $x = 0.34$.[Batlogg94]

The characteristic signatures of the pseudogap state in the dc resistivity[Bucher93] are seen clearly in LSCO[Batlogg94, Uchida91]. There are the striking deviations below a temperature T^* from the high temperature linear resistivity, resulting in a clear break in slope at T^*. It was found by B. Batlogg *et al.* [Batlogg94] that in LSCO T^* decreases from 800 K to approximately 300 K as the doping level is increased from the strongly underdoped to just over the optimal doped level. Similar behavior at $T = T^*$ has been observed in the Hall effect coefficient and the magnetic susceptibility.[Hwang94, Topygo96]

The pseudogap can also be observed if the conductivity is measured in the frequency domain, $\sigma(\omega)$, where it shows up as a striking depression in the frequency dependent scattering rate at low frequency. It is found that below a frequency $\Omega_p \approx 600$ cm^{-1}, the scattering rate drops below its high temperature, high frequency, linear behavior. This effect has been clearly identified in the bilayer materials.[Basov96, Puchkov96c, Puchkov96a] One of the aims of this paper is to see if this behavior can also be observed in LSCO. A pseudogap state can be defined in terms of this suppression of scattering: the material is in the pseudogap state when the scattering rate falls below the high frequency straight-line extrapolation. In the low frequency limit the scattering rate is proportional to the dc resistivity. Due to this, the $1/\tau(\omega,T)$ suppression should be compared to the suppression of $\rho_{DC}(T)$ [Batlogg94] at temperatures below the linear T dependent region. The IR measurement gives us the possibility to see both the frequency and the temperature dependence of this feature.

A pseudogap feature can also be observed in the *c-axis* IR *conductivity* in the form of a gap-like region of depressed conductivity at low frequency. It has been reported in

the $YBa_2Cu_3O_{7-x}$ (Y123) and $YBa_2Cu_4O_8$ (Y124) materials[Basov96, Homes93b] as well as in LSCO[Basov95a, Uchida96]. In slightly underdoped LSCO the pseudogap state in the *c*-axis direction is not as well defined as it is in the two plane materials.[Basov96] However, as the doping is reduced further, the *c*-axis pseudogap state features below 0.1 eV become clearer.[Uchida96]

Previous work on the in-plane $\sigma(\omega)$ of the single layer lanthanum strontium cuprate includes work on the oxygen doped $La_2CuO_{4-\delta}$ material[Quijada95], thin films of a LSCO[Gao93] as well as work done on LSCO single crystal at room temperature[Uchida91]. To our knowledge, a study of the temperature and doping dependence has not been done. We fill this gap here by performing optical measurements on high-quality LSCO single crystals at temperatures ranging from 10 K to 300 K at two different doping levels, both slightly underdoped. Also the optical properties of both the ab-plane and c-axis of $La_{1.87}Sr_{0.13}CuO_4$ were measured on the same crystal.

To better display the effect of increased coherence on $\sigma(\omega)_{ab}$ resulting from the formation of the pseudogap state we use the memory function, or extended Drude analysis. In this treatment the complex optical conductivity is modeled by a Drude spectrum with a frequency-dependent scattering rate and an effective electron mass.[Götze72, Allen71] While the optical conductivity tends to emphasize free particle behavior, a study of the frequency dependence of the effective scattering rate puts more weight on displaying the interactions of the free particles with the elementary excitations of the system.[Gold82] The temperature evolution of the frequency dependent scattering rate and effective mass spectra are of particular interest and are defined as follows:

$$1/\tau(\omega,T) = \frac{\omega_p^2}{4\pi} Re\left(\frac{1}{\sigma(\omega,T)}\right) \tag{3.1}$$

$$\frac{m^*(\omega,T)}{m_e} = \frac{1}{\omega}\frac{\omega_p^2}{4\pi} Im\left(\frac{1}{\sigma(\omega,T)}\right) \tag{3.2}$$

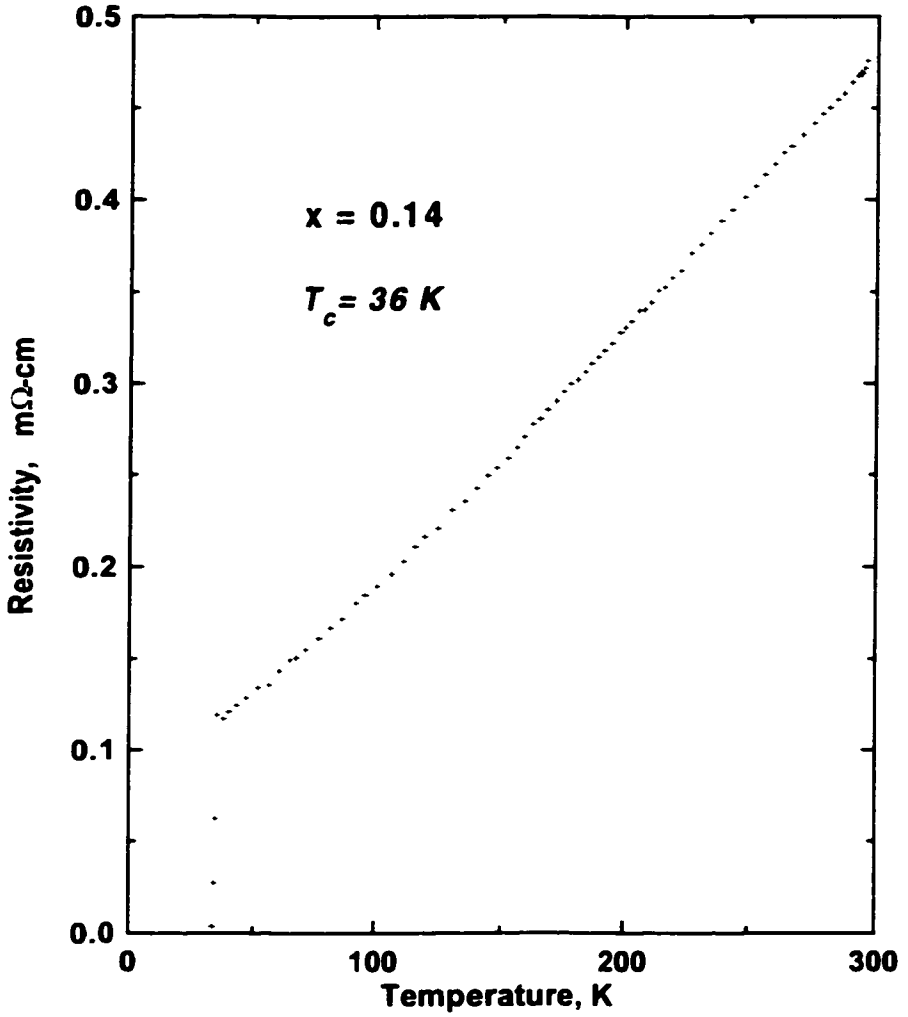

Figure 3.1: The temperature dependence of the in-plane resistivity of $La_{1.86}Sr_{0.14}CuO_4$ is shown with a sharp superconducting transition at 36 K.
The shape of the curve is consistent with T^* being greater than 300 K.

Here, $\sigma(\omega, T) = \sigma_1(\omega, T) + i\sigma_2(\omega, T)$ is the complex optical conductivity and ω_p is the plasma frequency of the charge carriers.

The single crystals of $La_{2-x}Sr_xCuO_4$, with approximate dimensions 5x3x3 mm^3, were grown by the traveling-solvent floating zone technique at Oak Ridge [Cheng91] in the case of $x = 0.14$ and in Tokyo [Kimura92] in the case of $x = 0.13$. The critical temperature was determined by both SQUID magnetization and resistivity measurements and was found to be 36 K for the nominal concentration of Sr $x = 0.14$ and 32 K for $x = 0.13$. Since the highest T_c in the LSCO system has been found to be 40 K for $x = 0.17$, we conclude that both crystals are underdoped.

The crystal with $x = 0.14$ was aligned using Laue diffraction and polished parallel to the CuO_2 planes. The crystal with $x = 0.13$ was polished in Tokyo to yield both ab-plane and ac-plane faces. Both surfaces were measured. Polarizers were used for the ac-face data to separate the contribution of CuO_2 planes from the c-axis optical response.

To get an uncontaminated ab-plane measurement it is important to have the sample surface accurately parallel to the *ab*-plane to avoid any c-axis contribution to the optical conductivity.[Orenstein88] The miscut angle between the polished surface normal and the c-axis was checked by a high precision triple axis x-ray diffractometer and was determined to be less than 0.8%.

All reflectivity measurements were performed with a Michelson interferometer using three different detectors which cover frequencies ranging from 10 to 10000 cm^{-1} (1.25 meV - 1.25 eV). The experimental uncertainty in the reflectance data does not exceed 1%. The dc resistivity measurements were carried out using a standard 4-probe technique.

The result of the resistivity measurement on the same $La_{1.86}Sr_{0.14}CuO_4$ single crystal used in the optical measurements is shown in Fig. 3.1. It is commonly accepted that the DC-resistivity is linear at high temperatures for LSCO and that the pseudogap begins to form near the temperature where the resistivity drops below this linear trend.[Batlogg94]

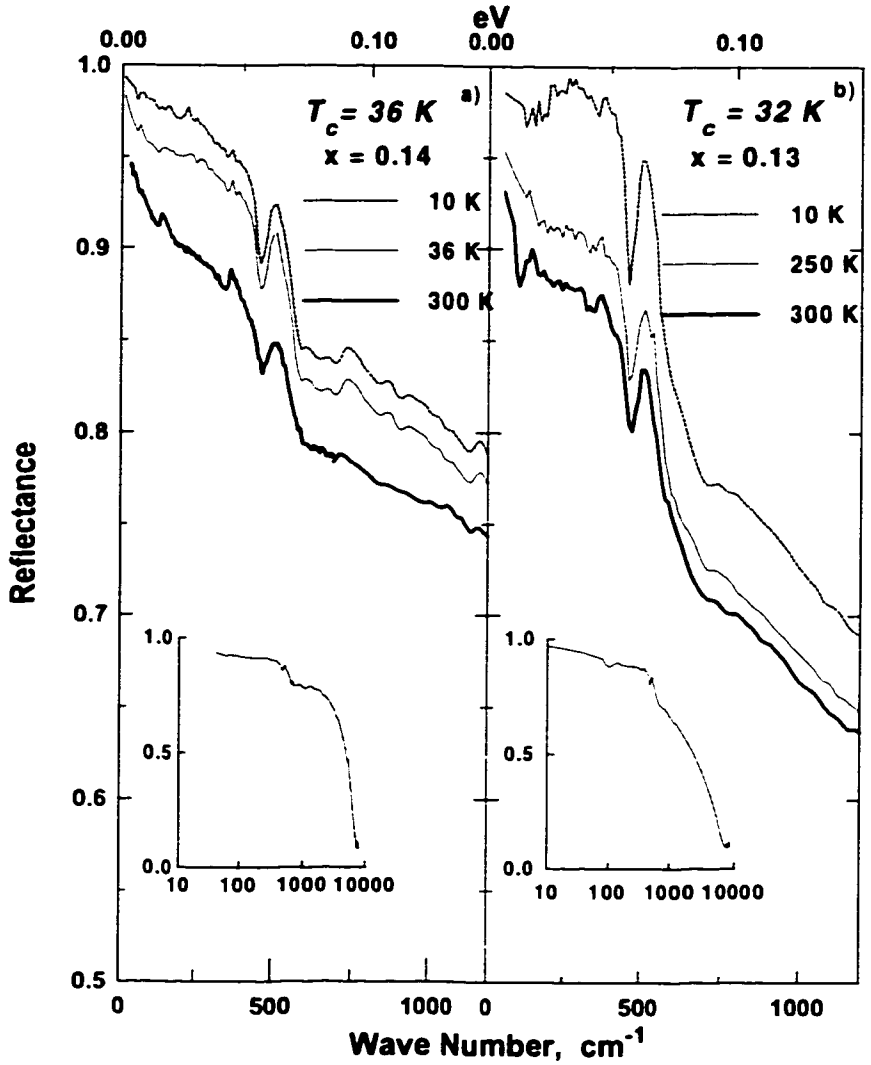

Figure 3.2: The reflectance of $La_{1.86}Sr_{0.14}CuO_4$ (a) and $La_{1.87}Sr_{0.13}CuO_4$ (b). The solid lines show the normal state spectra, while the dashed curve shows superconducting state spectrum. The thinest line shows the spectrum at the temperature closest to T_c. The insert in the left panel is a semi-log graph of the reflectance at 300 K which shows a plasma edge around 7000 cm^{-1}.

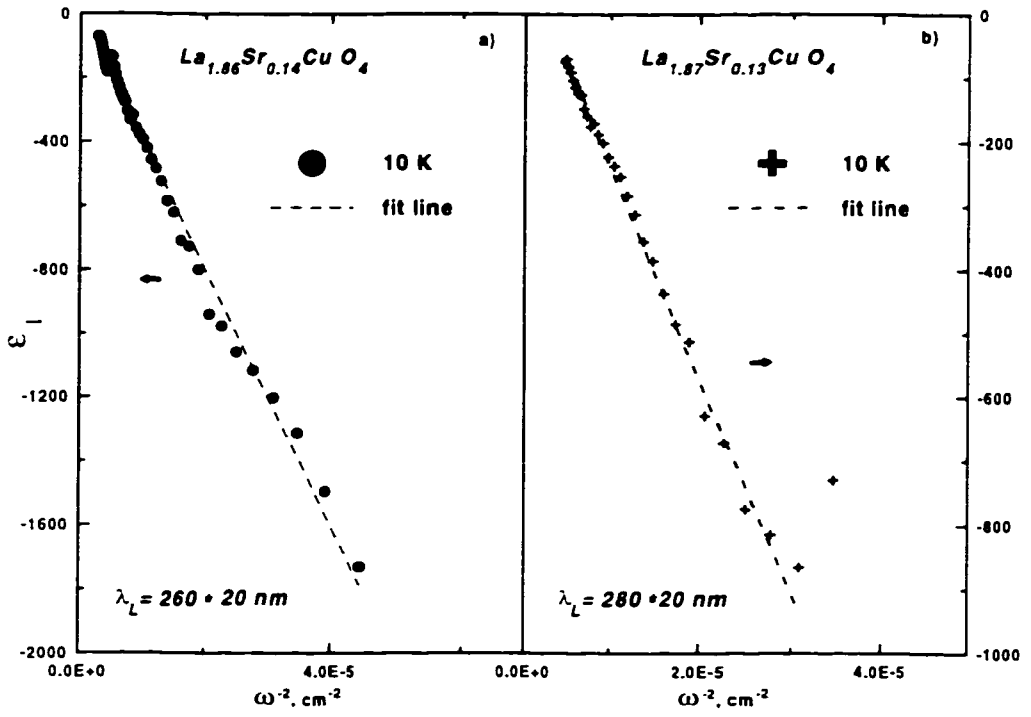

Figure 3.3: The real part of the dielectric function as a function of ω^{-2} for $La_{1.86}Sr_{0.14}CuO_4$ at 10 K is shown in panel a) and for $La_{1.87}Sr_{0.13}CuO_4$ at 25 K is shown in panel b).
The dashed line is linear fit. The slope of the fit gives the values of the London penetration depth.

At lower temperatures there is a region of superlinear temperature dependent resistivity. The T^* value for our samples with $x = 0.13$ and $x = 0.14$ extracted from the phase diagram of Batlogg *et al.*,[Batlogg94] are 650 K and 450 K, respectively. In agreement with this, the resistivity shows a superlinear temperature dependence below room temperature as expected in the pseudogap region.

In Fig. 3.2 we present the reflectivity data at temperatures above and below T_c for the two samples. For clarity, only three temperatures are shown: $T = 300$ K, an intermediate temperature above the superconducting transition and a low temperature (≈ 10 K) in the superconducting state. In the frequency region shown the reflectance is strongly temperature dependent for both materials, dropping by approximately 10% as the temperature is increased from the lowest temperature to $T = 300$ K. The plasma edge is observed at 7800 cm^{-1} (see insert of Fig. 3.2). The distinct peaks at approximately 135 and 365 cm^{-1} in the LSCO reflectivity spectra correspond to the excitation of ab-plane TO phonons and the peak at 500 cm^{-1} corresponds to a LO phonon.[Tajima90] As in all other HTSC materials, the ab plane has a coherent response with very high reflectance. Note, that the reflectance of the samples with $x = 0.13$ is lower than those with $x = 0.14$ for frequencies above 500 cm^{-1}. This will manifest itself in the form of a lower overall conductivity. The low values of both the reflectance and conductivity in LSCO($x = 0.13$) can be explained by a possible oxygen deficiency. Thus, it is plausible that these samples are even more underdoped than expected.

The complex optical conductivity, $\sigma(\omega)$, was obtained by Kramers-Kronig analysis of the reflectivity data. Since, in principle, this analysis requires knowledge of the reflectance at all frequencies, reflectivity extensions must be used at high and low frequencies. The Hagen-Rubens formula was used for the low frequency reflectivity extrapolation, with parameters taken from the dc resistivity measurements on the same sample with $x = 0.14$ shown in Fig. 3.1 and the results of H. Takagi *et al.*[Takagi92] for the sample with

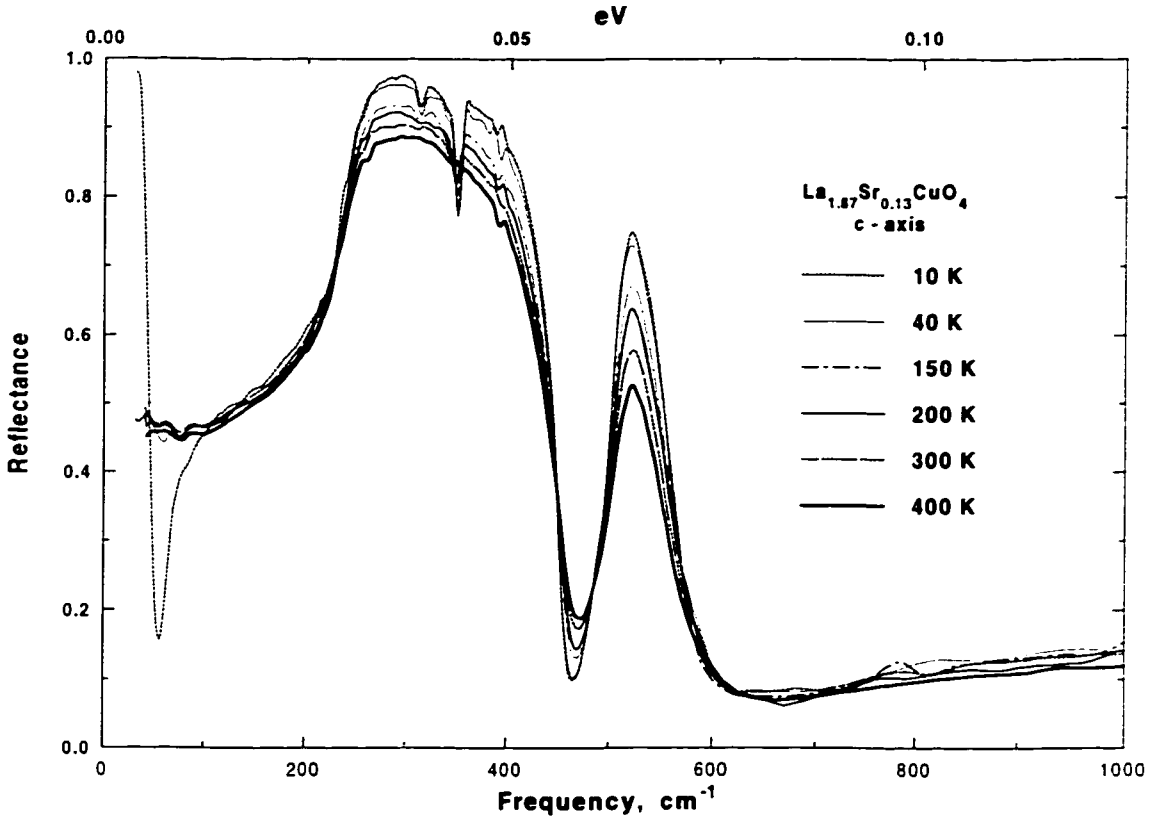

Figure 3.4: The reflectance of $La_{1.87}Sr_{0.13}CuO_4$ with $E \parallel c$ axis. The temperature sequences are 10 K, 40 K, 150 K, 200 K, 300 K and 400 K.

$x = 0.13$. For the high-frequency extension for $\omega > 8000$ cm^{-1} we used the reflectivity results of Uchida *et al.*[Uchida91] At frequencies higher than 40 eV the reflectivity was assumed to fall as $1/\omega^4$.

We calculate the plasma frequency of the superconducting charge carriers and the London penetration depth using the following formula:[Timusk89]

$$\epsilon_1 = 1 - \frac{\omega_{ps}^2}{\omega^2}. \tag{3.3}$$

The slope of the low-frequency dielectric function, $\epsilon_1(\omega)$, plotted as a function of ω^{-2} in Fig. 3.3a,b gives plasma frequencies of 6100 cm^{-1} and 5700 cm^{-1} in the superconducting state. The corresponding London penetration depths are $\lambda_L = 1/2\pi\omega_{ps} = 250$ nm and 280 nm for $La_{1.86}Sr_{0.14}CuO_4$ and $La_{1.87}Sr_{0.13}CuO_4$, respectively. These values are in good agreement with those obtained previously by Gao *et al.* in films[Gao93] ($\lambda_L = 275 \pm 5$ *nm*) and by muon-spin-relaxation[Aeppli87] ($\lambda_L = 250$ *nm*).

The c-axis reflectance of the $x = 0.13$ sample is shown in Fig. 3.4. The corresponding conductivity is low and is dominated by optical phonons (Fig. 3.5).

In YBCO 123 and 124 the pseudogap along the c-axis manifests itself as a depression in the conductivity at low frequencies.[Homes93b, Basov96, Homes95] There is no coherent Drude peak and the conductivity is flat and frequency independent. In the temperature and doping range where a pseudogap is expected a low frequency depression of the conductivity is seen with an edge in the 300-400 cm^{-1} region where the conductivity rises to the high frequency plateau.

In order to isolate the electronic features of our LSCO c-axis spectrum we magnify the low value region of σ_{1c} (Fig. 3.5). There is no sharp pseudogap edge in the low-frequency infrared data for underdoped LSCO as there is in the case of Y123. It is possible that such a feature could be hidden under the large phonon structure. Efforts to subtract the phonons in order to extract the background conductivity were found to be extremely

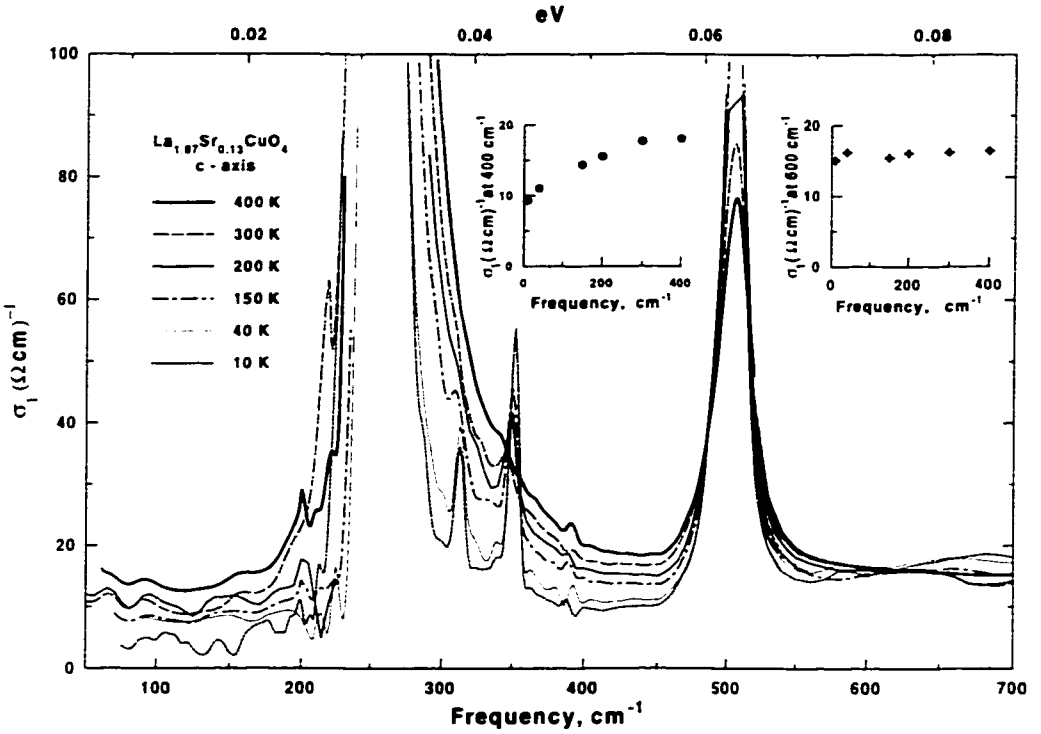

Figure 3.5: The c-axis conductivity of $La_{1.87}Sr_{0.13}CuO_4$ is shown at various temperatures. Since the phonon peaks are dominant in the direction perpendicular to CuO_2 planes, the graph is focused at the background conductivity. The two inserts are the c-axis conductivity of the underdoped $La_{1.87}Sr_{0.13}CuO_4$ measured at 450 cm^{-1} and at 600 cm^{-1}. The c-axis conductivity at 450 cm^{-1} is depressed below 300 K, however, it is almost constant above 600 cm^{-1}. This could be a signature of the pseudogap formation with the size of 500 cm^{-1} for temperatures less than 300 K.

sensitive to the choice of their shape in fitting procedures. Nonetheless, the raw data clearly shows that there is a low frequency depression of the c-axis conductivity. Conductivity at 450 cm^{-1} is uniformly suppressed below T=300 K (Fig. 3.5insert), whereas the conductivity at 600 cm^{-1} is nearly constant at all temperatures. Based on this analysis one can conclude that the pseudogap state in the c-axis opens up below 300 K and its size is approximately equal to 500 cm^{-1}.

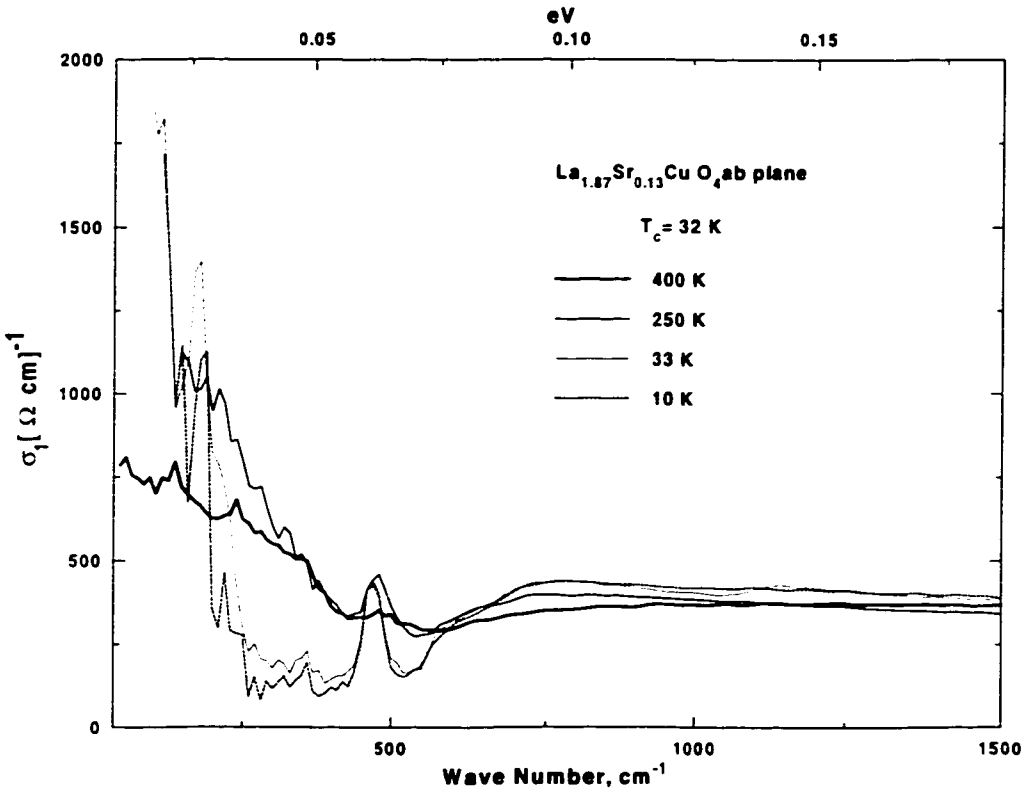

Figure 3.6: The ab-plane conductivity of $La_{1.87}Sr_{0.13}CuO_4$ is shown at different temperatures.

Manifestations of the pseudogap in the *ab*-plane conductivity exist as a loss of spectral

weight between 700 and 200 cm^{-1} balanced by increases both below and above this frequency. In both Fig. 3.6 and Fig. 3.7 one can see the temperature evolution of the sharp depression in ab-conductivity below 700 cm^{-1} at temperatures above T_c. A much clearer picture of the pseudogap state can be seen from the effective scattering rate, $1/\tau(\omega,T)$, calculated from the conductivity using equation (1) which is shown along with the effective mass in Fig. 3.8 and Fig. 3.9. The $1/\tau(\omega,T)$ spectra can conveniently be divided into two regions. In the high frequency region, starting at about 700 cm^{-1}, the scattering rate varies linearly with frequency while in the low frequency region there is a clear suppression of $1/\tau(\omega,T)$ below this linear trend.[Puchkov96d] The temperature where this suppression first appears serves as a definition of T^*, the onset temperature of the pseudogap state. As the temperature is lowered below T^* this suppression becomes deeper. We find that for underdoped $La_{2-x}Sr_xCuO_4$ $T^* \geq 400$ K, an order of magnitude higher than the superconducting transition temperature T_c (32 K). This is significantly different from previous results on cuprates where T^* more or less coincides with T_c near optimal doping.

The temperature dependence above 700 cm^{-1} is strongly influenced by the level of Sr doping. In the underdoped sample the high frequency scattering rate is nearly temperature independent up to a certain temperature (Fig. 3.8a and Fig. 3.9a), which we will call T^{**} above which a pronounced temperature dependence of $1/\tau(\omega,T)$ is seen (Fig. 3.8b and Fig. 3.9b). In the $x = 0.13$ sample $T^{**} \approx 200$ K while in the $x = 0.14$ sample $T^{**} \approx 150$ K. It is iteresting to note that these values are in a good agreement with the crossover temperature found in NMR expriment by Yasuoka *et al.*[Yasuoka9] defined as the temperature where $1/T_1T$ has a maximum and equal to 175 K and 140 K for $x = 0.13$ and $x = 0.14$, respectively. We find that in the overdoped samples the scattering rate above 700 cm^{-1} increases uniformly with temperature[Startseva98b] at all temperatures suggesting $T^{**} \rightarrow 0$ in that limit. This behavior is also seen in other

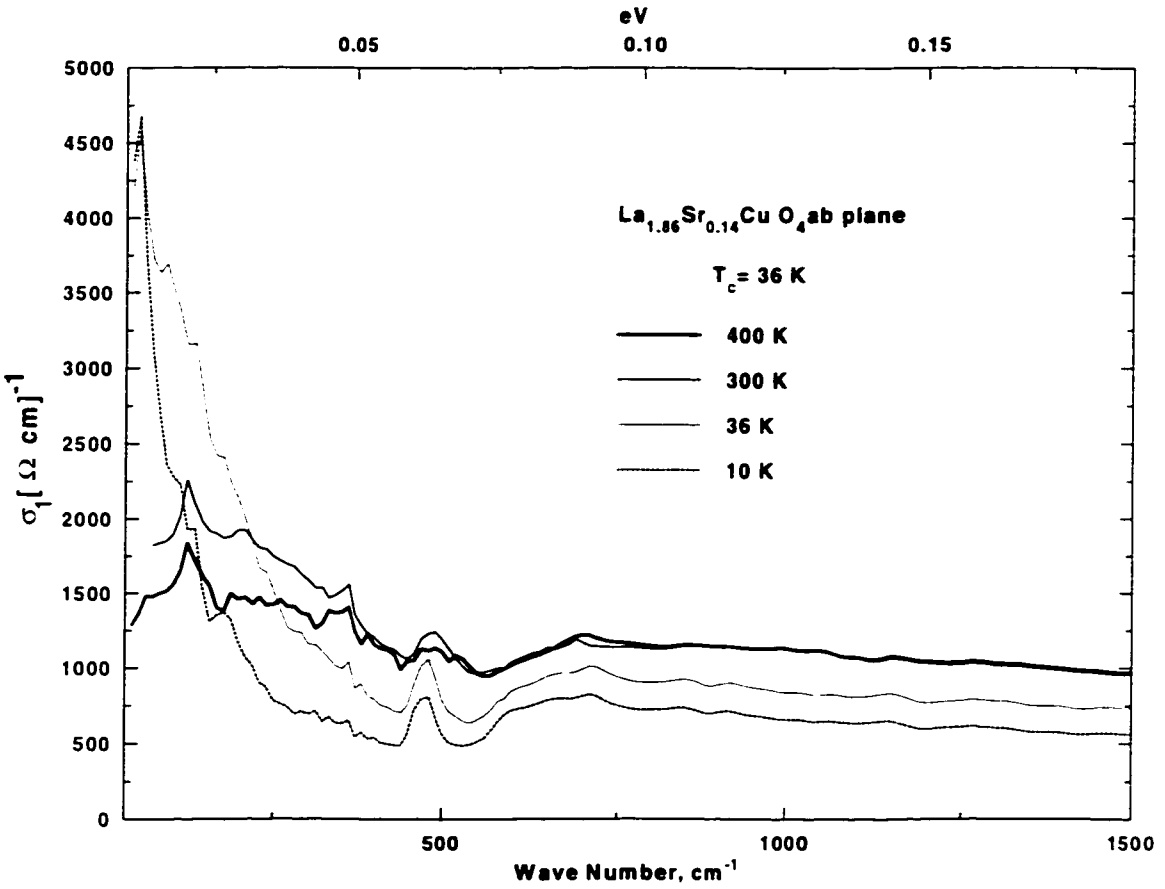

Figure 3.7: The ab-plane conductivity of $La_{1.86}Sr_{0.14}CuO_4$ is shown at various temperatures.

overdoped HTSC.[Puchkov96d] The physical meaning of the T^{**} is not clear at this time. We note however that the state above T^{**} has the properties of the marginal Fermi liquid where there is linear temperature and frequency dependence of the quasiparticle self energy leading to linear resistivity and frequency dependence of the scattering rate.[]

If one extrapolates the 300 K scattering rates to zero frequency one finds, that for the $x = 0.13$ sample, a scattering rate of $1/\tau_0 \approx 2500$ cm^{-1} and for the $x = 0.13$ sample this rate is $\approx$ 1500 cm^{-1}. These scattering rates are much higher than what is seen for the higher T_c materials reviewed by Puchkov *et al.*[Puchkov96d] where at 300 K $1/\tau_0 \approx 1000 \pm 200$ cm^{-1} for several families and many doping levels. This high residual scattering differentiates the LSCO material from the other cuprates.

If we call the frequency below which the scattering rate is suppressed the *ab*-plane pseudogap $\omega_{ab} \approx 700$ cm^{-1} we find that it is clearly bigger than the c-axis pseudogap frequency $\omega_c \approx 500$ cm^{-1}.

In addition to the pseudogap depth and the temperature dependence, several other features seen in Figures 9 and 10 should be mentioned. The position of the pseudogap remains at 700 cm^{-1} for all temperatures. There are also several peaks positioned at 500 cm^{-1} in the scattering rate which complicate the analysis, particularly in the case of the sample with $x = 0.14$. These peaks have been observed by other groups and have been attributed to polaronic effects.[Yagil94, 1] Another possible explanation is the correlation of the ab-plane conductivity with c-axis LO phonons. We did observe a difference in the contribution of LO phonons to the ab plane reflectance with different propagation directions, an effect first observed by Reedyk *et al.*,[Reedyk92] and also seen in the $k \parallel c$ vs. $k \perp c$ spectra obtained by Tanner's group.[Quijada95] In Fig. 3.10 the reflectance with $E \parallel a$ and $k \parallel c$, is compared with the reflectance with $E \parallel ab$ and $k \parallel a$, for the $La_{1.87}Sr_{0.13}CuO_4$ sample at room temperature. There is an extra feature observed at 500 cm^{-1} in the spectra with $k \parallel c$. Further evidence that the c-axis LO phonons

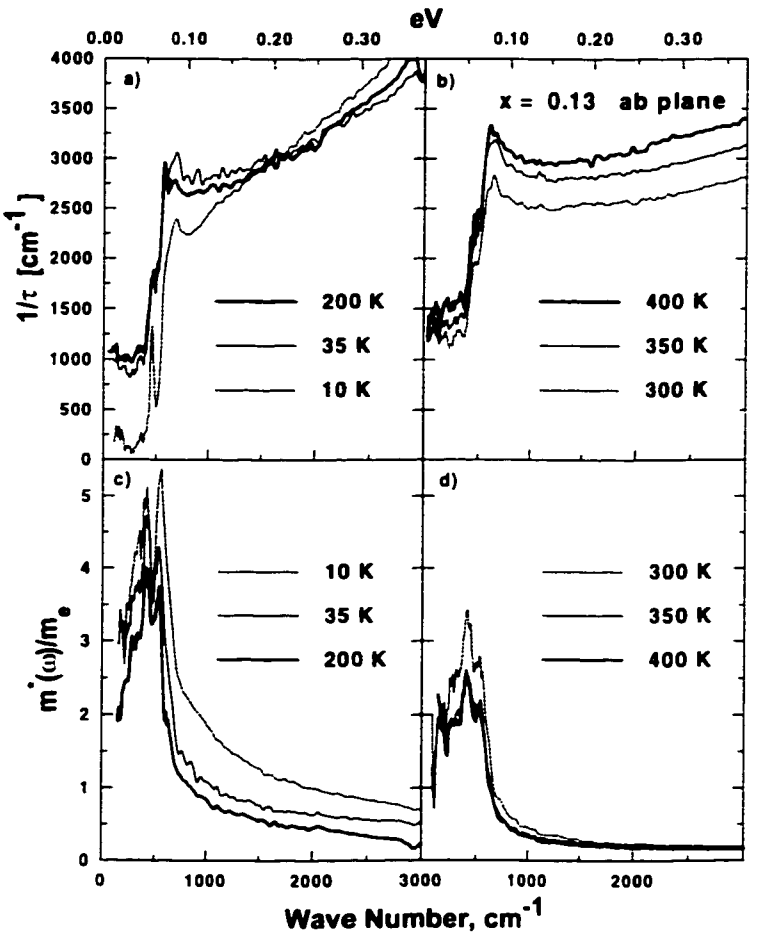

Figure 3.8: The frequency dependent effective scattering rate and the effective mass of $La_{1.87}Sr_{0.13}CuO_4$.
Top panel: the low temperature frequency dependent scattering rate of $La_{1.87}Sr_{0.13}CuO_4$ below T**(a) and above T**(b) is calculated using Equation (1). The onset of the suppression in the conductivity corresponds to a drastic change in the frequency dependence of the scattering rate below T*. Above 700 cm^{-1} the scattering rate is nearly temperature independent and has a linear frequency dependence below T**. Below 700 cm^{-1} the scattering rate varies as $\omega^{1+\delta}$ and shows a strong temperature dependence. Bottom panel: The effective mass of $La_{1.87}Sr_{0.13}CuO_4$ below T**(a) and above T**(b) is calculated using Equation (2). The onset of the enhancement of $\frac{m^*(\omega)}{m_e}$ corresponds to the onset of the suppression in the scattering rate.

couples to ab plane features can be seen in Fig. 3.11. A comparison between the peaks in the effective scattering rate at 450 cm^{-1} and 580 cm^{-1} to the peaks in Im(- $1/\epsilon_c$) shows the same strong correlation seen in many other cuprates.[Reedyk92]

For completeness we also plot the effective mass of the underdoped samples at low temperatures(Fig. 3.8c) and high temperatures(Fig. 3.9c,d). As expected, $\frac{m^*(\omega)}{m_e}$ rises to a maximum of ≈ 3 forming a peak at ≈ 400 cm^{-1}. This enhancement of the effective mass in the pseudogap state as well as the upper limit of $\frac{m^*(\omega)}{m_e}$ are similar to what has been previously reported for Y123, Y124 and Bi2212.[Puchkov96d]

Before closing this chapter we compare our results with the data of Gao *et al.*[Gao93] on $La_{2-x}Sr_xCuO_{4+\delta}$ films and Quijada *et al.*[Quijada95] on oxygen doped $La_2CuO_{4+\delta}$. Our results in the underdoped case are comparable with those of the oxygen doped material, although Quijada *et al.* did not carry out a frequency dependent scattering rate analysis for their underdoped sample. The film results of Gao *et al.* are quite different from our findings. The films used in that study had a strontium level that would correspond to optimal doping in crystals. However, the $1/\tau(\omega)$ curves deviate markedly from what we observe for slightly under and overdoped samples. The authors performed an extended Drude analysis and found a strongly temperature dependent scattering rate even at low temperatures. This is in sharp contrast to our results which would suggest a very weak temperature dependence in this temperature region. Based on our work, their samples should be in the pseudogap state since they have an x value near optimal doping. Comparing these results with other systems, in particular with Tl2202, two factors suggest the possibility that the films may be overdoped. First, their T_c was near 30 K, lower than that expected for optimal doping. Secondly, it is known that the oxygen level in films can vary substantially and in LSCO oxygen can have a major influence on the doping level[ZhangH94]. On the other hand, we cannot completely rule out the possibility that all the crystal results are affected by the polishing process, and

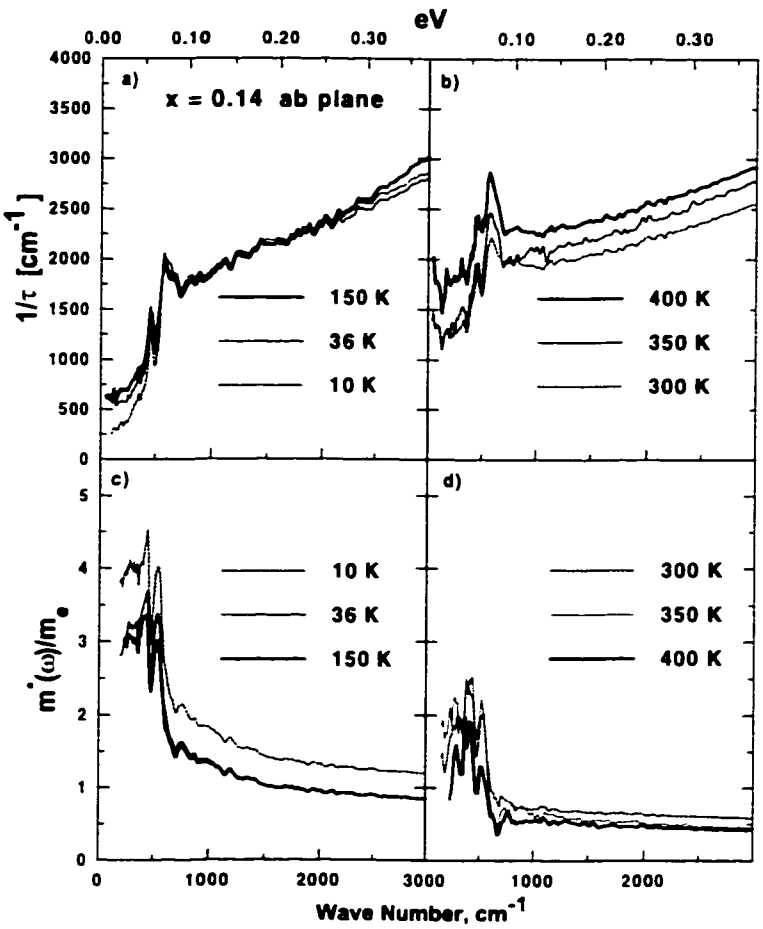

Figure 3.9: The frequency dependent effective scattering rate and the effective mass of $La_{1.86}Sr_{0.14}CuO_4$.
Top panel: the high temperature effective scattering rate of $La_{1.86}Sr_{0.14}CuO_4$ below T** (a) and above T** (b) is calculated using Equation (1). Above 700 cm^{-1} the scattering rate has a linear frequency dependence and is temperature independent below T** (a) and temperature dependent above T**(b). Below 700 cm^{-1} the scattering rate varies as $\omega^{1+\delta}$ and shows a strong temperature dependence. Bottom panel: The effective mass of $La_{1.87}Sr_{0.13}CuO_4$ below T**(a) and above T**(b) is calculated using Equation (2).

that the films better represent the bulk material. It is clearly important to measure films where the oxygen content is controlled by selective annealing.

In conclusion, the optical data in the far-infrared region, taken on two underdoped *single-layered* high-T_c superconductors, shows clear evidence of *a pseudogap state* in both the scattering rate and the conductivity along CuO_2 planes. This pseudogap state extends to higher temperatures than that observed in the multi-layered underdoped cuprates such as YBCO and BSCO.

The scattering rate is similar for both systems in the pseudogap state. At low frequencies, $\omega \leq 700$ cm^{-1}, the scattering rates are *temperature* dependent and change with frequency in a *non-linear* fashion. Above 700 cm^{-1} this behavior becomes *linear*. Within experimental uncertainty the observed high frequency scattering rate of the underdoped sample is *not affected by temperature* up to certain temperature T**. This temperature is equal to 200 K in case of $La_{1.87}Sr_{0.13}CuO_4$ and 150 K in case of $La_{1.86}Sr_{0.14}CuO_4$. Above T** the high frequency scattering rate is temperature dependent. This behavior is identical to the high-frequency effective scattering rate of an overdoped HTSC.[Puchkov96d]

Our findings in the direction perpendicular to the CuO_2 planes showed that the depression of the c-axis conductivity is not as prominent as the one found in the two-layer HTSC. Nevertheless, the signature of the pseudogap can be seen at frequencies below 500 cm^{-1} up to room temperature.

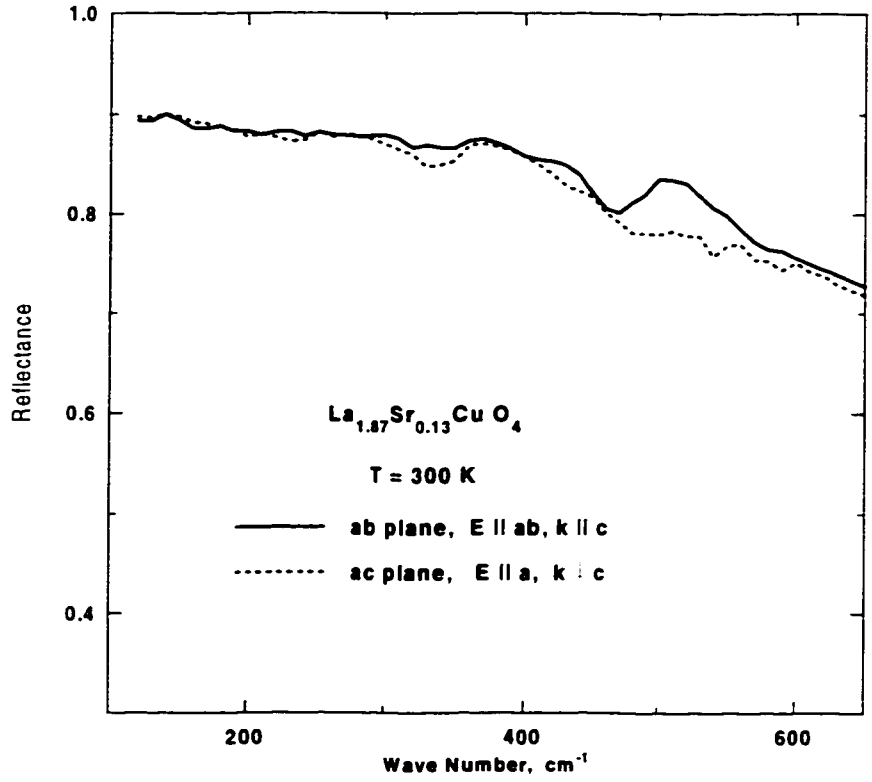

Figure 3.10: Comparison of the reflectance of $La_{1.87}Sr_{0.13}CuO_4$ measured from ab plane with $k \parallel c$ and from ac plane with $k \perp c$.

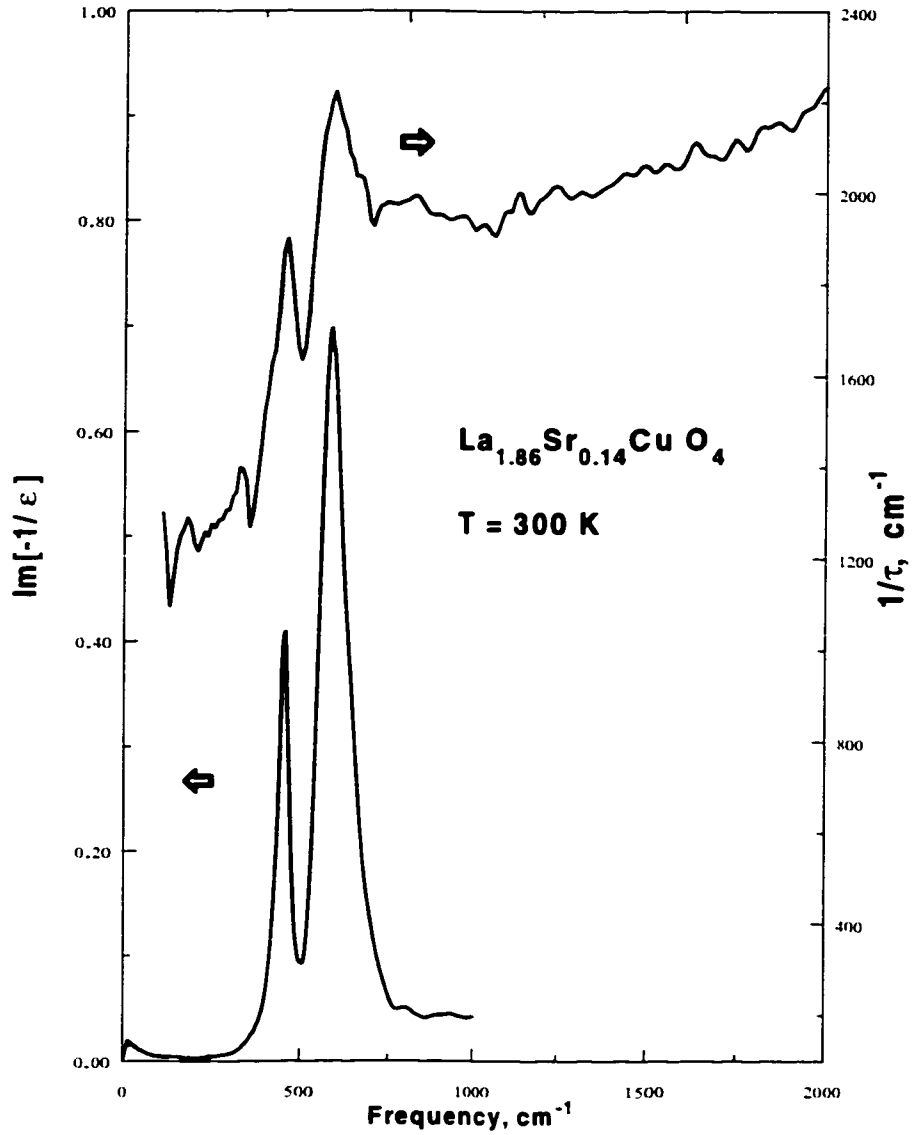

Figure 3.11: Comparison of the position of the peak at 450 and 580 cm^{-1} in the dielectric loss function of the c-axis phonons with the room temperature effective scattering rate of $La_{1.86}Sr_{0.14}CuO_4$.
The correspondence of the peaks positions, width and the relative strength suggests that the nature of the peak may lie in the coupling of a ab-plane spectra to the c-axis longitudinal optical phonons.

Chapter 4

THE PSEUDOGAP STATE OF OVERDOPED $La_{2-x}Sr_xCuO_4$

The pseudogap phenomenon in high temperature superconductors has been well established with a number of experimental techniques. Probes such as NMR,[Warren89, Timusk98] angle resolved photoemission (ARPES),[Marshall96b] tunneling, [Tao87, Renner98], electronic specific heat,[Loram94] IR spectroscopy,[Timusk98, Homes93b, Puchkov96d, Homes95] and a number of transport measurements[Ito93, Batlogg94] all show evidence of a partial gap or a pseudogap in the normal state. This gap forms below a temperature T^*, which is well above the superconducting transition temperature T_c. ARPES reveals that the pseudogap has a $d_{x^2-y^2}$ symmetry with the gap going to zero in the $\mathbf{k_x} = \mathbf{k_y}$ direction with a maxima at the zone boundary in the $\mathbf{k_x} = \mathbf{k_y} = \mathbf{0}$ direction. Transport experiments such as the DC and infrared conductivity show that the pseudogap forms in the spectrum of low-energy electronic excitations that scatter the charge carriers. As the pseudogap forms, the scattering rate, $1/\tau(\omega, T)$, is reduced for both the temperature and spectral regions where the gap occurs. Furthermore, infrared spectroscopy shows that a depression in the scattering develops below ≈ 700 cm^{-1}. Above this frequency, there is no temperature dependent scattering. All experiments point to a depressed density of states below an energy $\Delta \approx 40meV$ and a temperature T^*. Both parameters decrease as the doping level increases.

A number of theoretical interpretations of the pseudogap have been advanced and a number of these have incorporated the idea that there should be a crossing of the two temperature scales that vary with doping: the rising scale of T_c and the decreasing scale

of T^*.[Lee97, Emery95b, Chubukov97] It is predicted that the two temperature scales are equal at optimal doping. Indeed, in most of the families of cuprates this is approximately what is observed. In particular, optimally doped $YBa_2Cu_3O_{6.95}$(Y123) shows no sign of a pseudogap for temperatures 10 K above T_c. In $Bi_2Sr_2CaCu_2O_{8+\delta}$(Bi2212), however, there is evidence that the pseudogap extends slightly into the overdoped state[Puchkov96d]. Batlogg *et al.*[Batlogg94] performed an extensive study of $La_xSr_{2-x}CuO_{4+\delta}$'s (LSCO) transport properties. From the studies of the resistivity, the Hall coefficient and the susceptibility, they found that the pseudogap temperature, T^*, is significantly higher than T_c all the way up to the nominal Sr concentration of x =0.34. Overdoped LSCO, the subject of this chapter, forms the extreme exception to the simple picture of the crossing of the two temperature scales at optimal doping. While the superconducting critical temperature of LSCO is quite low compared to the other cuprates, the onset temperature of the pseudogap, T^*, is unusually high. For example, overdoped LSCO with x = 0.22 has $T^* \sim 5T_c$.[Batlogg94]

There are other important differences between the pseudogap's behavior in LSCO and those superconductors with maximum T_c of 90 K. Both NMR[Millis93] and neutron scattering results[Mason92] suggest that the pseudogap in LSCO is very weak. The suppression of the spin susceptibility is different in the two HTSC families. The temperature dependence of the spin susceptibility suggests that a pseudogap may be present in the underdoped lanthanum compound, but the copper spin–lattice relaxation rate shows no sign of a pseudogap for any strontium concentration between $0.075 \leq x \leq 0.15$.[Ohsugi91] The sharp depression in the c-axis conductivity, characteristic of Y123's pseudogap,[Homes93b] is also absent in recent infrared (IR) spectroscopy experiments on LSCO[Basov95a, Uchida96, Startseva98a]. Instead a weaker drop in the c-axis conductivity, is observed. However, the energy scale of the pseudogap in the ab-plane

and along *c*-axis in LSCO is remarkably similar to the superconductors with a maximum T_c of 90 K. The size of the pseudogap in the *ab*-plane is approximately equal to 700 cm^{-1}.[Puchkov96d]

The most striking property of the LSCO system is the very high scale of T^* in both the optimally and overdoped states. Thus, it is advantageous to find the spectroscopic evidence responsible for such a large energy scale. The goal of this chapter is to investigate the *ab*-plane scattering rate in two different overdoped samples of LSCO.

The crystals used in this work were grown using the traveling-solvent floating zone technique.[Kimura92] The critical temperature for LSCO with x = 0.184 and x = 0.22 was determined by SQUID magnetization measurements and were found to be 32 K and 30 K, respectively. The sample's surface was oriented using Laue X-ray diffraction and was polished parallel to the direction of CuO_2-planes. The possible miscut between the *ab*-plane and the sample's surface is $\leq 2°$.

All reflectivity measurements were performed with a Michelson interferometer using three different detectors which cover frequencies ranging from 10 to 10000 cm^{-1}. After the sample's reflectance was measured a thin layer of gold was evaporated onto it to account for surface irregularities. The sample's absolute reflectance was then obtained by comparing its reflectance to the same sample coated with gold.[Lynch91] The experimental uncertainty in the reflectance data does not exceed 1%. In the case of LSCO ($x = 0.184$), the *c*-axis contribution to the reflectance due to any miscut errors was eliminated by placing a polarizer normal to the plane of incidence. The angle between the *c*-axis and the polarizer axis is less than 1°.

The reflectance of LSCO with a nominal concentration of strontium equal to 0.184 was measured with the light polarized along either the *a*- or *b*- directions (see Fig. 4.1). The reflectance of $La_{1.78}Sr_{0.22}CuO_4$ was measured without polarizers along the CuO_2-planes. As a result, strong phonon features can be observed at $\approx$ 250 and 500 cm^{-1}.

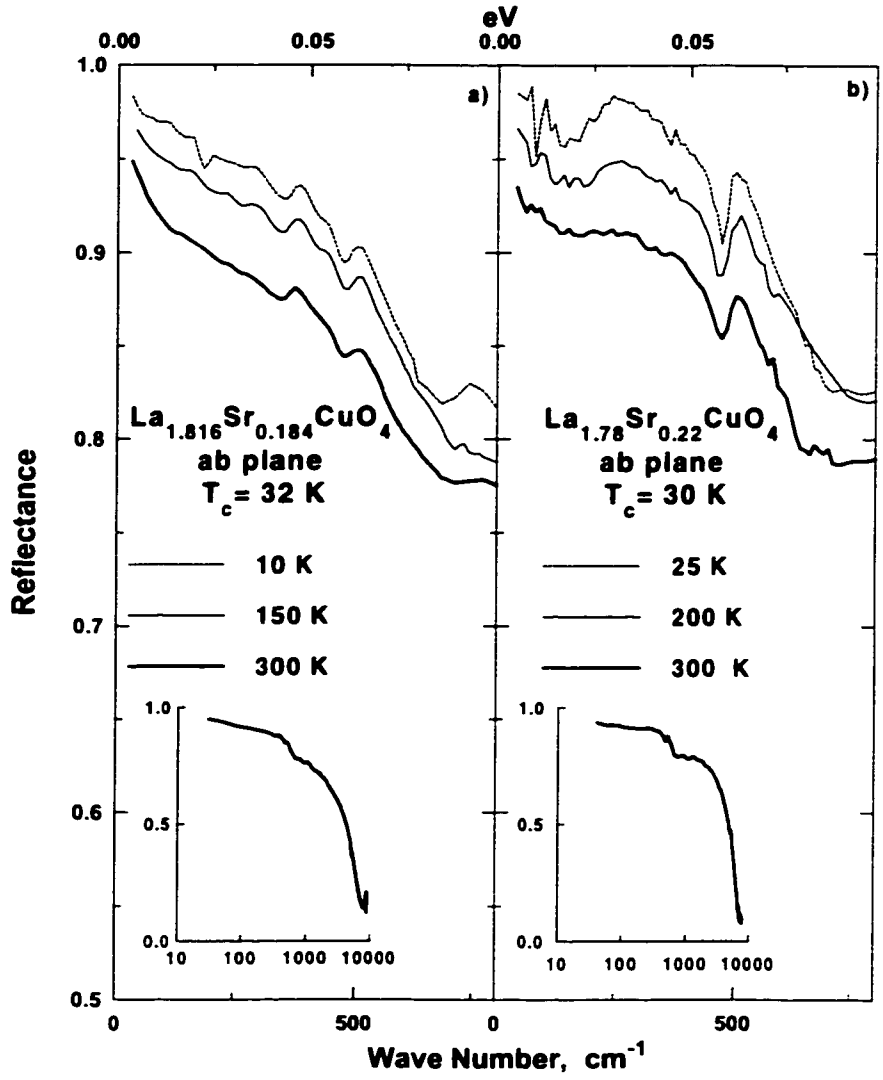

Figure 4.1: The temperature dependence of the reflectance of $La_{1.816}Sr_{0.184}CuO_4$ (a) and $La_{1.78}Sr_{0.22}CuO_4$ (b).
The former has the light polarized along the *a*- or *b*- axis while the latter has the light polarized in the *ab*-plane. At low frequencies the reflectance approaches unity thereby indicating a metallic-like behavior. In the case of $La_{1.78}Sr_{0.22}CuO_4$ (b) the peaks at $\approx$250 and 500 cm^{-1} indicate a coupling to the c-axis longitudinal phonons. The inserts show the normal state reflectance up to 9000 cm^{-1}.

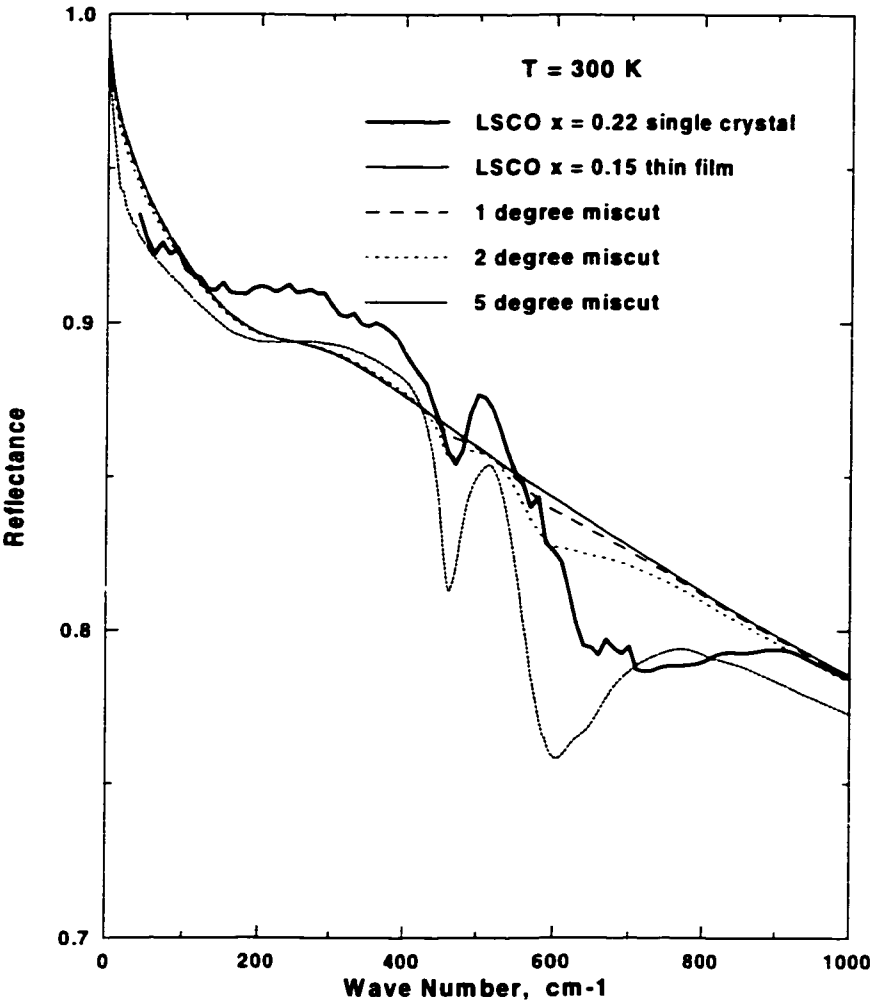

Figure 4.2: The comparison of the reflectance of $La_{1.78}Sr_{0.22}CuO_4$ with the reflectance calculated from the data taken on a LSCO thin film by Quijada *et al.*
The dashed curves are calculations showing the film reflectance when 1 °, 2 ° and 5 ° miscuts are added. Note that a 5 ° miscut is sufficient to show a significant contribution to the *c*-axis reflectance.

There are several possible explanations for this phenomenon that involve a coupling between the *ab*-plane properties and the longitudinal (LO) phonons polarized along the *c*-axis. One is in terms of surface miscut, where a 5° difference between the surface of the sample and the direction of CuO_2-planes would be sufficient to make c-axis LO phonons visible in the *ab*-plane reflectance. Figure 4.2 shows the room temperature reflectance of LSCO(x=0.22) in comparison to the reflectance obtained from a LSCO thin film[Gao93], displaying no evidence of phonons. Also shown is a calculation of the film's reflectance when a hypothetical miscut of 1°, 2° and 5° is added. From Figure 4.2 one can see that while the broad feature at 300 cm^{-1} is stronger in the experimental data, the peak at 500 cm^{-1} in our crystal is weaker than what the 5° miscut model predicts. The elimination of the *c*-axis phonons was the main reason for using polarized light in the case of LSCO(x=0.184). However, the introduction of a polarizer significantly reduces the amount of signal detected which, in turn, increases the noise level. This is especially true for small samples. The other possible mechanism is a direct, microscopic, coupling between the *ab*-plane conductivity and *c*-axis LO phonons. Such an effect was first observed by Reedyk *et al.*[Reedyk92] The difference in the contribution of LO phonons to the *ab*-plane reflectance with different propagation directions has also been seen in the $\mathbf{k} \parallel c$ vs. $\mathbf{k} \perp c$ spectra.[Quijada95, Startseva98a]

The optical conductivity was calculated by a Kramers-Kronig (KK) transformation of the reflectance. In order to perform KK analysis several extrapolations have been used. For the low frequency extrapolation, the Hagen-Rubens formula, $(1 - R) \propto \omega^{-1/2}$, was applied with parameters taken from the results of Takagi *et al.*[Takagi92] For the high-frequency extension ($\omega > 8000$ cm^{-1}) we used the reflectivity results of Uchida *et al.*[Uchida91] At frequencies higher than 40 eV the reflectivity was assumed to fall off as $1/\omega^4$.

The real part of the conductivity for the two materials is shown in Fig. 4.3. Clearly,

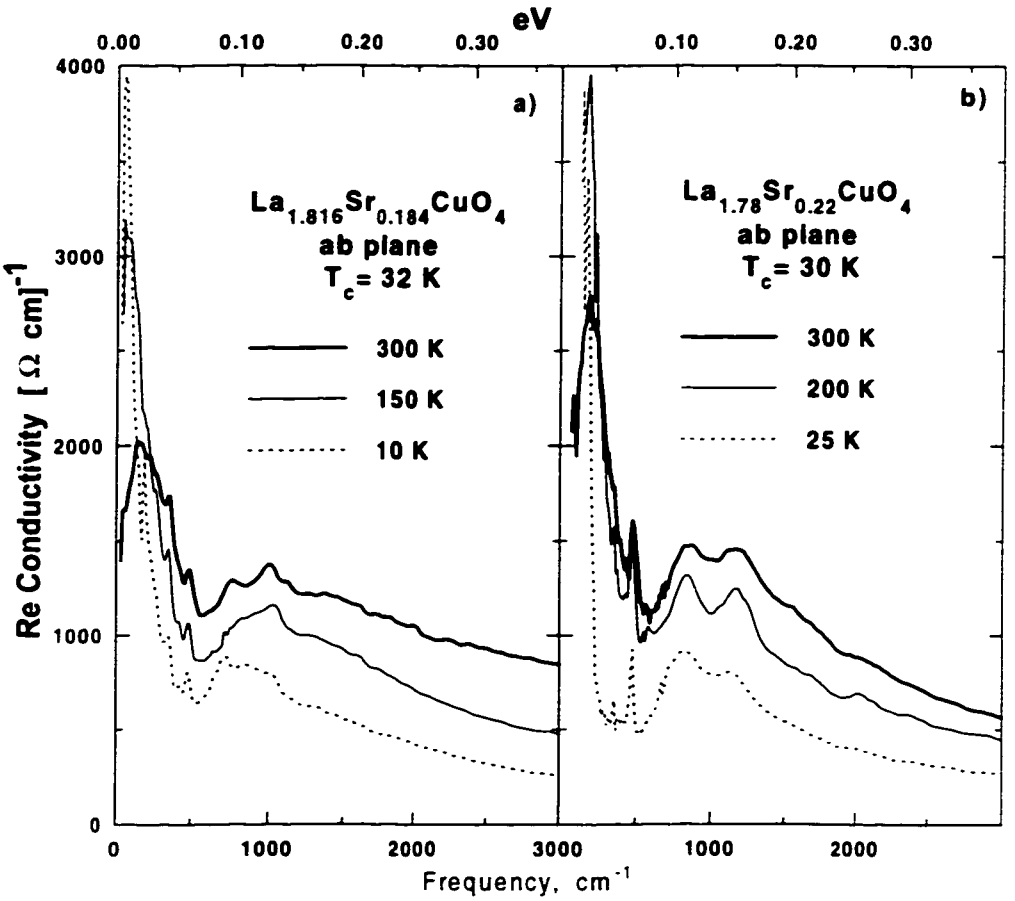

Figure 4.3: The temperature dependence of the optical conductivity (σ_1) of $La_{1.816}Sr_{0.184}CuO_4$ (a) and $La_{1.78}Sr_{0.22}CuO_4$ (b).
The former has the light polarized along the *a*- or *b*- axis while the latter has the light polarized in the *ab*-plane. In both materials a gap-like depression opens up below 750 cm^{-1} for temperatures below and above T_c (32 K), but the conductivity is non-zero even in the superconducting state.

σ_1 has a Drude-like peak which narrows as the temperature decreases which is in agreement with the metallic temperature dependence of the DC resistivity. The conductivity of LSCO is temperature-dependent in the mid IR frequency region as well. There are strong deviations from the Drude shape in the form of an onset or a step in the conductivity at $\sim$ 700 cm^{-1}. Unlike the Y123, Y124, and $Bi_2Sr_2CaCu_2O_{8+\delta}$ (Bi2212) materials which show similar features only at low temperatures, the optical conductivity of $La_{1.816}Sr_{0.184}CuO_4$ shows this 700 cm^{-1} threshold at room temperature. The sharpness of the threshold is related to the presence of phonon features in the reflectance spectra.

Another deviation from the Drude form is a shift in the Drude peak from zero frequency to 150 cm^{-1}. It is clearly seen in the room temperature σ_1 spectra presented in Figure 4.3. This peak grows in magnitude and narrows as the Sr doping level increases. A similar peculiarity was observed by Quijada *et al.*[Quijada95] in the conductivity of a single crystal of La_2CuO_4 ; but was absent in $La_{2-x}Sr_xCuO_4$ thin films.[Gao93] The peak has also been observed in other HTSC systems, but its origin is still unclear. Localization has been suggested as a possible cause.[Timusk95] An artifact of the polished surface is another possible explanation. However, in the previous IR measurements on LSCO(x = 0.13) this peculiar shift of the Drude-like peak was not seen.[Startseva98a] The surface of this underdoped LSCO was prepared using an identical procedure to those used in the present study. We believe that this feature is an intrinsic attribute of overdoped LSCO. The doping dependence of the peak suggests its connection to either disorder or the higher carrier concentration. Yet, the resistivity measurements favour the carrier concentration explanation for the peak's shift because of the dramatic decrease in resistivity with increasing Sr doping. This is a clear indication of the dominance of the effect of varying the carrier concentration over changing the amount of disorder in the compound.[Boebinger96]

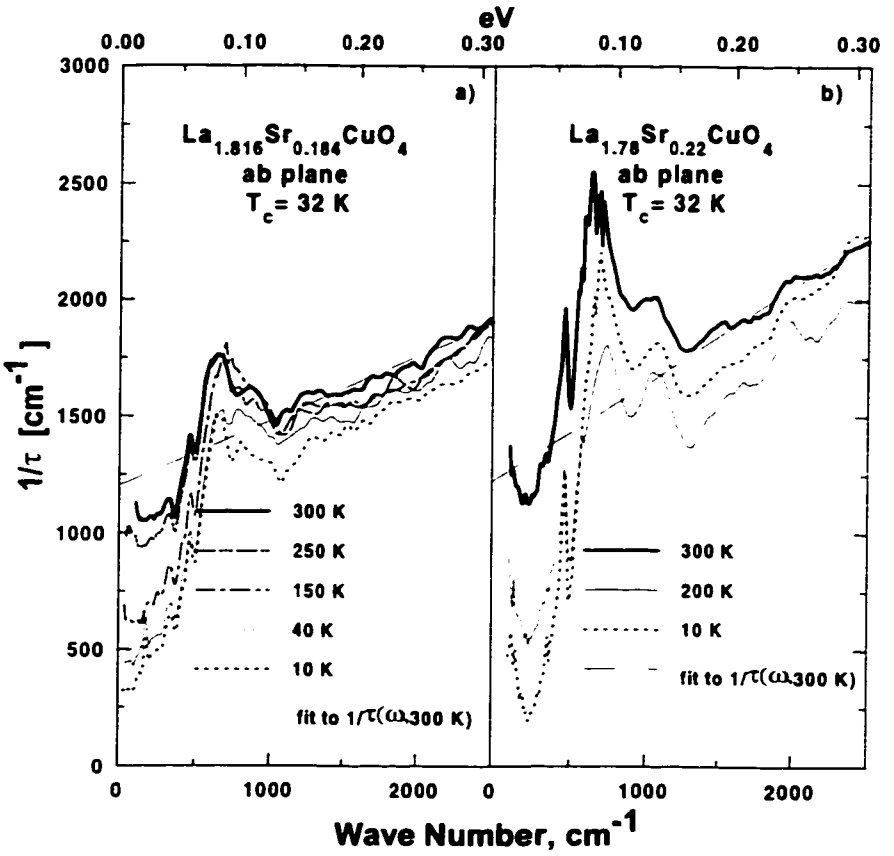

Figure 4.4: The frequency dependent effective scattering rate of $La_{1.816}Sr_{0.184}CuO_4$ (a) and $La_{1.78}Sr_{0.22}CuO_4$ (b) as calculated using Equation (2.37).
The onset of the suppression in the conductivity corresponds to a drastic change in the frequency dependence of the scattering rate. The dashed lines are linear fits ($1/\tau = \alpha \times \omega + \beta$) to the scattering rate above 700 cm^{-1} with the parameters $\alpha = 0.29$, 0.50 and $\beta = 1180$, 1065 for LSCO with $x = 0.184$ and $x = 0.22$, respectively. Below this frequency the scattering rate varies as $\omega^{1+\delta}$ and shows a strong temperature dependence.

A more dramatic manifestation of the pseudogap state is seen in the frequency dependent effective scattering rate, $1/\tau$, shown in Figure 4.4 which can be calculated using the following equation,

$$1/\tau(\omega,T) = \frac{\omega_p^2}{4\pi} Re(\frac{1}{\sigma(\omega,T)}), \tag{4.1}$$

where $\sigma(\omega,T) = \sigma_1(\omega,T) + i\sigma_2(\omega,T)$ is the complex optical conductivity and ω_p is the plasma frequency of charge carriers.

There are two distinct regimes in Figure 4.4: below and above $\approx$ 1000 cm^{-1}. At high frequencies the scattering rate varies approximately linearly with ω. The numerical value of $1/\tau$ is comparable to the corresponding frequency, thereby violating the Fermi liquid approximation which assumes $1/\tau << \hbar\omega$. The other observation that can be made from Figure 4.4 is that there is little change in the effective scattering rate on entry into the superconducting state. The quasiparticle scattering above 1000 cm^{-1} in the superconducting state drops by, at most, 15% from the room temperature value. Similar behavior has been previously seen in the underdoped cuprates such as Bi2212, Y123 and Y124.[Puchkov96d] The usual trend for the overdoped systems, however, is a strong temperature dependence of the scattering rate at high frequencies. For example, in the overdoped Bi2212 compound containing Pb (Bi2212/Pb) the difference between the scattering rates in the normal and the superconducting states at 2000 cm^{-1} is of the order of 50%. In the case of overdoped LSCO, by contrast, the temperature dependence of $1/\tau$ is significantly smaller than that in Bi2212/Pb. On the other hand, there are noticeable differences between the linear part of the scattering rate in underdoped and overdoped LSCO. The value of $1/\tau$ for the underdoped LSCO(x=0.13 and 0.14) varies by only 8% between 10 K and 200 K.[Startseva98a]

The dashed lines in Figure 4.4 are extrapolations of the high frequency linear behavior to zero frequency. A well-defined depression below this linear trend develops at $\omega <$ 750 cm^{-1} in both samples signaling the onset of the pseudogap state. In this state the scattering rate has a strong temperature dependence and a sublinear frequency dependence, $\sim \omega^{1+\delta}$. The pseudogap state is more prominent in LSCO with x = 0.184. In this sample the depression is present right up to room temperature. For the $x = 0.22$ sample the depression gradually vanishes as temperature is increased.

One explanation of the scattering rate's suppression may be the fact that the quasiparticles are heavily dressed with interactions. The other possible explanation of the suppression of $1/\tau$ is the existence of a gap in the scattering excitation spectrum. Nevertheless, one would expect the saturation of $1/\tau$ at high frequencies as soon as all the scattering channels were filled.

There is considerable uncertainty in the size of the pseudogap due to the presence of two overlapping peaks at $\sim$ 450 cm^{-1} and 580 cm^{-1}. In accordance with our previous discussion these peaks could originate from a microscopic coupling between the *c*-axis LO phonons and the *ab*-plane conductivity.[Reedyk92] The inset in Figure 4.4 shows a comparison of the peak positions at 450 cm^{-1} and 580 cm^{-1} in the dielectric function of the *c*-axis phonons[Startseva98a] to those found in the $1/\tau$ spectra. There is agreement between the position of the peaks, their width and the relative strength with the model of coupling between LO phonons and the *ab*-plane IR response. The best we can do in view of these uncertainties is to suggest an approximate energy range 750$\pm$200 cm^{-1} for the pseudogap similar to the size of the pseudogap in the other cuprates. However we should note that in a recent study with ARPES it was found that the normal state gap is significantly bigger in LSCO than in Bi2212 or Y123.[Ino98] The estimated value of Δ is 0.1 eV (800 cm^{-1}) which would correspond to at least 1600 cm^{-1} in the IR spectra. However, authors points out that because of the technical difficulties the error introduced

in this estimation is of the order of 0.05 eV.

We found that for $La_{1.816}Sr_{0.184}CuO_4$ the pseudogap critical temperature, T^* ($\geq$ 300 K), (Fig. 4.4a) is an order of magnitude higher than the superconducting transition temperature T_c (32 K). This is significantly different from the previous results on overdoped cuprates. Theoretical considerations have led to the suggestion that T^* coincides with the temperature of the superconducting transition at the optimal doping level.[Lee92] This seems to apply to Y123 and Y124 where the T^* and T_c curves cross near the optimal doping level.[Basov96] However, this is clearly not the case here. A detailed examination of the scattering rate curves in Fig. 4.4b indicates that in the overdoped sample with x=0.22 the suppression of the scattering disappears near room temperature, implying that T^* is close to 200 K for $x = 0.22$. As Figure 4.5 shows, our findings of a pseudogap in overdoped LSCO are consistent with the phase diagram of Batlogg *et al.* for this material.

There was a suggestion[Stojković97], based on the fact that the pseudogap stretches to the chemically overdoped regime, to define the overdoped systems as those where the antiferromagnetic correlations are weak and the temperature dependent uniform susceptibility has a maximum only below T_c. The examples are Tl2212 with T_c = 40 K and LSCO with x > 0.24. According to this definition both of the systems studied in this chapter are "magnetically underdoped".

J.G. Naeini *et al.*[Naeini98] studied a crystal from the same source as the present sample with a strontium content equal to 0.22 using electronic Raman scattering. The scattering rate was obtained from the B_{1g} spectra at different temperatures. Distinct changes in both the magnitude and slope were found at a temperature of $\sim$ 160 K. By applying nearly antiferromagnetic Fermi liquid theory (NAFL) the authors suggested that the pseudogap is absent in LSCO (x = 0.22) and that a pseudoscaling regime is prevalent below 160 K. According to our findings the pseudogap state exists below 200 K

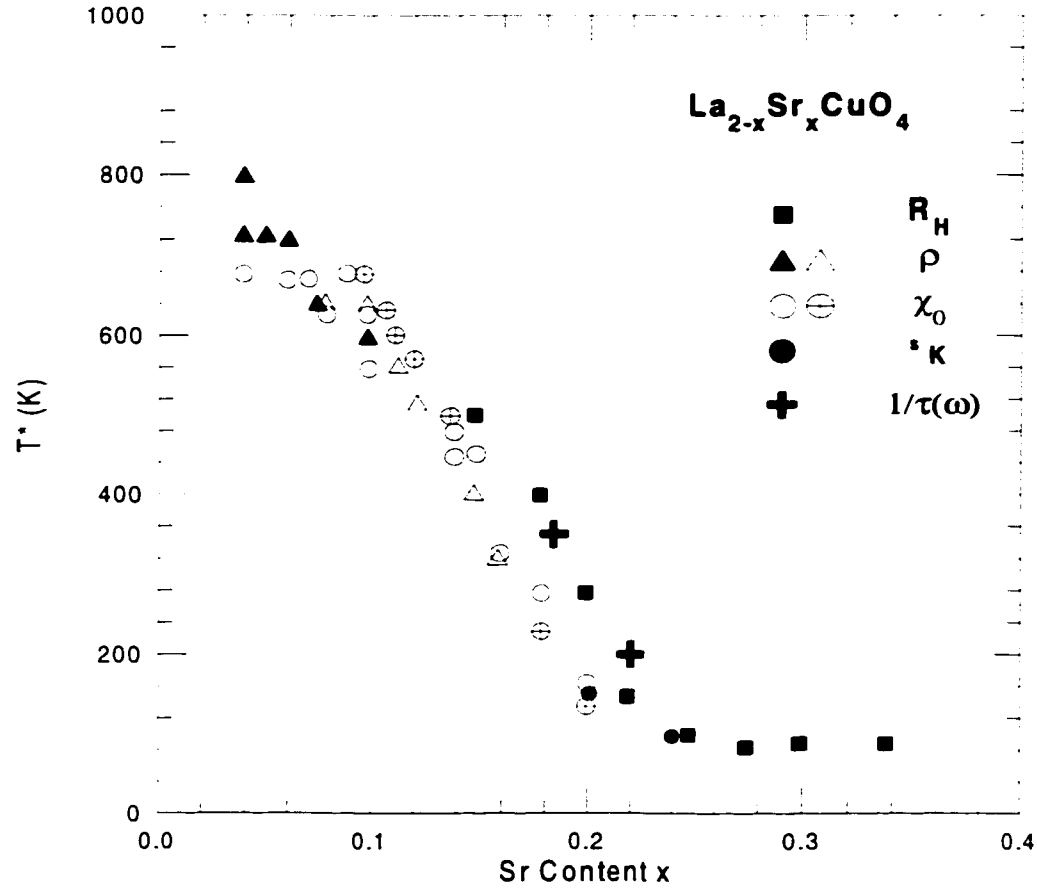

Figure 4.5: The phase diagram T* vs x for $La_{2-x}Sr_xCuO_4$.
The data from Hall effect, resistivity, magnetic susceptibility and NMR experiments were taken from the work of Batlogg *et al.* and references therein. The value of T* estimated from the effective scattering rate (see Fig. 4) is shown by + symbols.

in this sample. The nature of the disagreement may be in the choice of the particular definition used to characterize the pseudogap. However, the transport measurements mentioned above concur with the statement that the pseudogap exists in the overdoped LSCO (Fig. 4.5).[Batlogg94]

For completeness we also calculated the effective mass enhancement which is related to the effective scattering rate by the Kramers-Kronig relation:

$$m^*/m_e = 1 + \lambda(\omega) = \frac{2}{\pi}\mathcal{P}\int_0^\infty \frac{1/\tau(\Omega)}{\Omega^2 - \omega^2}d\Omega \tag{4.2}$$

where $\lambda(\omega)$ is the mass enhancement factor. It also can be calculated from the complex conductivities using the equation:

$$m^*/m_e = -\frac{\omega_p^2}{4\pi}\frac{1}{\omega}Im(\frac{1}{\sigma(\omega)}). \tag{4.3}$$

In Figure 4.6 the mass enhancement calculated using Equation 4.3 is shown for temperatures below and above the superconducting transition temperature. Note that m^*/m_e is intensified in the same energy range where the effective scattering rate is depressed. The maximum value of m^*/m_e ranges from 1.5 to 4. The mass enhancement seems to be higher for x=0.22 than for x=0.184. Both the range and the maximum values of the mass enhancement are in good agreement with the previously reported results.[Puchkov96d]

In summary, we have observed clear evidence for the pseudogap state in two overdoped samples of LSCO. Unlike the YBCO system, where the normal state's pseudogap feature is only seen in the underdoped system, the LSCO compound exhibits this feature in the overdoped regime at a temperature substantially above the superconducting transition temperature. In this material the crossover from the underdoped to the overdoped regime does not suppress T^* below T_c.

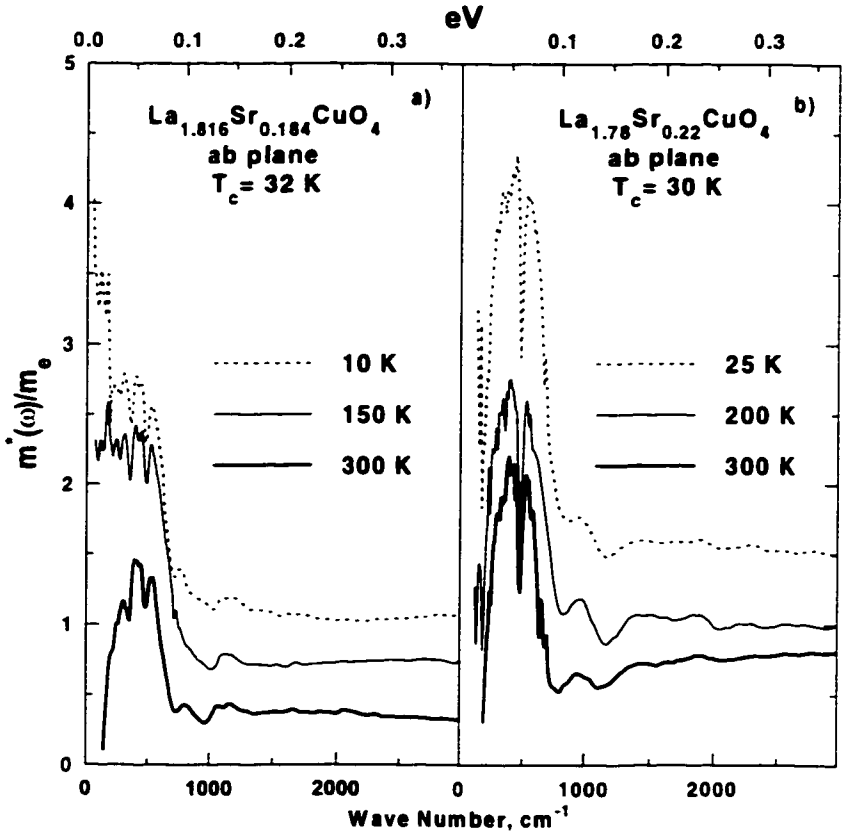

Figure 4.6: The frequency dependent effective mass of $La_{1.816}Sr_{0.184}CuO_4$ (a) and $La_{1.78}Sr_{0.22}CuO_4$ (b) as calculated using Equation 3.

Chapter 5

OPTICAL PROPERTIES OF $HgBa_2Ca_2Cu_3O_{8+\delta}$

Since its discovery,[Putilin93, Schilling93] the $HgBa_2Ca_{n-1}Cu_nO_{2(n+1)+\delta}$ (Hg12$(n-1)n$)) system has attracted a tremendous amount of attention. When n = 3, the compound has a superconducting transition temperature (T_c) of 136 K at ambient pressure[Isawa94] which rises to values above 150 K under pressure.[Chu93, Takahashi93] Both of these values are records for the HTSC. It is also possible to vary the critical temperature in this material by changing the number of CuO_2 planes, n, within a single unit cell. The diversity of n in this system gives a unique opportunity to characterize the dynamics of the inter-plane coupling as well as to study the dependence of the critical temperature upon the number of CuO_2 planes. In addition, it has been found that the Hg-O_δ blocks supply excess oxygen to the CuO_2 planes. This provides another avenue for modifying T_c. Based on the value of the critical temperature there are three classes of high-T_c superconductors. The first class includes materials such as LSCO and the related NdCe cuprates. They can be characterized by a low T_c, which at optimal doping does not exceed 40 K, and only one CuO_2 plane per unit cell. The second class is the most studied one. It includes materials such as YBCO and PSYCCO and is characterized by a maximum critical temperature in the vicinity of 90 K. The third class which includes Hg12$(n-1)n$ and the compound studied here as well as the Bi and Tl cuprates exhibits an optimal T_c that varies with the system but increases dramatically with the number of copper layers. This unusual behavior makes this class of materials an excellent candidate for studying the mechanism behind the high transition temperatures in the cuprate superconductors.

In this work the triple layered Hg-cuprate is investigated in the underdoped regime.

The high value of the transition temperature directed attention towards the properties of the superconducting state. Nevertheless, the normal state properties are as anomalous and intriguing as the superconducting ones. It is important to see whether or not the value of T_c, as well as large number of CuO_2 planes, affects the temperature, T^*, and energy scale of the pseudogap. At present, the highest values for T^* have been found for the cuprates with the lowest T_c[Batlogg94, Startseva98a, Startseva98b]. However, the size of the pseudogap as measured by the *ab*-plane scattering rate seems to be material independent.[Puchkov96d]

The peculiar normal properties previously seen in the majority of underdoped cuprates have also been found in the Hg-cuprates. Several transport studies [Carrington94, Fukuoka97] have shown the presence of a clear downward suppression from the linear temperature dependent resistivity. According to Fukuoka *et al.*[Fukuoka97] the characteristic temperature of this anomaly, T^*, spans from 220 K to 280 K for Hg1223 single crystals having different oxygen contents.

An even higher range of T^* based on NMR is reported by Julien *et al.*[Julien96]. The measurements presented in this work were performed on the samples grown by the same group that supplied the crystals for NMR work. Both the in-plane resistivity[Carrington94] and the uniform spin susceptibility suggest a value for T^* near 370 K. It has also been argued that the characteristic energy of the spin fluctuations of Hg1223 is higher than that of underdoped $YBa_2Cu_3O_{7-\delta}$(Y123). This magnetic energy scale was found to be 95 meV, whereas for Y123, the number does not exceed 75 meV.[Takigawa94] Nevertheless, the magnitude and the temperature dependence of the uniform spin susceptibility are comparable in both materials. The NMR measurements performed on the single layer Hg-cuprates indicate that the value of T^* is similar to that of the triple layer Hg1223 compound.[Bobroff97] Thus, there is only an insignificant connection between T^* and the

coupling between adjacent layers.

There are a number of other studies on the Hg1223 compound (Raman spectroscopy [Sakuto97], specific heat[Carrington97], transport measurements[Bertinotti97]), but there have been no investigations of the far-infrared optical properties for the triple layer Hg-cuprate. This work presents the first measurements on the optical properties of Hg1223 over a wide frequency range, at temperatures below and above T_c. The main reason for the lack of optical data on this system is the extremely small size of the available samples. A sensitive overfilling technique combined with an improved rapid scan Fourier-transform spectrometer made this measurement possible. While the infrared experiments do not provide information about the k-space dependence of the normal state gap they do have an advantage over, for example, DC transport measurements in that they possess the ability to obtain detailed information about scattering processes and the coupling between the carriers as a function of frequency.

The growth procedures as well as the characterization performed on the crystals used in this study are described elsewhere.[Bertinotti97] The dimensions of the crystals used were typically 0.5x0.4x0.03 mm^3 (the shortest dimension being along the c-axis). Magnetization measurements showed a transition temperature of 121 K, which is somewhat lower than the optimum value of 133 K. The samples measured were as-grown and oxygen deficient, thus underdoped.[Bertinotti97]

The reflectance of a single crystal of Hg1223 was measured with the electromagnetic radiation polarized parallel to the ab plane. The far-infrared reflectance is shown in Fig. 5.1. The dotted curves represent reflectance for temperature below the superconducting transition and the solid curves describes the reflectance above T_c. The reflectance clearly deviates from a simple Drude behavior. Moreover, the reflectance does not monotonically increase as frequency decreases. Instead, it develops a sharp step-like

suppression below 325 cm^{-1}. This feature almost vanishes in the noise at room temperature. However, it seems to strengthen below T_c. A similar suppression was previously observed in a number of cuprates and was assigned to a localization effect.[Timusk95] Several study has shown that the step-like suppression below 325 cm^{-1} is enhanced by impurities such as Zn, by radiation damage or by disorder associated with oxygen doping.[Basov94, Basov98a] Nevertheless, it has also been seen in the reflectance of a high purity Y123 crystal grown in a zirconia crucible,[Rõõm98] suggesting that the suppression may be intrinsic. An interesting aspect of the Y123 measurements is that the feature only occurs in the a-direction (i.e. the direction without chains). It is conceivable that this suppression is also an intrinsic feature of Hg1223.

The real part of the optical conductivity is shown in Fig. 5.2. Both the real and imaginary parts of conductivity have been calculated from the reflectance data using Kramers-Kronig analysis. To implement this calculation extrapolations were used. At low frequency, the reflectance followed a Hagen-Rubens dependence in the normal state and a $(1 - R) \sim \omega^2$ dependence in the superconducting state. The room temperature high frequency data was measured up to 3.5 eV. Beyond this frequency the reflectance is assumed to be constant up to 37 eV. At higher frequencies free-electron behavior is used.

The in-plane response of Hg1223 is approximately Drude-like: the real part of conductivity decreases with increasing ω. Nevertheless, a few deviations from the Drude form should be mentioned. Firstly, the typical Drude peak, usually centered at the zero frequency, is shifted towards 300 cm^{-1}. The precursor of this shift was a suppression in the reflectance below 300 cm^{-1}. Secondly, the width of the peak is significantly lower at temperatures below 225 K. It seems that most of the spectral weight below 1250 cm^{-1} is displaced to the condensate delta function at $\omega = 0$. In order to analyze the differences we show the frequency dependence of the effective scattering rate, $1/\tau(\omega)$, calculated using the extended Drude model.

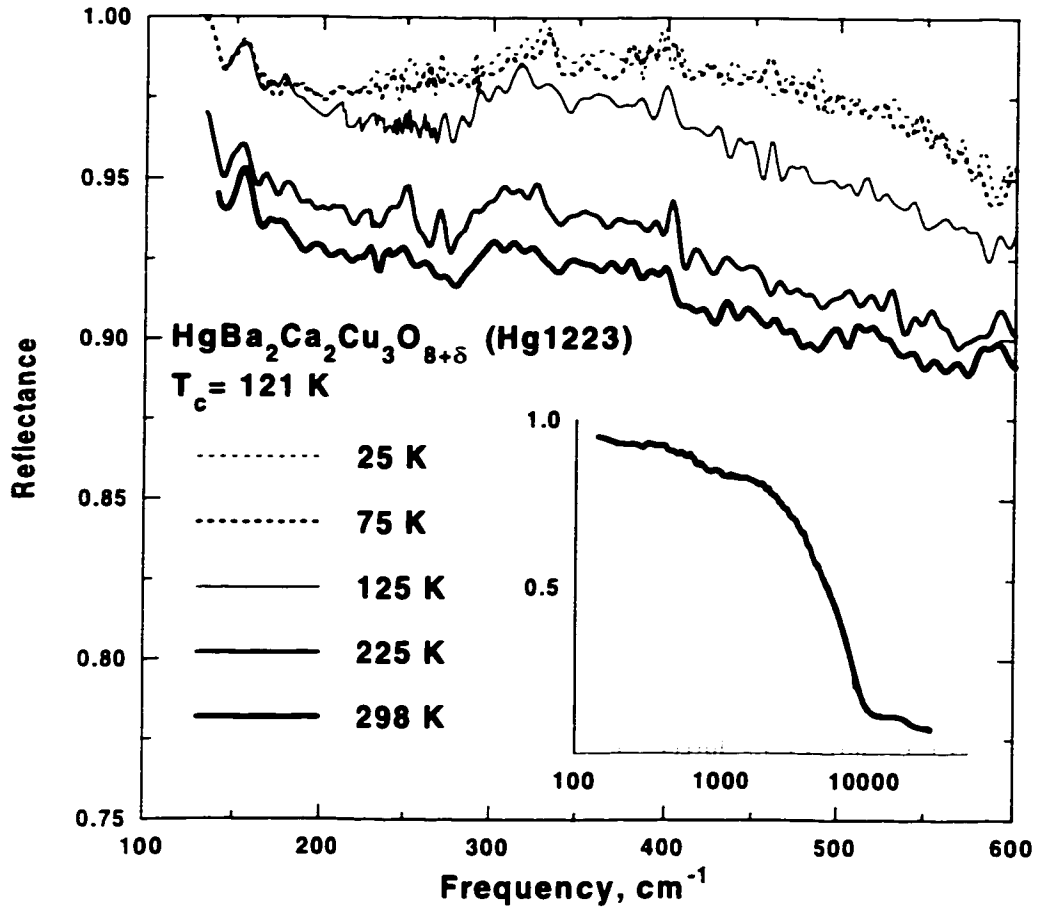

Figure 5.1: The frequency dependence of the in-plane reflectance of $HgBa_2Ca_2Cu_3O_{8-\delta}$ is shown for temperatures below and above T_c.
The dotted curves corresponds to temperatures below the superconducting transition and the solid curves belong to the normal state. Inset: The reflectance at 298 K over a broad frequency range.

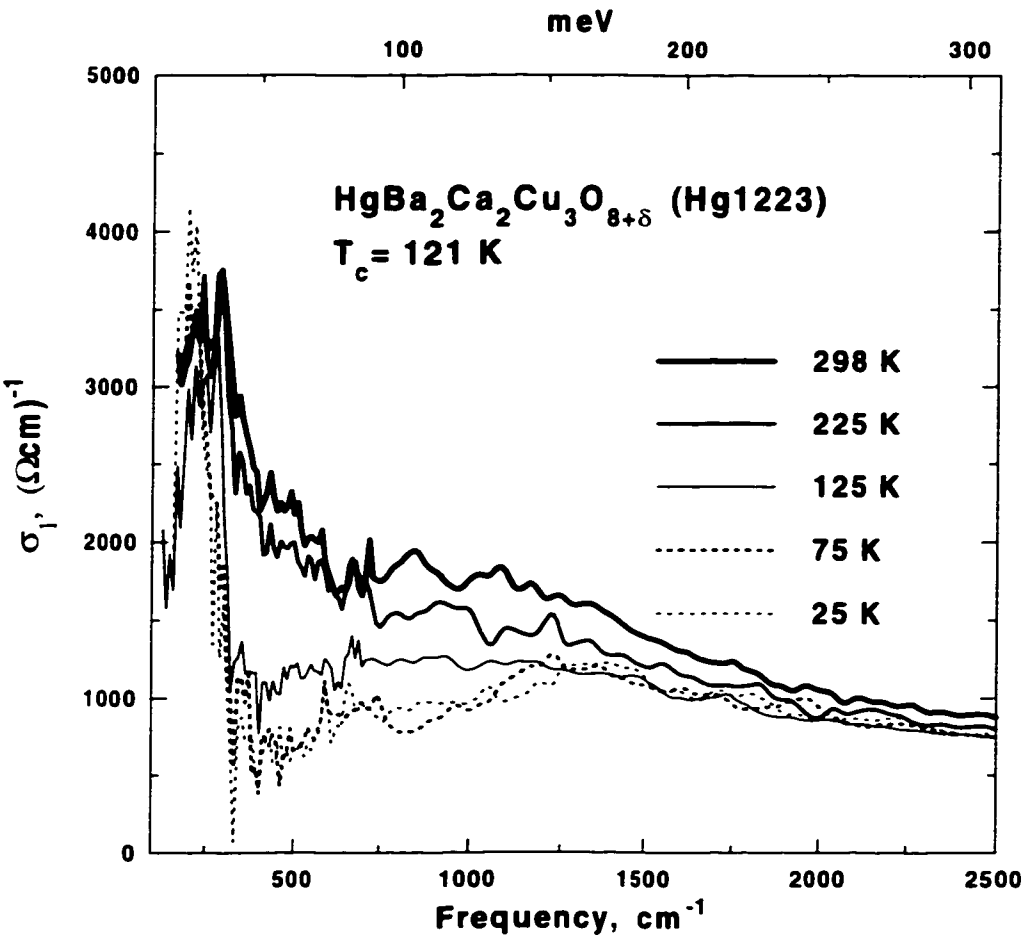

Figure 5.2: The real part of the optical conductivity vs frequency for $HgBa_2Ca_2Cu_3O_{8+\delta}$ with $E \perp c$.
The dotted curves correspond to temperatures below the superconducting transition (T = 25 and 75 K) and the solid curves belong to the normal state (T = 298, 225 and 125 K). In the normal state, the conductivity is similar in appearance to a Drude conductivity. However, there is a visible suppression of σ_1 below 1250 cm^{-1}. This suppression is enhanced in the superconducting state. Also the usual Drude peak centered at the zero-frequency is shifted to a finite frequency equal to 200 cm^{-1}

It is well known that the effective scattering rate in the underdoped samples can be divided into two well defined regions.[Puchkov96d] At high frequencies (ω >750 cm^{-1}), the scattering is strong and linear as a function of frequency. In addition, the temperature dependence of $1/\tau$ is weak below 300 K. At low frequencies (ω <750 cm^{-1}) the strong scattering regime abruptly fades. The remaining scattering rate is diminished and strongly temperature dependent. The frequency at which the crossover from the strong to the weak scattering regime occurs can be used to define the size of the pseudogap. It has been shown, based on the measurements from the different high-T_c superconductors, that the size of the pseudogap is the same for both the normal and superconducting states.

Similar behavior is observed for the case of Hg1223 (Fig. 5.3). There are two distinct regions: one region is where the scattering rate is somewhat linear and practically temperature independent and the other where a sublinear frequency dependence develops along with a strong variation in $1/\tau$ as a function of temperature. The suppression of the scattering rate below the linear-ω trend persists above the highest measured temperature suggesting that $T^* > 298\ K$. This is in agreement with the previous estimation of T^*.[Carrington94] For completeness, the effective mass is shown in the inset to Fig. 5.3. The value of m^*/m_e is enhanced in the frequency range corresponding to a suppression of the scattering rate.

In the previously measured cuprates, the transition between the superconducting and normal states is very subtle. However, the spectra in Fig. 5.3 reveals a distinct difference in the size of the pseudogap for temperature below and above T_c. In the normal state (solid curves on Fig.. 5.3) it is equal to $\sim$ 750 cm^{-1} which is in accord with the characteristic energy scale of spin fluctuations.[Julien96] However, below T_c the crossover from a strong to weak scattering regime occurs at a frequency nearly double that of the normal state. The physics behind this shift is unclear. The possibility exists that

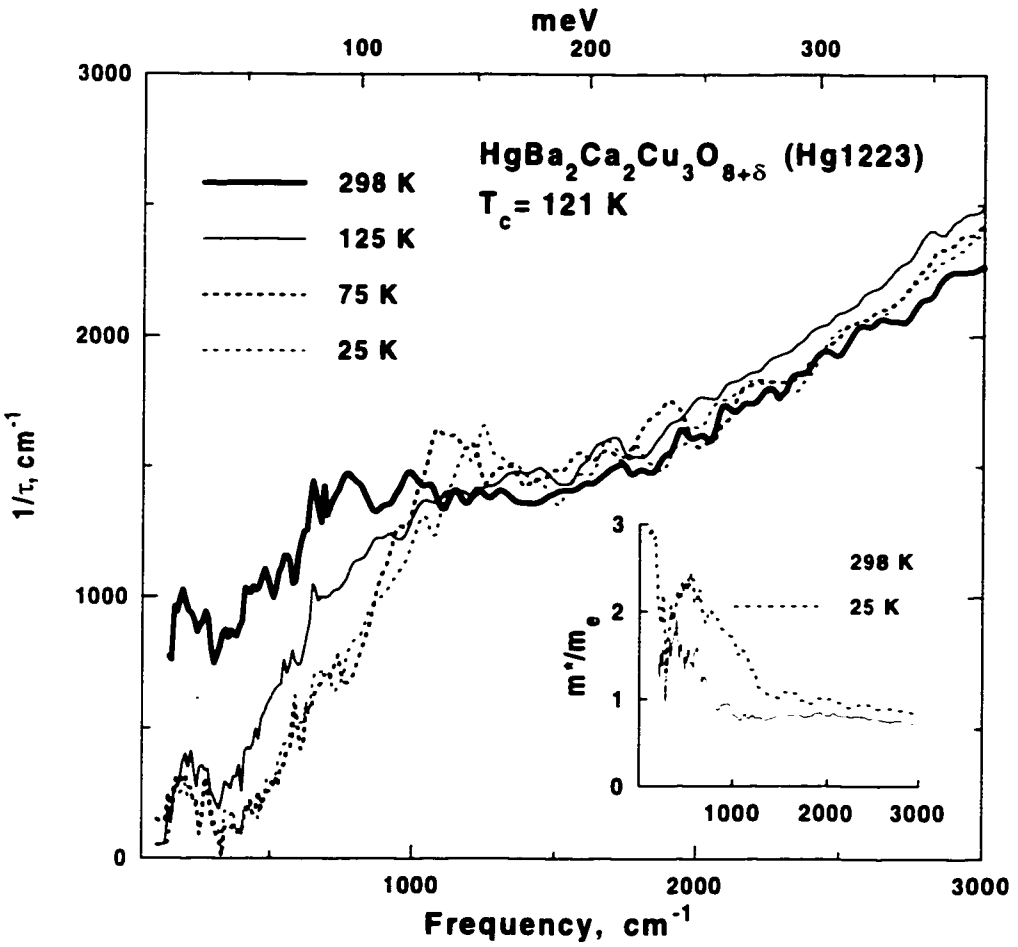

Figure 5.3: The frequency dependent effective scattering rate for $HgBa_2Ca_2Cu_3O_{8+\delta}$ with $E \perp c$.

The dotted curves correspond to temperatures below the superconducting transition (T = 25 and 75 K) and the solid curves belong to the normal state (T = 298, 225 and 125 K). The onset of the suppression in the conductivity corresponds to a drastic change in the frequency dependence of the scattering rate. In the superconducting state, a gap-like feature opens up at 1250 cm^{-1}. In the normal state, this suppression is also present, but the onset of the pseudogap shifts towards lower frequencies. Inset: The frequency-dependent mass enhancement in the normal and the superconducting states.

it may be related to the extremely high value of T_c. One might expect that a high critical temperature at optimal doping would lead to a bigger superconducting energy gap. For comparison the scattering rate of several underdoped cuprates is shown in Fig. 5.4. In the underdoped Bi2212 with a $T_c = 67$ K (upper middle panel) a slight difference in the size of the pseudogap between the normal and superconducting states is noticeable. In underdoped Y123, with a lower T_c of 58 K (lower middle panel), the difference vanishes. The size of the pseudogap in LSCO (bottom panel), discussed elsewhere,[Startseva98a] is equal to 750 cm^{-1}. On the other hand, the critical temperature is a mere 32 K. In the BCS framework, the value of the superconducting gap is proportional to the value of T_c. In this case one would expect that the small value of T_c corresponds to the smaller value of the superconducting gap. This conjecture would be consistent with the measurements performed on LSCO if one assumes that the superconducting gap and the pseudogap are two different entities. In this case the pseudogap could dominate in both the normal and superconducting states of LSCO. There is, however, no direct verification of the proportionality between the superconducting gap and T_c in HTSCs. Another possible scenario is that there are two competing processes. One process is responsible for the superconducting gap and the other process forms the pseudogap. Yet, there is evidence from ARPES[Norman97] that both the pseudogap and the superconducting gap trace the shape of the Fermi surface. This suggests that the processes responsible for gap formation have the same origin at temperatures above and below T_c.

Significant information about the electronic structure can be obtained from the partial conductivity sum rule. The plasma frequency of the condensate (or the missing area under the curve of $\sigma_1(\omega)$) can be obtained from the following expression[Basov98b]:

$$\omega_{pS}^2 = S_n(\omega) - S_s(\omega) \tag{5.1}$$

$$= \frac{120}{\pi}\int_0^{\omega}[\sigma_{1n}(\omega) - \sigma_{1s}(\omega)]d\omega, \tag{5.2}$$

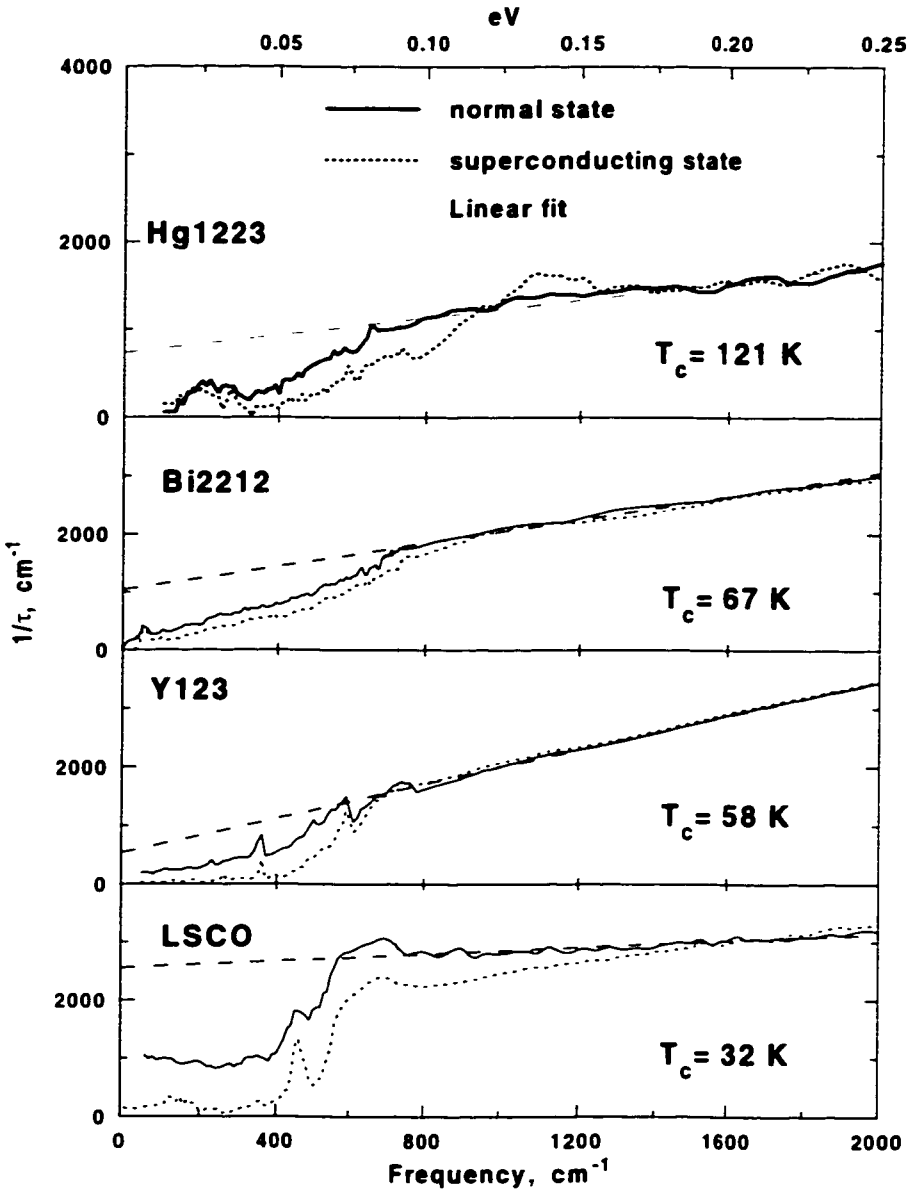

Figure 5.4: The frequency dependent effective scattering rate with $E \perp c$ for Hg1223 (top panel), Bi2212 (middle panel) (After A.V. Puchkov[Puchkov96d]), Y123 (bottom panel) (After D.N. Basov[Basov96]) and LSCO.
The dotted curves correspond to temperatures below the superconducting transition and the solid curves belong to the normal state. The scattering rate curves are essentially temperature independent above 1000 cm^{-1}. Yet, at low frequencies, a depression develops below the high-frequency extrapolation (the dash line). The size of the pseudogap, taken as the frequency where the onset of the suppression develops, is essentially material independent for both the normal and superconducting states for Bi2212, Y123 and LSCO. By contrast, in the superconducting state of Hg1223, the size of the gap-like feature is significantly bigger than that of the normal state.

where $\sigma_{1n}(\omega)$ and $\sigma_{1s}(\omega)$ are the conductivities at temperatures above and below T_c, respectively. This equation with a cutoff frequency of $\omega = 1$eV yields $\omega_{pS} = 7850 \pm 50$ cm^{-1} at 25 K for Hg1223 . The curves corresponding to the integrals, $S_n(\omega)$ and $S_s(\omega)$, are shown in Fig. 5.5. Below 1500 cm^{-1} the curves rise sharply. There is a considerable difference between the values of $S_n(\omega, 298\text{K})$ and $S_s(\omega, 25\text{K})$. This is associated with the appearance of the superconducting condensate. The numerical difference occurs because the weight of the delta function is not included in the conductivity sum rule. It important to note that the value of $S_n(\omega, 125\text{K})$ is comparable to the corresponding values of the superconducting state. Thus there is a significant loss of low frequency spectral weight even at 125 K. This suggests that there is an unusually large low frequency peak below the frequency of 100 cm-1 where our conductivity measurements stop. This peak may be associated with paraconductivity due to preformed pairs as suggested by some theories of the pseudogap state.

The oscillator strength of the condensate can also be estimated from the real part of the dielectric function in the superconducting state (see Eq. 2.22). The real part of the dielectric function at various temperatures is shown in Fig. 5.6. The sharp decrease in $\epsilon_1(\omega)$ is a signature of the suppression of the quasiparticle scattering rate. Note, that the decrease in the superconducting dielectric function (dotted line) occurs at a higher frequency than in the normal state. The inset to Fig. 5.6 shows the plot of ϵ_1 versus ω^{-2}. The slope obtained from the linear regression fit at 25 K gives a value for the plasma frequency of the condensate equal to 8000 ± 500 cm^{-2}. This value is in good agreement with the value obtained from the partial sum rule. Based on both results the London penetration depth can be estimated to be $\lambda_L = 1/2\pi\omega_{pS} = 200 \pm 30$ nm which is in agreement with the penetration depth measurements of Panagopoulos *et al.* done on magnetically aligned powders in a low field susceptometer.[Panagopoulos97]

It has been pointed out that the strength of the condensate is directly proportional

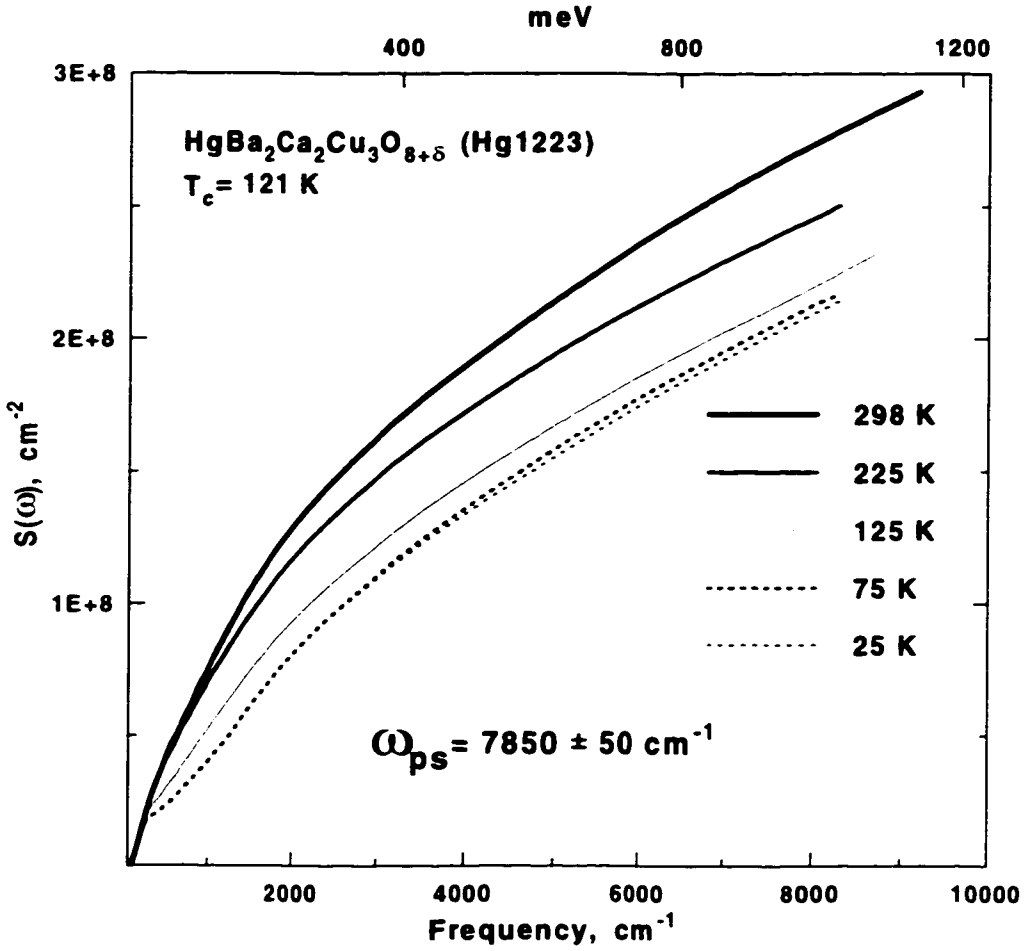

Figure 5.5: The area under the curve of $\sigma_1(\omega)$) as a function of frequency. The dotted curves correspond to temperatures below the superconducting transition and the solid curves belong to the normal state. The plasma frequency of the condensate is estimated from the difference of $S_(\omega)$ in the normal and superconducting states.

to the critical temperature. This relationship is commonly referred to as the Uemura line.[Uemura91] Both optimally doped and underdoped HTSC from a wide variety of families seem to follow this relationship. The Hg1223 compound, however, is unique in that it falls significantly below the line. This suggests that the physics of this compound has a few distinct characteristics.

In conclusion, we have used, for the first time, reflectance measurements in the far infrared frequency region to study single crystals of underdoped Hg1223. In agreement with previous experiments on other cuprates, our results indicate that the pseudogap is formed in this material with $T^* > 298$ K. Two different energy scales were observed within the pseudogap. In the superconducting state, the size of the pseudogap is approximately 1250 cm^{-1}. In contrast, the size of the normal state's pseudogap assumes the lower value found in all other high-T_c superconductors. Also, a shift in the Drude-like peak from the usual zero position towards 325 cm^{-1} was observed. The magnitude of the peak increases upon entry into the superconducting state. Based on both the conductivity sum rule and the dielectric function analysis the value of the London penetration depth was found to be 200± 30 nm.

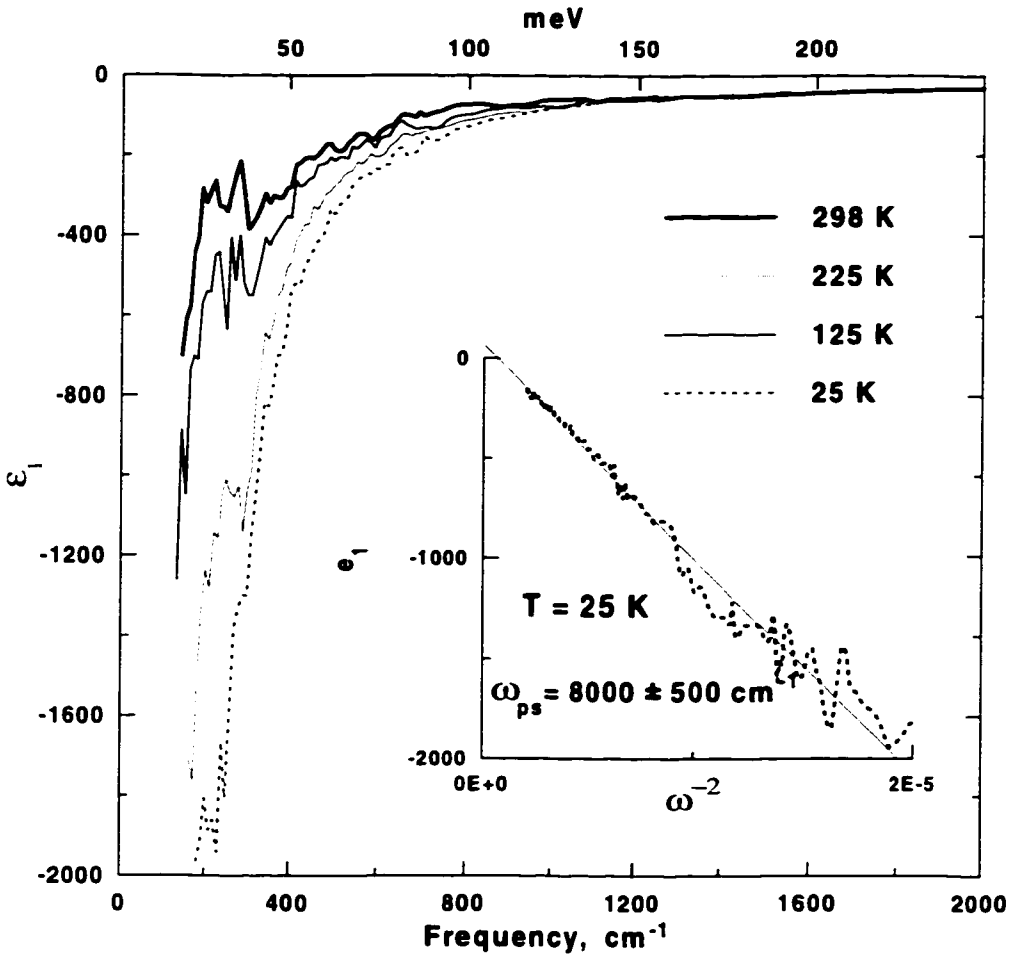

Figure 5.6: The real part of the dielectric function vs frequency for $HgBa_2Ca_2Cu_3O_{8-\delta}$ with $E \perp c$.
The dotted curves correspond to temperatures below the superconducting transition vs and the solid curves belong to the normal state. Inset: a plot of $\epsilon_1(\omega)$ ω^{-2}. In the clean limit case, the slope of this plot is ω_{pS}^2.

Chapter 6

CONCLUSIONS

To a large extent, the underlying theme behind this work has been the investigation of the pseudogap state in various cuprates. At the beginning of the work the question was addressed whether or not the pseudogap state is universal among all HTSCs. If the answer were positive, then how would it depend on the number of CuO_2 planes as well as on the value of the critical temperature? Another motivation for this work was the suggestion that the pseudogap strongly depends on the interlayer coupling, making it specific to only bilayer compounds such as Y123, Y124 and Bi2212. In an attempt to answer these and many other questions, this work has concentrated on two cuprate systems: LSCO and Hg1223.

A comparison of LSCO and Hg1223 with the other cuprates such as Y123 or Bi2212 shows a significant number of similarities. For all of the underdoped cuprates, the pseudogap is a fundamental property of the normal state. The characteristic temperature of the pseudogap is strongly doping dependent and exceeds room temperature in some cases. It decreases as doping increases until, finally, it matches T_c in the overdoped region. However, T^* is not a direct measure of the pseudogap's energy scale. The energy scale itself has proved to be weakly dependent upon the doping regime. Moreover, in all investigated materials, the suppression in the effective scattering rate spectra, which corresponds to the pseudogap, occurs at 750 cm^{-1} for temperatures between T_c and T^*. Remarkable similarities are displayed, not only in the position of the suppression, but

also in both the temperature and the frequency dependence of $1/\tau(\omega,T)$. For the frequencies below 750 cm^{-1} and for temperatures below T^*, the scattering rate becomes both the temperature and ω dependent. Above 750 cm^{-1} and below the characteristic temperature T^{**}, $1/\tau(\omega,T)$ is nearly a linear function of frequency and does not show any indication of a temperature dependence.

Even with all these similarities there are still a number of important differences between the various cuprates. In Y123, Y124, Bi2212 and LSCO the crossover between the normal and superconducting states is an elusive one. Yet, in the Hg1223, the transition is obvious. Here, the energy scale of the gap-like feature differs for temperatures above and below T_c. At 25 K the suppression in the effective scattering rate, which suggests the opening of a gap in the excitation spectrum, occurs at 1250 cm^{-1}. This is a significant shift from the energy scale of the $1/\tau$ suppression at T, where $T_c < T < T^*$. Also, it is generally believed that the pseudogap is a unique property of the underdoped cuprates. However, in LSCO the existence of the pseudogap extends into the strongly overdoped region. The cumulative data collected on LSCO suggests the presence of paramagnetic centers.

Two entirely novel aspects were introduced in this thesis. The previous measurements showed the optical spectra only up to room temperature. For the first time the reflectance of the underdoped LSCO compound was obtained at temperatures as high as 400 K. As a result, in the underdoped sample, the temperature dependence of the effective scattering rate was observed even above 750 cm^{-1}. This suggested the possibility of another temperature scale within the phase diagram T^* vs T.

Also this work presents the first optical spectra of Hg1223 single crystals. Besides the study of the pseudogap in this material, the optical conductivity, as well as the dielectric function, were investigated. Based on this study, the London penetration length was found to be 200 $\pm$30 nm. Surprisingly, the value of the condensate $\delta \propto \lambda_L^{-2}$ as

a function of T_c does not follow the relationship commonly referred as the Uemura line.[Uemura91] Namely, Uemura *et al.* pointed out that the strength of the condensate δ varies monotonically with T_c. Many underdoped and optimally doped materials such as LSCO, Y123 and Bi2212 are well described by the Uemura relationship. However, the value of δ in Hg1223 falls significantly below the Uemura line, suggesting that the physical processes determining superconductivity are different for this material.

The c-axis conductivity of LSCO also shows evidence of a pseudogap. However, a clear gap-edge feature like that seen for Y123 was not observed. The feature is weak and can be seen at frequencies below 500 cm^{-1}.

Taken together the experimental and theoretical work on high temperature superconductors has not yet provided a consistent explanation for the pseudogap phenomenon. Such an explanation will only arise through further experimental investigations of the anomalous normal state. Moreover, it is these studies that will direct our understanding towards the true nature of the pseudogap and pave the way towards a theory describing the essence of high temperature superconductivity.

Appendix A

Energy units:

1 eV = 8065.5 cm^{-1} = 2.41796×10^{14} Hz = 11600.4 K = 1.602×10^{-19} J.

Appendix B

Material abbreviations:

$La_{2-x}Sr_xCuO_4$ (LSCO)

$HgBa_2Ca_2Cu_3O_{8+\delta}$ (Hg1223)

$YBa_2Cu_3O_{7-\delta}$ (Y123)

$YBa_2Cu_4O_4$ (Y124)

$Tl_2Ba_2CuO_{6+\delta}$ (Tl2201)

$Bi_2Sr_2CaCu_2O_{8+\delta}$ (Bi2212)

$Bi_{2-x}Pb_xSr_2CaCu_2O_{8+\delta}$ ((Bi/Pb)2212)

$Ba_{1-x}K_xBiO_3$ (BKBO)

$Ba_{1-x}Pb_xBiO_3$ (BPBO)

Bibliography

[Aeppli87] Aeppli G., R.J. Cava, E.J. Ansaldo, J.H. Brewer, S.R. Kreitzman, G.M. Luke, D.R. Noakes, and R.F. Kiefl, Phys. Rev. B, **35**, 7129 (1987).

[Allen71] Allen P.B., Phys. Rev. B **3**, 305 (1971).

[Allen76] Allen P.B., and J.C. Mikkelsen, Phys. Rev. B **15**, 2953 (1976).

[Allen87] Allen P.B., W.E. Pickett, and H. Krakauer, Phys. Rev. B **36**, 3926 (1987).

[Anderson73] Anderson P.W., Mat. Res. Bull. **8**, 153 (1973).

[Ashcroft76] Ashcroft N.W., and N.D. Mermin, *Solid State Physics*, Saunders College, Philadelphia, 1976.

[Atkinson97] Atkinson W.A. and J.P. Carbotte, Phys. Rev. B **55**, 3230 (1997).

[Bardeen57] Bardeen, J., L.N. Cooper, and J.R. Schrieffer, Phys. Rev. **108**, 1175 (1957).

[Basov94] Basov D.N., T. Timusk, B. Dabrowski and J.D. Jorgensen, Phys. Rev. B **50**, 3511 (1994).

[Basov95a] Basov D.N., H.A. Mook, B.Dabrowski, and T. Timusk, Phys. Rev. B **52**, R13141 (1995).

[Basov95a] Basov D.N., H.A. Mook, B.Dabrowski, and T. Timusk, Phys. Rev. Lett. **74**, 598 (1995).

[Basov96] Basov D.N., R. Liang, B. Dabrowski, D.A. Bonn, W.N. Hardy, and T. Timusk, Phys. Rev. Lett., **77**, 4090 (1996).

[Basov98a] Basov D.N. and T. Timusk, to be published (1998).

[Basov98b] Basov D.N. S.I. Woods, A.S. Katz, E.J. Singley, R.C. Dynes M. Xu, D. Hinks, C.C. Homes and M. Strongin, to be published (1998).

[Batlogg88] Batlogg B., R.J. Cava, L.W. Rupp, Jr., A.M. Mujsce, J.J. Krajewski, J.P. Remeika, W.F. Peck, Jr., A.S. Cooper and G.P. Espinosa, Phys. Rev. Lett. **61**, 1670 (1988);

[Batlogg89] Batlogg B., in *Mechnisms of High Temperature Superconductivity*, Editors: H. Kamimure, A. Oshiyama, Springer Series in Material Science, Vol. 11, p.342 (1989).

[Batlogg94] Batlogg B., H.Y. Hwang, H. Takagi, R.J. Cava, H.L. Kao, and J. Kwo, Physica C **235–240**, 130 (1994).

[Bednorz86] Bednorz J.G., and K.A. Müller, Z. Phys. B **64**, 189 (1986).

[Bertinotti97] Bertinotti A., D. Colson, J.-F. Marucco, V. Viallet, G. Le Bras, L. Fruchter, C. Marcenat, A. Carrington, and J. Hammann, Editor: Narlikar, Nova Science Publisher Vol. 23, (1997).

[Blumberg97] Blumberg G., M. Kang, M.V. Klein, K. Kadowaki, C. Kendziora, Science **278**, 1427 (1997).

[Bobroff97] Bobroff J., H. Alloul, P. Mendels, V. Viallet, J.-F. Marucco, and D. Colson, Phys. Rev. Lett. **78**, 3757 (1997).

[Bonn88] Bonn D.A., J.D. Garret, and T. Timusk, Phys. Rev. Lett. **61**, 1305 (1988).

[Bonn92] Bonn D.A., P. Dosanih, R. Liang, and W.N. Hardy, Phys. Rev. Lett. **68**, 2390 (1992).

[Bourges95] Bourges P., Y. Sidis, L.P. Regnault, B. Hennion, R. Villeneuve, G. Collin, C. Vettier, J.Y. Henry, and J.F. Marucco, J. Phys. Chem Solids, **56**, 1937 (1995).

[Boebinger96] Boebinger G.S., Y. Ando, and A. Passner, T. Kimura, M. Okuya, J. Shimoyama and K. Kishio, K.Tamasakyu, N. Ichikawa, and S. Uchida, Phys. Rev. Lett. **77**, 5417 (1996).

[Branch97] Branch D.G., McMaster Ph.D. Thesis(1990).

[Bucher93] Bucher B., P. Steiner, J. Karpinski, E. Kaldis, and P. Wachter, Phys. Rev. Lett. **70**, 2012 (1993).

[Carbotte90] Carbotte J.P., Rev. Mod. Phys. **62**, 1027 (1990).

[Carbotte95] Carbotte J.P., C. Jiang, D.N. Basov, and T. Timusk, Phys. Rev. B **51** 11798 (1995).

[Carrington94] Carrington A., D. Colson, Y. Dumont, C. Ayache, A. Bertinotti, and J.F. Marucco, Physica C **234**, 1 (1994).

[Carrington97] Carrington A., C. Marcenat, F. Bouquet, D. Colson, A. Bertinotti, J.F. Marucco, and J. Hammann, Phys. Rev. B **55**, R8674 (1997).

[Cava89] Cava R.J., and B. Batlogg, MSR Bull. **14** (1), 49 (1989).

[Cheng91] Cheng S.-W., G. Aeppli, T.E. Mason, H. Mook, S.M. Hayden, P.C. Canfield, Z. Fisk, K.N. Clausen, and J.L. Martinez. Phys. Rev. Lett., **67**, 1791 (1991).

[Chen89] Chen Yi-Hong., F. Wilczek, E. Witten, and B.I. Halperin, Int. J. Mod. Phys. **3**, 1001 (1989).

[Chu93] Chu C.W., L. Gao, F. Chen, Z.J. Huang, R.L. Meng, and Y.Y. Xue, Nature,**365**, 323 (1993).

[Chubukov97] Chubukov A. V., and J. Schmalian, cond-mat/9711041 (1997).

[Collins90] Collins R.T., Z. Schlesinger, F. Holtzberg, P. Chaudhari, and C. Feild, Phys. Rev. Lett. **39**, 6571 (1990).

[Ding96] Ding H., T. Yokoya, J.C. Campuzano, T. Takahashi, M. Randeria, M.R.Norman, T. Mochiku, K. Kadowaki, and J. Giapitzakis, Nature **382**, 51 (1996).

[Ding97] Ding H., M.R.Norman, T. Yokoya, T. Takahashi, M. Randeria, J.C. Campuzano, T. Takahashi, T. Mochiku, and K. Kadowaki, Phys. Rev. Lett. **78**, 2628 (1997).

[Dolgov95] Dolgov O.V., and S.V. Shulga, J. of Superconductivity **8**, 611 (1995).

[Emery95a] Emery V.J., and S.A. Kivelson, Phys. Rev. Lett. **74**, 3253 (1995).

[Emery95b] Emery V.J., and S.A. Kivelson, Nature **374**, 434 (1995).

[Farnworth74] Farnworth B. and T. Timusk, Phys. Rev. B **10**, 1970 (1974).

[Fukuoka97] Fukuoka A., A. Tokiwa-Yamamoto, M. Itoh, R. Usami, S. Adachi, and K. Tanabe, Phys. Rev. B **55**, 6612 (1997).

[Fukuyama92] Fukuyama H., Prog. Theor. Phys. Supp. **108**, 287 (1992).

[Fukuzumi96] Fukuzumi Y., K. Mizuhashi, K. Takenaka, and S. Uchida, Phys. Rev. Lett. **76**, 684 (1996).

[Gagnon94] Gagnon R., C. Lupien, and L. Taillefer, Phys. Rev. B **50**, 3458 (1994).

[Gao93] Gao F., D.B. Romero, D.B. Tanner, J. Talvacchio, and M.G. Forrester, Phys. Rev. B **47**, 1036 (1993).

[Geshkenbein] Geshkenbein V.G., L.B. Ioffe, and A.I. Larkin, Phys. Rev. B **55**, 3173 (1997).

[Glover57] Glover R.E., III, and M.Tinkham, Phys. Rev. **108**, 243 (1957).

[Gold82] Gold A., S.J. Allen, B.A. Wilson and D.C. Tsui, Phys. Rev.B. **25**, 3519 (1982).

[Götze72] Götze W., and P. Wölfe, Phys. Rev. B **6**, 1226 (1972).

[Graf93] Graf M.J., D. Rainer, and J.A. Sauls, Phys. Rev. B **47**, 12089 (1995).

[Gurvitch87] Gurvitch M., and A.T. Fiory, Phys. Rev. Lett. **59**, 1337 (1987).

[Hardy93] Hardy W.N., D.A. Bonn, D.C. Morgan, R. Liang, and K. Zhang, Phys. Rev. Lett. **70**, 3999 (1993).

[Harris96] Harris J.M., Z.-X. Shen, P.J. White, D.S. Marshall, and M.C. Schabel, cond-mat/9611010 (1996).

[Hazen90] Hazen R.M., Crystal Structures of High-Temperature Superconductors, in *Physical Properties of High Temperature Superconductors II*

D.M. Ginsberg, editor, (World Scientific, Singapore, 1990) pp. 121-198.

[Hinks88] Hinks D.G., D.R. Richards, B. Dabrowski, D.T. Marx, and A.W. Mitchell, Nature **335**, 419 (1988).

[Homes93a] Homes C.C., M.A. Reedyk, D.A. Crandles, and T. Timusk, Applied Optics **32**, 2976 (1993).

[Homes93b] Homes C.C., T. Timusk, R. Liang, D.A. Bonn, and W.N. Hardy, Phys. Rev. Lett. **71**, 1645 (1993).

[Homes95] Homes C.C., T.Timusk, R. Liang, D.A. Bonn, and W.H. Hardy, Physica C, **254**, 265-280, (1995).

[Humlíček90] Humlíček J., E. Schmidt, L. Bočánek, M. Carriga, and M. Cardona, Solid State Comm. **73**, 127 (1990).

[Hwang94] Hwang H.Y., B. Batlogg, H. Tagaki, H.L. Kao, J. Kwo, R.J. Cava, and J.J. Krajewski, Phys. Rev. Lett.,**72**, 2636 (1994).

[Ino98] Ino A., T. Mizokawa, K. Kobayashi and A. Fujimori, Phys. Rev. Lett. **81**, 2124 (1998).

[Isawa94] Isawa K., A. Tokiwa-Yamamoto, N. Itoh, S. Adachi, and H. Yamauchi, Physica C,**222**, 33 (1994).

[Ishida93] Ishida K., Y. Kitaoka, N. Ogata, T. Kamino, K. Asayama, and J.R. Cooper, J. Phys. Soc. Jpn. **62**, 2803 (1993).

[Ito93] Ito T., K. Takenaka, and S. Uchida, Phys. Rev. Lett. **70**, 3995 (1993).

[Ioffe93] Ioffe L.B., A.I. Larkin, A.A. Varlamov, L. Yu, Phys. Rev. B **47**. 8936 (1993).

[Jiang96] Jiang C., E. Schachinger, J.P. Carbotte, D. Basov, and T. Timusk. Phys. Rev. B **54**, 1264 (1996).

[Julien96] Julien M.-H., P. Carretta, M. Horvatic, C. Berthier, Y. Berthier. P. Segransan, A. Carrington, and D. Colson, Phys. Rev. Lett. **76**. 4238 (1996).

[Kendziora93] Kendziora C., M.M. Martin, J. Hartge, and L. Mihaly, Phys. Rev. B **48**, 3531 (1993).

[Kimura92] Kimura T., K. Kishio, T. Kobayashi, Y. Nakayama, N. Motohira, K. Kitazawa, and K. Yamafuji, Physica C(Amsterdam), **192**. 247 (1992).

[Kirtley95] Kirtley J.R., C.C. Tsuei, J.Z.. Sun, C.C. Chi, L.-S. Yu-Jahnes, A. Gupta, M. Rupp, M.B. Ketchen, Nature,**373**, 225 (1995).

[Kittel86] Kittel C., *Introduction to Solid State Physics*, John Wiley & Sons. Inc.. (New York), 1986.

[Kostur96] Kostur V.N., Phys. Rev. B **53**, 2273 (1996).

[Kotliar88] Kotliar G., and J. Liu, Phys. Rev. B **38**, 5142 (1988).

[Landau84] Landau L.D., and E.M. Lifshits, *Electrodynamics of Continuous Media*. Pergamon (New York) (1984).

[Laughlin88] Laughlin R.B., Science **242**, 525 (1988).

[Lee92] Lee P.A., and N. Nagaosa, Phys. Rev. B **46**, 5621 (1992).

[Lee97] Lee P.A. and X.-G. Wen, Phys. Rev. Lett. **78**, 4111 (1997).

[Legget92] Leggett A.J., Braz. J. Phys. B **50**, 496 (1994).

[Liang92] Liang R., P. Dosanih, D.A. Bonn, D.J. Baar, J.E. Carolan, and W.N. Hardy, Physica C **195**, 51 (1992).

[Lynch85] Lynch D.W., Interband Absorption - Mechanisms and Interpretation, in *Handbook of Optical Constants*, E.D. Palik, Editor (Academic Press, 1985).

[Lynch91] Lynch D.W. and W.R. Hunter, in *Handbook of Optical Constants*, E.D. Palik, Editor (Academic Press, 1991) p.286.

[Litvinchuk92] Litvinchuk A.P., C. Thomsen, and M. Cardona, Solid State Comm. **83**, 343 (1992).

[Loram93] J.W. Loram, K.A. Mirza, J.R. Cooper, and W.Y. Liang, Phys. Rev. Lett., **71**, 1740 (1993).

[Loram94] Loram J.W., K.A. Mirza, J.R. Cooper, and W.Y. Liang, J. of Superconductivity, **7**, 261 (1994).

[Loeser96] Loeser A.G., Z.-X. Shen, D.S. Dessau, D.S. Marshall, C.H. Park, P. Fornier, and A. Kapitulnik, Science **273**, 325 (1996).

[Marshall96a] Marshall D.S., D.S. Dessau, A.G. Loeser, C.H. Park, Z.-X. Shen, A.Y. Matsuura, J.N. Eckstein, I. Bozovik, P. Fornier, A. Kapitulnik, W.E. Spicer, and Z.-X. Shen, Phys. Rev. Lett. **76**, 4841 (1996).

[Marshall96b] D.S. Marshall, A.G. Loeser, Z.-X. Chen, and D.S. Dessau, Physica **C**, **263**, 208, (1996).

[Marsiglio95] Marsiglio F., and J.P. Carbotte, Phys. Rev. B **52**, 16192 (1995).

[Marsiglio98] Marsiglio F., T. Startseva, and J.P. Carbotte, to be published in Phys. Rev. Lett.,(1998).

[Mason92] Mason T.E., G. Aeppli, and H.A. Mook, Phys. Rev. Lett., **68**, 1414 (1992).

[Millis88] Millis A.J., S. Sachdev, and C.M. Varma, Phys. Rev. B **37**, 4975 (1988).

[Millis90] Millis A.J., H. Monien, and D. Pines, Phys. Rev. B **42**, 167 (1990).

[Millis93] Millis A.J. and H. Monien, Phys. Rev. Lett., **70**, 2810 (1993).

[Montoux92] Monthoux P., and D. Pines, Phys. Rev. Lett. **69**, 961 (1992).

[Naeini98] J.G. Naeini, X.K. Chen, K.C. Hewitt, and J.C. Irwin, preprint (1998).

[Nemetschek97] Nemetschek R., M. Opel, C. Hoffman, P.F. Müller, R. Hackl, H. Berger, L. Forró, A. Erb and E. Walker Phys. Rev. Lett. **78**, 4837 (1997).

[Niedermayer93] Niedermayer Ch., C. Bernhard, U. Binninger, H. Glücker, J.L. Tallon, E.J. Ansaldo, J.I. Budnick, Phys. Rev. Lett. **71**, 1764 (1993).

[Norman97] Norman M.R., H. Ding, J.C. Capuzano, T. Takeuchi, M. Randeria, T. Yokaya, T. Takahashi, T. Mochiku and K. Kadowaki Phys. Rev. Lett. **79**, 3506 (1997).

[Ohsugi91] Ohsugi S., Y. Kitai, K. Ishida, and K. Asayama, J. Phys. Soc. Jpn. **60**, 2351 (1991).

[Orenstein88] J. Orenstein and D.H. Rapkine, Phys. Rev. Lett., **60**, 968 (1988).

[Orenstein90] Orenstein J., G.A. Thomas, A.J. Millis, S.L. Cooper, D. Rapkine, T. Timusk, L.F. Schneemeyer, and J.V. Waszszak, Phys. Rev. B **42**, 6342 (1990).

[Panagopoulos97] Panagooulos C., J.P. Copper, T. Xiang, G.P. Peacock, I. Gameson and P.P. Edwards, Phys. Rev. Lett. **79**, 2320 (1997).

[Palik85] Handbook of Optical Constants, E.D. Palik, Editor (Academic Press, 1985).

[Puchkov95a] Puchkov A.V., T. Timusk, W.D. Mosley, R.N. Shelton, Phys. Rev. B. **50**, 4144 (1995).

[Puchkov95b] Puchkov A.V. *et al.*, unpublished; A.V. Puchkov, T. Timusk, S. Doyle, and A.M. Hermann, Phys. Rev. B **51**, 3312 (1995).

[Puchkov95c] Puchkov A.V., T. Timusk, M.A. Karlow, S.L. Cooper, P.D. Han, and D.A. Payne, Phys. Rev. B **52**, R9855 (1995).

[Puchkov96a] Puchkov A.V., P. Fournier, T. Timusk, and N.N. Kolesnikov, Phys. Rev. Lett. **77**, 1853 (1996).

[Puchkov96c] Puchkov A.V., P. Fournier, D.N. Basov, T. Timusk, A. Kapitulnik, and N.N. Kolesnikov, Phys. Rev. Lett. **77**, 3212 (1996).

[Puchkov96d] Puchkov A.V., D.N. Basov, and T. Timusk, J. Phys.: Condens. Matter,**8**, 10049 (1996).

[Putilin93] Putilin S.N., E.V. Antipov, O. Chmaissem, and M. Marezio, Nature,**362**, 323 (1993).

[Quijada95] Quijada M.A., D.B. Tanner, F.C. Chou, D.C. Johnston and S.-W. Cheong, Phys. Rev. B, **52**, 15485 (1995).

[Quinlan96] Quinlan S.M., P.J. Hirshfeld, and D.J. Scalapino, Phys. Rev. B **53**, 8575 (1996)

[Randeria97] Randerial M., cond-mat/9710223.

[Reedyk88] Reedyk M., D.A. Bonn, J.D. Garrett, J.E. Greedan, C.V. Stager, T. Timusk, K. Kamarás, and D.B. Tanner, Phys. Rev. B **38**, 11981 (1988).

[Reedyk92] Reedyk M., and T. Timusk, Phys. Rev. Lett. **69**, 2705 (1992).

[Reedyk97] Reedyk M., T. Timusk, Y.-W. Hsueh and B.W Statt, J.S. Xue and J.E. Greedan, Phys. Rev. B **56**, 9129, (1997) .

[Renker88] Renker B., F. Gompf, E. Gering, D. Ewert, H. Rietschek, and A. Dianoux, Z. Phys. B – Cond. Matt. **73**, 309 (1988).

[Renner98] Ch. Renner, B. Revaz, J.-Y. Genoud, K. Kadowaki, and O. Fischer, Phys. Rev. Lett. **80**, 149, (1998).

[Rieck95] Rieck C.T., W.A. Little, J. Ruvalds, and A. Virosztek, Phys. Rev. B **51**, 3772 (1995).

[Rice92] Rice T.M., in *The Physics and Chemistry of Oxide Superconductors*, edited by Y. Iye and H. Yasuoka (Springer-Verlag, Berlin, 1992), p. 313.

[Richards60] Richards P.L. and Tinkham M., Phys. Rev. **119**, 575 (1960).

[Romero92] Romero D.B., C.D. Porter, D.B. Tanner, L. Forro, D. Mandrus, L. Mihaly, G.L. Carr, and G.P. Williams, Phys. Rev. Lett. **68**, 1590 (1992).

[Rõõm98] Rõõm T. and T. Timusk (unpublished) (1998).

[Rossat-Mignod91] Rossat-Mignod J., L.P. Regnault, C. Vettier, P. Bourges, P. Burlet, J. Bossy, J.Y. Henry, and G. Lapertot, Physica C **185-189**, 86 (1991).

[Rotter91] L.D. Rotter, Z. Schlesinger, R.T. Collins, F. Holtzberg, C. Feild, U. Welp, G.W. Crabtree, J.Z. Liu, Y. Fang, K.G. Vandervoort, and S. Flesher Phys. Rev. Lett. **67**, 2741 (1991).

[Sakuto97] Sakuto A., R. Combescot, N. Bontemps, P. Monod, V. Viallet and D. Colson, Europhys. Lett. **39**(2), 207 (1997).

[Sato89] Sato H., S. Tajima, H. Takagi, and S. Uchida, Nature **338**, 241 (1989).

[Schilling93] Schilling J.S.M. Cantoni, J.D. Guo, H.R. Ott, Nature,**363**, 56 (1993).

[Schlesinger89] Schlesinger Z., R.T.Collins, J.A. Calise, D.G. Hinks, A.W. Mitchell, Y. Zheng, B. Dabrowski, N.E. Bickers, and D.J. Scalapino, Phys. Rev. B **40**, 6862 (1989).

[Schlesinger90] Schlesinger Z., R.T. Collins, F. Holtzberg, C. Feild, S.H. Blanton, U. Welp, G.W. Crabtree, Y. Fang, and J.Z. Liu, Phys. Rev. Lett. **65**, 801 (1990).

[Schlesinger94] Schlesinger Z., R.T. Collins, L.D. Rotter, F. Holtzberg, C. Field, U. Welp, G.W. Grabtree, J.Z. Liu, Y. Fang, K.G. Vandervoort, and S. Fleshler, Physica C **235-240**, 49 (1994).

[Shen93] Shen Z.-X., D. S. Dessau, B. O. Wells, D. M. King, W. E. Spicer, A. J. Arko, D. Marshall, L. W. Lombardo, A. Kapitulnik, P. Dickinson,

S. Doniach, J. diCarlo, T. Loeser, and C. H. Park, Phys. Rev. Lett. **70**, 1553 (1993).

[Shulga91] Shulga S.V., O.V. Dolgov, and E.G. Maksimov, Physica C **178**, 266 (1991).

[Slakey90] Slakey F., M.V. Klein, J.P. Rice, and D.M. Ginsberg, Phys. Rev. B **42**, 2643 (1990).

[Schmalian96] Schmalian J., D. Pines and Stojković B., Phys. Rev. Lett. **80**, 3839 (1998).

[Smith85] Smith D.Y., Dispersion theory, Sum Rules, and Their Application to the Analysis of Optical Data, in *Handbook of Optical Constants*, E.D. Palik, Editor (Academic Press, 1985).

[Startseva98a] Startseva T., T. Timusk, A.V. Puchkov, D.N. Basov, M. Okuya, T. Kimura, and K. Kishio, submitted to Phys. Rev. B (1998).

[Startseva98b] Startseva T., T. Timusk, M. Okuya, T. Kimura, and K. Kishio, submitted to Physica C.

[Stojković96] Stojković B., and D. Pines, Phys. Rev. Lett. **78**, 811 (1996).

[Stojković97] Stojković B., and D. Pines, cond-mat/9706247 (1997).

[Stromer88] Stormer H.L., A.F.J. Levi, K.W. Baldwin, M. Anzlowar, and G.S. Boebinger, Phys. Rev. B **38**, 2472 (1988).

[Sugai89] Sugai S., Y. Yntomoto, and T. Murakami, Sol. State Comm. **72**, 1193 (1989).

[Tajima90] Tajima S., S. Uchida, S. Ishibashi, T. Ido and H. Takagi, T. Arima and Y. Tokura, Physica C, **168**, 117 (1990).

[Tajima95] Tajima S., J, Schützmann, and S. Miyamoto, Solid State Comm. **95**, 759 (1995).

[Takagi92] Takagi H., B. Batlogg, H.L. Kao, J. Kwo, R.J. Cava, J.J. Krajewski, and W.F. Peck, Jr., Phys. Rev. Lett. **69**, 2975 (1992).

[Takahashi93] Takahashi H., A. Tokiwa-Yamamoto, M. Mori, S. Adachi, H. Yamauchi, and S. Tanaka, Physica C,**218**, 1 (1993).

[Takegahara94] Takegahara K., J. Electron Spectrosc. Relat. Phenom. **66**, 303 (1994).

[Takigawa91] Takigawa M., A.P. Reyes, P.C. Hammel, J.D. Thompson, R.H. Heffner, Z. Fisk, and K.C. Ott, Phys. Rev. B **43**, 247 (1991).

[Takigawa94] Takigawa M., Phys. Rev. B **49**, 4158 (1994).

[Tallon95] Tallon J.L., Phys. Rev. B **51**, 12911 (1995).

[Tamasaku94] Tamasaku K., T. Itoh, T. Takagi, and S. Uchida, Phys. Rev. Lett., **72**, 3088 (1994).

[Tanner92] Tanner D.B., and T. Timusk, Optical Properties of High-Temperature Superconductors, in *Physical Properties of High Temperature Superconductors III* D.M. Ginsberg, editor, (World Scientific, Singapore, 1992) p. 105.

[Tao87] H.J. Tao, F. Lu, and E.L. Wolf, Physica C **282-287**, (1987).

[Timusk88] Timusk T., S.L. Herr, K. Kamarás, C.D. Porter, D.B. Tanner, D.A. Bonn, J.D. Garrett, C.V. Stager, J.E. Greedan, and M. Reedyk, Phys. Rev. B **38**, 6683, (1988).

[Timusk89] Timusk T., and D.B. Tanner, Infrared Properties of High T_c Superconductors, in *Physical Properties of High Temperature Superconductors I* D.M. Ginsberg, editor, (World Scientific, Singapore, 1989) p. 339.

[Timusk91] Timusk T., C.D. Porter, and D.B. Tanner, Phys. Rev. Lett. **66**, 663 (1991).

[Timusk95] T. Timusk, D.N. Basov, C.C Homes, A.V. Puchkov, and M. Reedyk, Journ. of Superconductivity, **8**, 437 (1995).

[Timusk98] T. Timusk and B. Statt, Rep. Prog. Phys. (to be published).

[Tinkham80] Tinkham M., *Introduction to Superconductivity*, Robert E. Krieger Publishing Company (Malabar, Florida), (1980).

[Thomas88] Thomas G.A., J. Orenstein, D.H. Rapkine, M. Capizzi, A.J. Millis, R.N. Bhatt, L.F. Schneemeyer, and J.V. Waszczak, Phys. Rev. Lett. **61**, 1313 (1988).

[Thomas91] Thomas G.A., D.H. Rapkine, S.L. Cooper, S.-W. Cheong, and A.S. Cooper Phys. Rev. Lett. **67**, 2906, (1991).

[1] Thomas G.A., D.H. Rapkine, S.L. Cooper, S.-W. Cheong, A.S. Cooper, L.S. Schneemeyer, and J.V. Waszczak, Phys. Rev. B, **45**, 2474 (1992).

[Topygo96] Tolpygo S.K., J.-Y. Lin, M. Girvich, S.Y. Hou, and Julia M. Phillips, Phys. Rev. **B, 53**, 12454 (1996).

[Tranquada92] Tranquada J.M., P.M. Gehring, G. Shirane, S. Shamoto, and M. Sato. Phys. Rev. **B 46**, 5561 (1992).

[Tsuei94] Tsuei C.C., J.R Kirtley C.C. Chi, L.-S. Yu-Jahnes, A. Gupta, T.M. Shaw, J.Z.. Sun and M.B. Ketchen, Phys. Rev. Lett. **72**, 593, (1994).

[Tsuei96] Tsuei C.C., J.R Kirtley, M. Rupp, J.Z.. Sun, A. Gupta, M.B. Ketchen, C.A. Want, Z.F. Ren, J.H. Wang, M. Bhushan, Science, (1996).

[Marel91] van der Marel D., H.-U. Habermeier, D. Heitmann, W. König, and A. Wittlin, Physica C **176**, 1 (1991).

[Uchida91] Uchida S., I. Ido, H. Takagi, T. Arima, Y. Tokura, and S. Tajima. Phys. Rev. **B 43**, 7942 (1991).

[Uchida96] Uchida S., K. Tamasaku, and S. Tajima, Phys. Rev. B **53**, 14558, (1996).

[Uemura89] Uemura Y.J., G.M. Luke, B.J. Sternlieb, J.H. Brewer, J.F. Carolan, W.N. Hardy, R. Kadono, J.R. Kempton, R.F. Kiefl, S.R. Kreitzman, P. Mulhern, T.M. Riseman, D.Ll. Williams, B.X. Yang, S. Uchida, H. Takagi, J. Gopalakrishnan, A.W. Sleight, M.A. Subramanian, C.L. Chien, M.Z. Cieplak, G. Xiao, V.Y. Lee, B.W. Statt, C.E. Stronach, W.J. Kossler, and X.H. Yu, Phys. Rev. Lett. **62**, 2317 (1989).

[Uemura91] Uemura Y.J., L.P. Le, G.M. Luke, B.J. Sternlieb, W.D. Wu, J.H. Brewer, T.M. Riseman, C.L. Seaman, M.B. Maple, M. Ishikawa,

D.G. Hinks, J.D. Jorgensen, G. Saito, and H. Yamochi, Phys. Rev. Lett. **66**, 2665 (1991).

[Walkes93] Walkes D.R., A. Carrington, A.P. Mackenzie, and J.R. Cooper. (unpublished), cited in M. Gabay, and P. Lederer. Phys. Rev. Lett. **47**. 14462 (1993).

[Warren89] Warren W.W., Jr., R.E. Walstedt, G.F. Brennert, R.J. Cava, R. Tycko. R.F. Bell, and G. Dabbagh, Phys. Rev. Lett. **62** 1193, (1989).

[Webb86] Webb B.C., A.J. Sievers, and T. Mihalisin, Phys. Rev. Lett **57**. 1951 (1986).

[Wen96] Wen X.-G., and P. Lee, Phys. Rev. Lett. **76**, 503 (1996).

[Wooten72] Wooten F., *Optical properties of solids*, Academic Press (New York). 1972.

[Yagil94] Yagil Y. and E.K.H Salje, Physica C, **235-240**, 1143 (1994).

[Yasuoka9] Yasuoka H., Physica C, **282-287**, 119 (1997).

[Yoshinari90] Yoshinari Y., H. Yasuoka, Y. Ueda, K. Koga, and K. Kosuge. J. Phys. Soc. Jpn. **59**, 3698 (1990); H. Alloul, T.Ohno, and P. Mendels. J. Less-Common Met. **164-165**, 1022 (1990).

[Yu92] Yu R.C., M.B. Salamon, J.P. Lu, and W.C. Lee, Phys. Rev. Lett. **69**. 1431 (1992).

[Zasadzinski89] Zasadzinski J.F., N. Tralshawala, D.G. Hinks, B. Dabrowski. A.W. Mitchell, D.R. Richards, Physica C **158**, 519 (1989).

[Zhang97] Zhang S.C., Science. **275**, 1089 (1997).

[ZhangH94] Zhang H., H. Sato, and G.L. Liedl, Physica C **234**, 185. (1994).

[ZhangK94] Zhang K., D.A. Bonn, S. Kamal, R. Liang, D.J. Baar, W.N. Hardy, D. Basov, and T. Timusk, Phys. Rev. Lett. **73**, 2484 (1994).

[Zheng93] Zheng G., T. Odaguchi, T. Mito, U. Kitaoka, K. Asayama, Y. Kodama, J. Phys. Soc. Jpn. **62**, 2591 (1993).